DOE/CH/10250--T1

DE93 001395

FIELD INVESTIGATION OF A WAKE STRUCTURE DOWNWIND OF A VAWT IN A WINDFARM ARRAY*

H.-T. Liu, J. W. Buck, A. C. Germain, M. E. Hinchee,
T. S. Solt, G. M. LeRoy and R. A. Srnsky

October 1987

DISCLAIMER

FLOW RESEARCH COMPANY
Applied Mechanics Division
21414-68th Avenue South
Kent, Washington 98032
(206) 872-8500

*This work was conducted under a cooperative agreement, DE-FC02-86CH10250, sponsored by the U.S. Department of Energy.

DISCLAIMER

ACKNOWLEDGEMENT

This field project was a cooperative effort between several organizations from private industries (Flow Research Company and FloWind Corporation), government agencies (Department of Energy, Solar Energy Research Institute, Pacific Northwest Laboratory, and Sandia National Laboratories), and utilities (Southern California Edison). The authors would like to acknowledge the contributions from these organizations, without which the field investigation could not have been accomplished. In addition to substantial cost sharing by Flow Research and FloWind through the provision of the wind system, instruments and equipment, they also provided administrative, research and O&M support. The project was monitored jointly by Mr. Warren Bollmeier of SERI and Dr. Larry Wendell of PNL. A Technical Review Team, including Mr. Bollmeier, Dr. Peter Tu of SERI, Mr. Paul Veers of Sandia Laboratories, and Mr. John Buck of PNL, was formed. Several onsite visits and review meetings of the test plan and the preliminary field data were conducted by the team members. Support of the project by SCE was made in the form of cash co-funding and furnishing of the research trailer through the coordination of Mr. Jay Stock. The stack-up towers and the Gill anemometers were installed and aligned by PNL technical personnel Mr. Owen Abbey and Mr. Gary Dennis. Many individuals from FloWind made various contributions to the project. First of all, the project was supported wholeheartedly by the management of FloWind, in particular, Dr. Y.-H. Pao and Mr. Art Wilder. Assistance was provided by FloWind's O&M crews, led by Mr. Bill Schindler, and onsite research personnel, specifically Mr. Henry Moore, in setting up the research trailer, the portable towers and the cup anemometers, as well as in keeping the turbine and tower arrays in good working order. Administrative assistance was provided by Mr. Uwe Moritz in coordinating with the California State Bureau of Land Management for permit applications and other legal matters. Last but not the least, the authors would like to acknowledge the consultation services of Mr. Tom Hiester and Dr. B. J. Im in the areas of site characterization and turbine performance.

ABSTRACT

The effects of upwind turbine wakes on the performance of a FloWind 17-m VAWT were investigated through a series of field experiments conducted at the FloWind windfarm on Cameron Ridge, Tehachapi, California. The field experiment was conducted within a VAWT array consisting of more than nine VAWTs with separations 3D crosswind by 8D downwind (where D is the turbine diameter) in a staggered configuration. The array is the upwind three rows of VAWTS in a total of six rows that are on top of the Cameron Ridge plateau. The terrain features in the vicinity are reasonably regular, with an upslope of 7 deg on the average; however, several local irregularities are present. The annual hourly averaged wind speed exceeds 8 m/s at the site. The primary wind season is from March to August, during which the wind is thermally driven due to cooler air masses rushing through the San Joaquin Valley to replenish the rising of hot air masses in the Mojave Desert. As a result, the wind pattern in terms of wind speed and direction is reasonably persistent during this time. In general, medium to high winds exceeding 9 m/s are confined in a narrow wind direction window between 295 and 310 deg. Therefore, turbines were selected to form an array with a major axis of 308 deg.

The wind field and the power outputs of nine turbines within the array were measured with wind sensors and power transducers. Nine Gill propeller and 18 Maximum cup anemometers and one direction sensor were mounted on portable and stack-up towers installed upwind and within the turbine array. Most of the wind sensors were mounted at 13.7 m above ground, slightly below the equator height, at various on-axis and off-axis locations with respect to the primary wake-producing turbine. Three other sensors were mounted at 6.1 m below (at -2D and 3D) and 13.7 m above (at 3D) for measuring the vertical gradients of the wind field and velocity deficit. A test matrix was designed and subsequently executed to obtain maximum data stratification and to provide results with adeqate accuracy and statistical significance.

From the field measurements, we derived the velocity and power/energy deficits under various turbine on/off configurations. Much information was provided to characterize the structure of VAWT wakes and to assess their effects on the performance of downwind turbines. A method to estimate the energy deficit was developed based on the measured power deficit and the wind speed and distributions. This method may be adopted for other turbine types and sites. Recommendations are made for optimizing windfarm design and operations as well as for wind energy management.

TABLE OF CONTENTS

LIST OF FIGURES

LIST OF TABLES

1. INTRODUCTION

Knowledge of turbine wake characteristics is crucial for optimizing the design of wind turbines (e.g., aerodynamic performance) and the configuration of turbine arrays (e.g., turbine spacings and array staggering). These characteristics include the wake geometry, i.e., the maximum wake height and width, the mean velocity deficit, the turbulence intensity and the blade-shed vortices. In the past, most of the research emphasis on the problem of wind turbine spacing was related to the momentum deficit and consequent loss of energy capture.

Numerical and laboratory simulations (Lissaman, 1979; Vermeulen, 1980) have been conducted to predict turbine wake behavior, and these studies have received limited verification in atmospheric tests of full-scale wind turbines (Vermeulen et al., 1979; Liu et al., 1983; Lissaman et al., 1983; Baker and Walker, 1982; Renne and Buck, 1985). No verification tests have been performed, however, in the wake of an array of full-scale vertical-axis wind turbines (VAWTs) 150 kW or larger. Our current understanding of the array effects on the performance of downwind turbines is, at best, very limited.

Many windfarms, with most of the turbines rated below 500 kW, have been established in recent years. The design criteria for the turbines (aerodynamic performance) and the array configurations (turbine spacings and array staggering) have relied mainly on information derived from numerical or laboratory simulations or from very limited full-scale results. Because the results of these simulations have not been thoroughly validated, most criteria are over-specified to allow sufficiently high safety factors. As a result, the costs of manufacturing and installation are unnecessarily high. Furthermore, because the array configurations in terms of packing density are not optimized, the energy capture and, hence, the revenues of the windfarm operations are by no means maximized. In other cases, the design of crucial components may not be adequate, so that stress concentration results in fatigue and premature failure.

Under a cooperative agreement with the Department of Energy (DOE) (DE-FC02-86CH10250), Flow Research Company (FLOW) and FloWind Corporation, as the Participant in cooperation with the Pacific Northwest Laboratory (PNL) and Southern California Edison (SCE), conducted a series of turbine wake measurements at the FloWind windfarm on Cameron Ridge, Tehachapi, California. The

The turbine wake project was divided into two phases. Phase I involved the development of the test plan for the field experiment. The test plan specified the selection of the turbine array, requirements for the instrumentation and equipment, the configuration of the wind sensors, the site preparation and support requirements, the test schedule, the plans for execution of the field experiment, and the procedure for data reduction and analysis. Phase II involved the execution of the field experiment according to the test plan and the data reduction and analysis of the results.

2. TEST SITE AND WIND SYSTEM

2.1 Test Site and Turbine Array

The wake project was conducted at the FloWind windfarm on Cameron Ridge in the Tehachapi Mountains, approximately 160 km (100 miles) northeast of Los Angeles in Kern County, California. Cameron Ridge (see Figure 1) is about 8 km (5 miles) long and ranges in elevation between 1.40 to 1.46 km (4600 and 4800 ft). The prevailing northwesterly wind in late spring to early summer is roughly perpendicular to the ridge. The annual average wind speed at the ridge exceeds 8 m/s (18 mph).

Cameron Ridge has strong winds in a wide variety of weather patterns. During the months of March through August, the air over California's Mojave Desert is warmed by the sun, causing a lower atmospheric pressure near the surface, which allows cooler, more dense air from the San Joaquin Valley to be drawn through the gaps and passes of the Tehachapi Mountains. This air movement is often strong and generally persistent during most of these warmer months. During the rest of the year (September through February), the temperature and pressure differentials between the desert and valley areas are less pronounced, and the winds are less frequent and not as strong. Winds during these cooler months are associated primarily with transitory weather patterns, such as storms and weather fronts, and not with the solar/thermal effects of the summer months.

The monthly and yearly average wind speeds at the Cameron Ridge windfarm, as projected by Stones and Webster and measured by FloWind in 1984-85, are listed in Table 1. Note that the mean wind speeds for all 12 months exceed the threshold speed for the FloWind 17-m VAWT, which is approximately 5.36 m/s or 12 mph (see Section 2.2). The projected speeds tend to be higher than the actual measurements conducted in 1984-85, especially for the months of July through September. Because Cameron Ridge is located further inland into the eastern desert, the thermally driven wind may weaken as the temperature on both sides of Tehachapi Pass equalizes during these hot summer months. This is different from the situation at passes closer to the Pacific coast, such as Altamont Pass where a large thermal gradient across the pass persists and the thermally driven wind is the strongest during the hot summer months. To obtain a worst-case scenario, therefore, the experiments were completed before early August 1986.

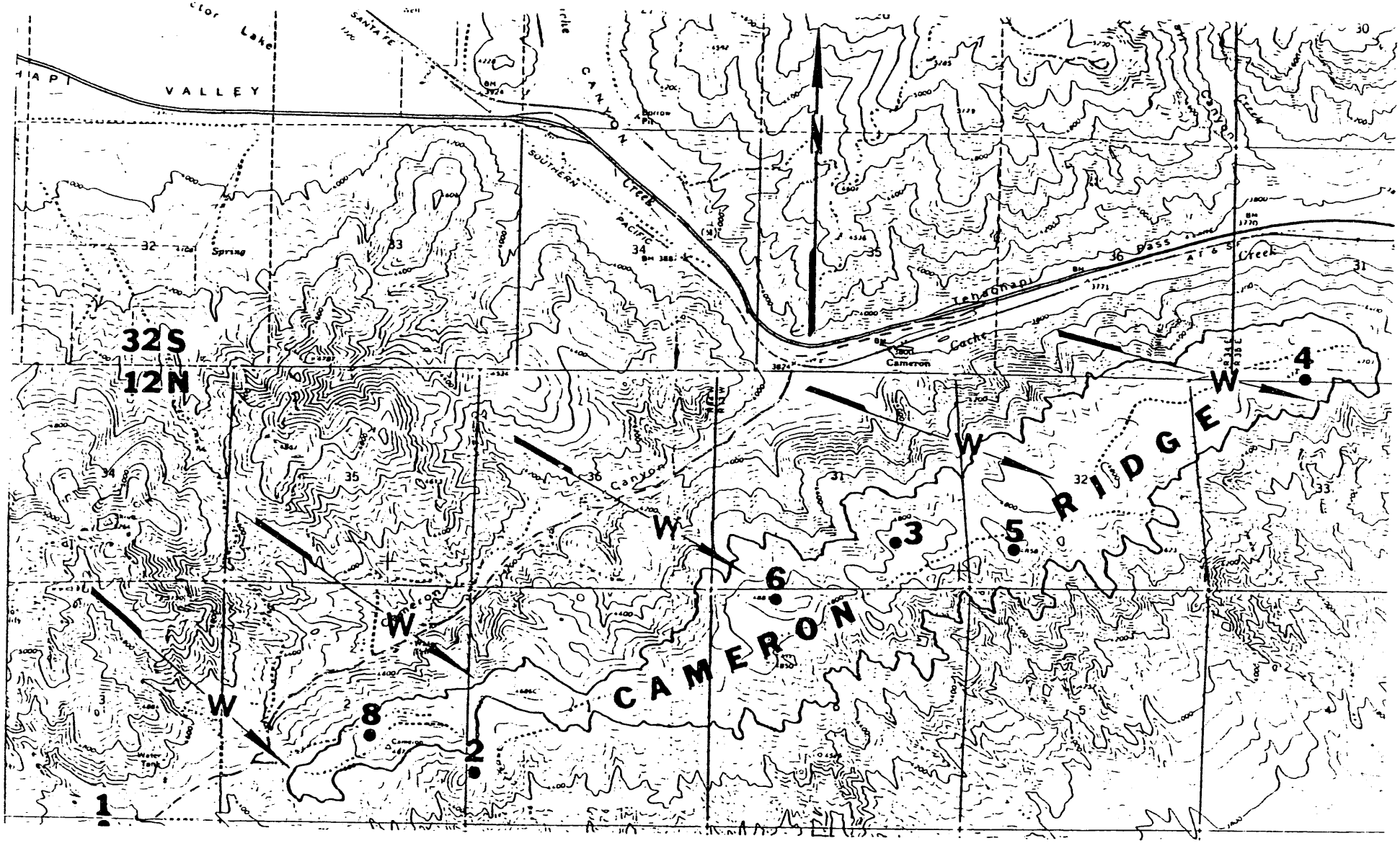

Figure 1. Topographical Map of Principal Portion of Cameron Ridge. Arrows with "W" indicate approximate wind direction responsible for over 98% of the wind energy. Numbers indicate wind measurement sites.

Table 1. Wind Speeds at Cameron Ridge Windfarm

Month	SWEC Projection (m/s) (16.8 m)	Actual Measurements (m/s) (14.6 m)	
January	7.93	5.68	1985
February	7.32	6.84	1985
March	10.98	9.39	1985
April	11.29	10.33	1985
May	13.42	10.51	1985
June	15.74	10.95	1985
July	13.30	6.75	1984
August	11.53	6.75	1984
September	10.68	6.30	1984
October	9.76	10.37	1984
November	8.18	8.27	1984
December	6.84	6.57	1984
Average	10.58	8.25	

The FloWind windfarm is equipped with approximately 200 FloWind 17-m VAWTs situated on the 4.9 km^2 site (see Figure 2). The site is well-developed, with roads, phone, water, gas and electricity in, and it has two buildings, one for operations and maintenance activities and the other a construction trailer. The power collection system consists of individual transmission lines running from each wind turbine to small transformers located nearby on concrete pads. These pad transformers step up the voltage from the 480 volts at which the electricity is produced by an individual wind turbine to 21,000 volts. The power is then transmitted to Southern California Edison through transmission lines and a substation. At the substation, the electric power is again stepped up from 21,000 volts to 66,000 volts for delivery to SCE.

The originally proposed site at which the wake measurements were to be conducted is located at the northeastern portion of Cameron Ridge (shaded area between Stations 3 and 4 in Figure 3) where the terrain features are relatively regular. In the vicinity of the test site, there are six rows of FloWind VAWTs (mostly 17-m and a few 19-m VAWTs), eight diameters apart downwind and three diameters apart crosswind. Inside the test site, we selected two nearby FloWind 17-m turbines as the wake-producing machines (adjacent to each other with one as the primary and the other as the backup system) for the field measurements.

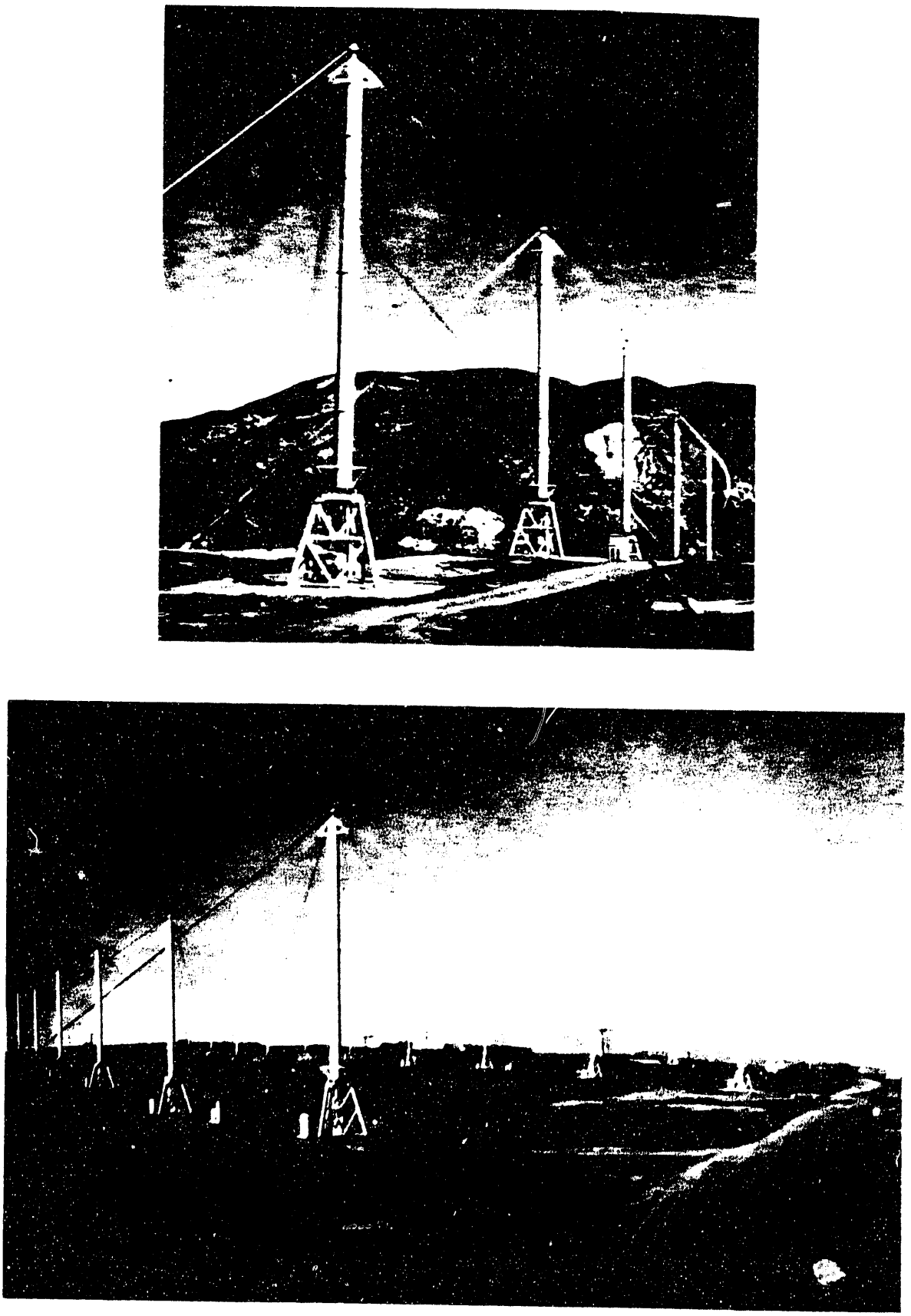

Figure 2. FloWind Windfarm on Cameron Ridge, Tehachapi, California.

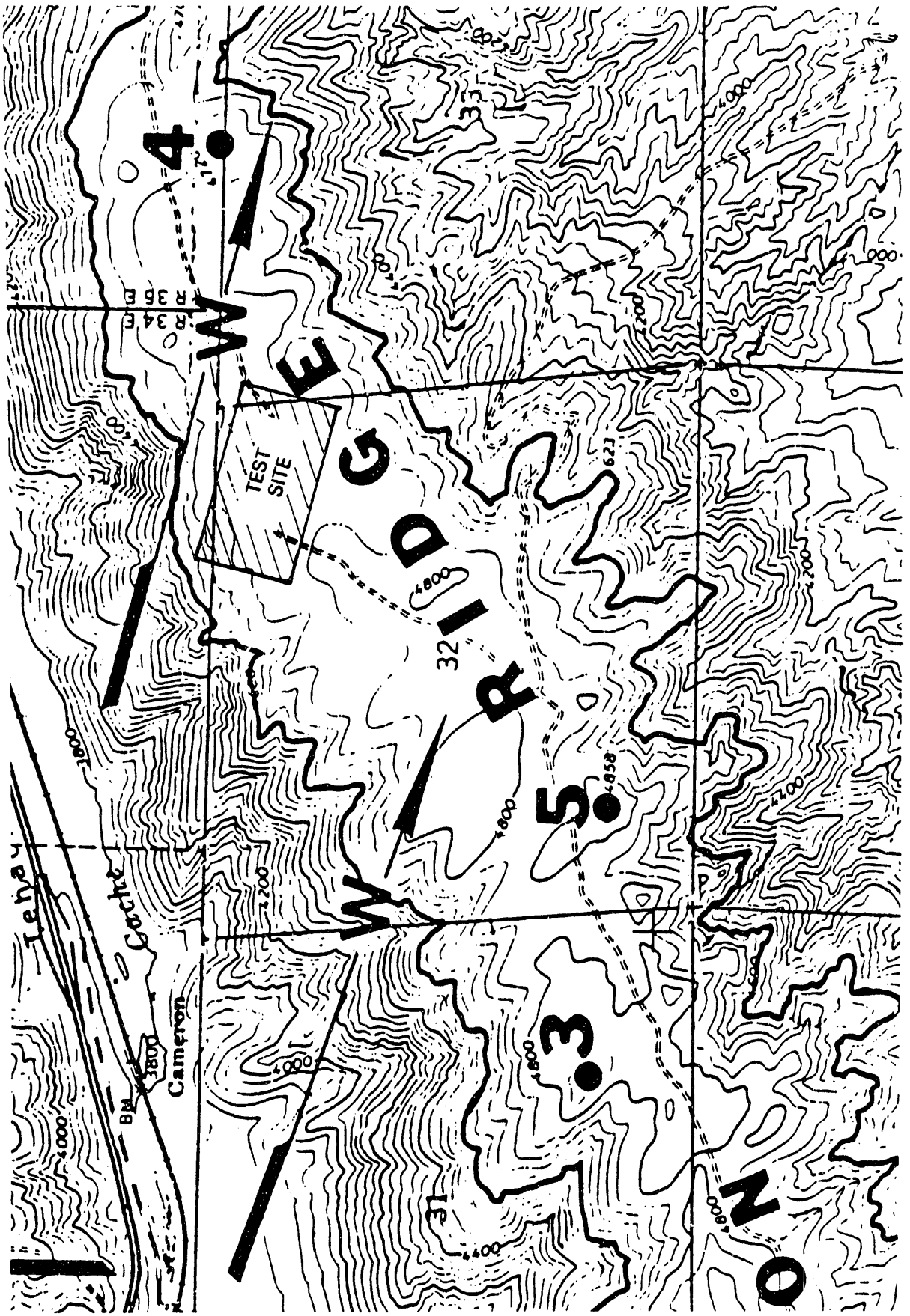

Figure 3. Location of the Test Site for Turbine Wake Measurements.

A preliminary site visit to the Tehachapi FloWind windfarm was made on December 3, 1985, by several members of the project management team and the Participant. Subsequently, the Participant conducted a review of historical and recent data available for the Tehachapi FloWind windfarm to gain a better understanding of the wind characteristics at various locations in the vicinity of the potential test sites and of the operational and performance characteristics of the wind turbines. Personnel in charge of windfarm operations were also contacted to ensure that our proposed field research project would be compatible with their operation. Based on the findings of the first phase, we developed a test plan (Liu, 1986a), which was then reviewed and approved by the project management team. In this report, we provide essential information not contained in the original test plan and an update of the final test plan.

One of the most important aspects of the test plan was to confirm the prevailing wind direction and its variations at potential test sites during the proposed test period. This information was required to finalize the selection of the turbine array, to configure the tower array for the wind sensors, and to schedule the field test. During the preliminary site visit, we examined two potential test sites, including the one originally proposed (with an array of F-17 VAWTs) (see Figure 3) and a backup site on the Horned Toad property at the northwest tip of the ridge (with an array of F-19 VAWTs). From a topographical point of view, the original site was preferable as it is located on a relatively flat plateau with up to six rows of F-17s spaced eight diameters downwind and three diameters crosswind. The topographic influence on the wake structure would be minimal. Figure 2 shows two photographs inside the Tehachapi windfarm; the proposed turbine array consisting of nine F-17s is located at the far left corner of the lower photograph. Other considerations, such as permit applications, also favored the original site. Therefore, we stayed with our original selection.

From the historical data, as shown in Table 1, the prevailing wind direction in the vicinity of the proposed test site during spring and summer is at about 285 to 290 deg. In 1985, measurements at two locations near the test site show that the prevailing wind exceeding 5 m/s has a narrow window between 270 and 315 deg, consistent with the historical data. More wind data gathered during the field experiments are presented in Section 5.1.

Based on the above findings, we selected the main axis of the tower array to be 308 deg, which coincided with the orientation connecting the primary

turbine (T123) and one of the downwind turbines (T102). A description of the turbine array together with the test configuration is given in detail in Section 4. Such a configuration was expected to have a high probability of covering all of the wind speed regimes. Furthermore, the spatial distribution of the portable towers was designed to provide adequate coverage of the wake for wind directions slightly off from 308 deg.

2.2 Wind Turbines

At the time the measurements were conducted for this project, there were over 300 FloWind 17-m (F-17) and 19-m (F-19) VAWTs in operation at the Tehachapi windfarm (the dimension refers to the diameter of the turbine at the equator height). These VAWTs are evolved versions of the original Sandia National Laboratories VAWT. The design and operation of the F-17 is given elsewhere (Hiester et al., 1983). Table 2 lists the specifications of the F-17 VAWT. The F-17 has a maximum power output of 160 kW (at sea level); the power output is about 42 kW at a wind speed of 8.9 m/s (20 mph). The power curve of the turbines is presented in Section 5.3. The F-19 is the largest FloWind VAWT in operation. An array of F-17s was used for the wake measurement experiments.

A review of the axial momentum theory, which forms the mathematical basis for the mechanisms by which a rotor extracts energy from or imparts energy to the wind field, has been given by Renne and Buck (1985). For the performance of an array of VAWTs, linear superposition of individual wakes was used to estimate the wake loss (Lissaman et al., 1982). At present, the adequacy of such linear superposition is yet to be confirmed due to limited availability of full-scale data for verification.

Table 2. Specifications of FloWind 17-m VAWT

System Configuration

Rotor Type	Vertical Axis
Rotor Diameter	17 m
Rotor Height	22.9 m
Ground Clearance	4.6 m
Total Height	28 m
Number of Blades	2
Blade Cross Section	NACA 0015 airfoil
Blade Chord	0.6 m
Rotor Support	Guyed on Top
Radius Guy Anchor	40 m

Control System

Intel 8085 Microprocessor Based
LED Status Display
Failsafe Relay Logic Backup
Battery Backup

Brake System

Service	Dual independent disk Hydraulic actuation
Park	Spring set disk Hydraulic release

Performance

Power	3-phase, 60 Hz, 480 volts AC induction motor, 149 kW
Rotor Speed	53 rpm
Generator Speed	1800 rpm

Operational Characteristics

Cut-in Wind Speed	5.4 m/s
Cut-out Wind Speed	26.8 m/s
Design Max. Wind Speed	71.3 m/s parked
Weight	13,607 kg
Installation	Crane erect or Hydraulic tilt-up

3. INSTRUMENTATION AND EQUIPMENT

3.1 Data Acquisition System

The data acquisition system used for the collection of the wind data from the vertical array of towers was a combination of a CDS 53A Smart data acquisition unit connected to an HP-9826 desktop computer system and two portable data loggers. The CDS 53A system is able to sample 40 channels at a rate of 1 Hz. The HP-9826 desktop computer system consisted of a desktop controller, a 20-Mb hard disk, a 5-1/4-inch cartridge tape drive, and a printer. All components of the data system were connected to the HP-9826 controller by HP-IB cables.

The signals sent by the Gill UVW anemometers were first filtered for spikes. These signals were also conditioned to account for signal loss from cable length and individual differences in the DC generators in each of the three Gill arms. The signals were then received by the CDS 53A Smart data acquisition system and converted from analog to digital signals within the range of -1.0 to 1.0 volt. These digital signals were then sent to the internal memory of the HP-9826 for intermediate storage and computations.

When the internal memory of the HP-9826 was full, the data were sent to the hard disk for permanent storage. Ten-minute averages of these data were sent to the printer for the operator to inspect. When the data collection session was over, the data set was transferred from the hard disk to the tape drive cartridge for backup and transferral to other computer systems.

The transferral of the data from the backup cartridge tapes to the mainframe computer for final data analysis was accomplished by connecting the HP-9826 system to a 9-track magnetic tape drive. A program was then run to convert the data from HP packed binary on the backup cartridges to standard ASCII data and to transfer these data to the 9-track magnetic tape. The data files on the 9-track tape are standard ASCII files that can be read by any computer system.

Two portable data loggers were used for recording the outputs of the Maximum cup anemometers and of the turbine power. The first was a microprocessor-based data logger (Windwatch 3, Atmospheric Research & Technology). The wind speed data with a 7.5-minute averaging period were recorded on the memory chip of the logger. The data were transferred to an IBM PC or compatible for analysis. The second was a programmable microcomputer data logger (Model CR21X, Campbell Scientific, Inc.). PNL provided four CR21X's for this project. One CR21X was used to record the power outputs of the three turbines

in each of the three rows. A total of three CR21X's was used with the fourth one as a spare. The turbine power was sampled and recorded on a cassette tape at several sampling/averaging rates (from 0.1 s/1 s to 0.2 s/30 s). The data were transferred via a cassette interface (Model C20, Campbell Scientific, Inc.) to an IBM PC or compatible for analysis.

3.2 Systems for Data Reduction and Analysis

The data recorded with the HP computer-based data acquisition system were transferred to magnetic tapes at PNL. The data on magnetic tapes were then loaded on FLOW's Masscomp MC5600 mainframe computer for reduction and analysis. The MC5600 is a real-time Unix-based computer with a virtual memory of 4 Gb and 4 Mb of semiconductor memory. The computer uses a 32-bit Motorola 68020 CPU chip along with a 68881 floating point processor chip. It has a Masscomp Lightning board that allows an execution speed of up to 3 MIPs. The MC5600 has two high-speed disk drives (300 and 133 Mb) and a 1600-bpi tape drive.

A Compaq Plus portable computer and several IBM PC and AT compatibles were also used for data retrieval, reduction and analysis. During the field experiment, the Compaq computer was brought to the test site for the above purpose. Data from the CR21X data loggers (on cassette tapes) and from the Windwatch 3 (on squirrels) were transferred to the Compaq computer for reduction and analysis. The software included programs written in BASIC/QUICKBASIC by Microsoft, LOTUS 123 and MANUSCRIPT by Lotus Development Corporation, and ASYSTANT by Macmillan Software Company.

FORTRAN programs run on the MC5600 were developed to convert the raw data into physical units by applying calibration coefficients and correction factors when appropriate. We then performed 7.5-minute averages on most of the data. The 7.5-minute averaged data were then downloaded to the Compaq Plus portable computer or IBM AT compatible personal computers for further reduction and analysis.

At the test site, it was necessary to operate the HP computer-based data acquisition system in a controlled environment close to the tower array. We installed an air-conditioned research trailer (2.6 m x 3.1 m) to provide the needed shelter for the data acquisition system and the operators. Most of the furniture inside the trailer was provided by SCE. Both 115- and 220-volt power sources were made available at the site. To anticipate possible power surges and irregularities in the power sources, a voltage regulator was incorporated

into the data acquisition system. In addition, a portable generator for emergency situations during power outages at the site was available at the onsite FloWind O&M Office.

3.3 Instrumentation

For measurements of the wind field, we used nine Gill UVW anemometers (R. M. Young Company) and 18 cup anemometers (Maximum Model 40). A Climatronics wind direction sensor (Model F460) was mounted on the upwind stack-up tower to obtain a visual indication of the wind direction and to provide duplicate measurements of the wind direction. The sensor of the Gill anemometer was a helicoid-shaped polypropylene propeller with a diameter of 23 cm and a pitch of 30 cm, which gives a distance constant of 3.3 m at 63% recovery. The frequency response of the Gill propellers is dependent on the wind speed. For example, the frequency response at a wind speed of 13.2 m/s is about 0.6 Hz. Gill anemometers have been used recently in a wake study of a DAF 500-kW VAWT (Renne and Buck, 1985). During the field test, a set of lightweight polystyrene propellers was used to replace the polypropylene ones for a short period of time. The polystyrene propellers have a distance constant of 0.8 m and a freqency response of 2.6 Hz at 13.2 m/s. These propellers, however, do not have the strength to withstand the extremely high winds that occur at the site, and they cannot be used unattended. The Maximum cup anemometers have a distance constant of 3.05 m. At a wind speed of 13.2 m/s, the frequency response is about 0.7 Hz.

For measurements of the turbine power, we made use of the existing electronic precision AC watt transducer (Model EW5-6B, Ohio Semitronics, Inc). Each unit was precalibrated at the factory to provide a 1-mA current output proportional to the electrical power delivered to a load.

3.4 Meteorological Towers

Two types of met towers were used. The first was a stack-up tower, which extended to 21.3 m (70 ft) above the ground. The Gill UVW anemometers, the wind direction sensor, and two of the cup anemometers were mounted on this type of tower. Seven stack-up towers were provided by PNL. The second type was a portable tower (Rohn Company), which reached to a maximum height of 13.7 m (45 ft) above the ground. The Maximum cup anemometers were mounted on these portable towers. FloWind provided 16 such towers for the project.

4. FIELD EXPERIMENT

4.1 Preparation

4.1.1 Layout of Experimental Setup

From the prevailing wind direction of around 310 deg and several other considerations, we selected for the field experiments a test site that contained nine F-17 turbines: T122, T123 (designated as the primary turbine), T124, T101, T102, T103, T77, T78 and T79. From the power production data recorded during 1985 (for May, June or the 10-month total), these nine turbines demonstrated similar performance (Liu, 1986a). During the wake measurement project, the power production from each of these nine turbines was recorded simultaneously with the wind measurements to correlate the power deficit with the velocity deficit. The four perimeter turbines on the side of rows 1 and 2 (T121, T125, T100 and T104) were also used to assess their effects, but their power outputs were not monitored.

Figure 4a shows a top view of the layout of the anemometers and towers. This layout is superposed onto a topographic map of the test site (Figure 4b) to show the overall configuration. The corresponding vertical configuration of the towers and wind sensors is shown in Figure 5. One of the main constraints was that, for safety considerations, any erected structure had to be at a minimum distance of 1.5 times its height from a turbine or a power line.

As shown in Figure 4, the major axis of the tower array was at 308 deg, which coincided with the alignment between turbines T123 and T102. The maximum height of the cup anemometers mounted on portable towers was 13.7 m, which is about 2.3 m below the equator height of the F-17 VAWT (i.e., 16 m). For the F-17 VAWT, the wake characteristics at these two levels are not expected to differ appreciably. Therefore, we installed all but four velocity sensors [the Gill UVW (small circles) and cup anemometers (crosses) as shown in Figure 4] at the 13.7-m level rather than the 16-m equator height. For the two taller stack-up towers at 2D upwind (where D is the rotor diameter dimension) and 3D downwind of the primary turbines, one Gill and one cup anemometer were mounted at 21.3-m and 6.1-m levels to monitor the vertical variations of the prevailing wind and of the wake characteristics.

Seven stack-up towers were used on which both types of wind sensors were mounted at -2D (13.7 m high), 1.5D, 3D (one on-axis and 21.3 m high and two $\pm$1D off-axis and 13.7 m high), 5D and 6.5D. Sixteen portable towers were equipped with only cup anemometers for greater spatial coverage (-3D, -1D, 5D,

a. Top View of the Layout Plan for the Anemometers and Towers

Figure 4. Top View of the Wind Sensor Layout Within the Turbine Array.

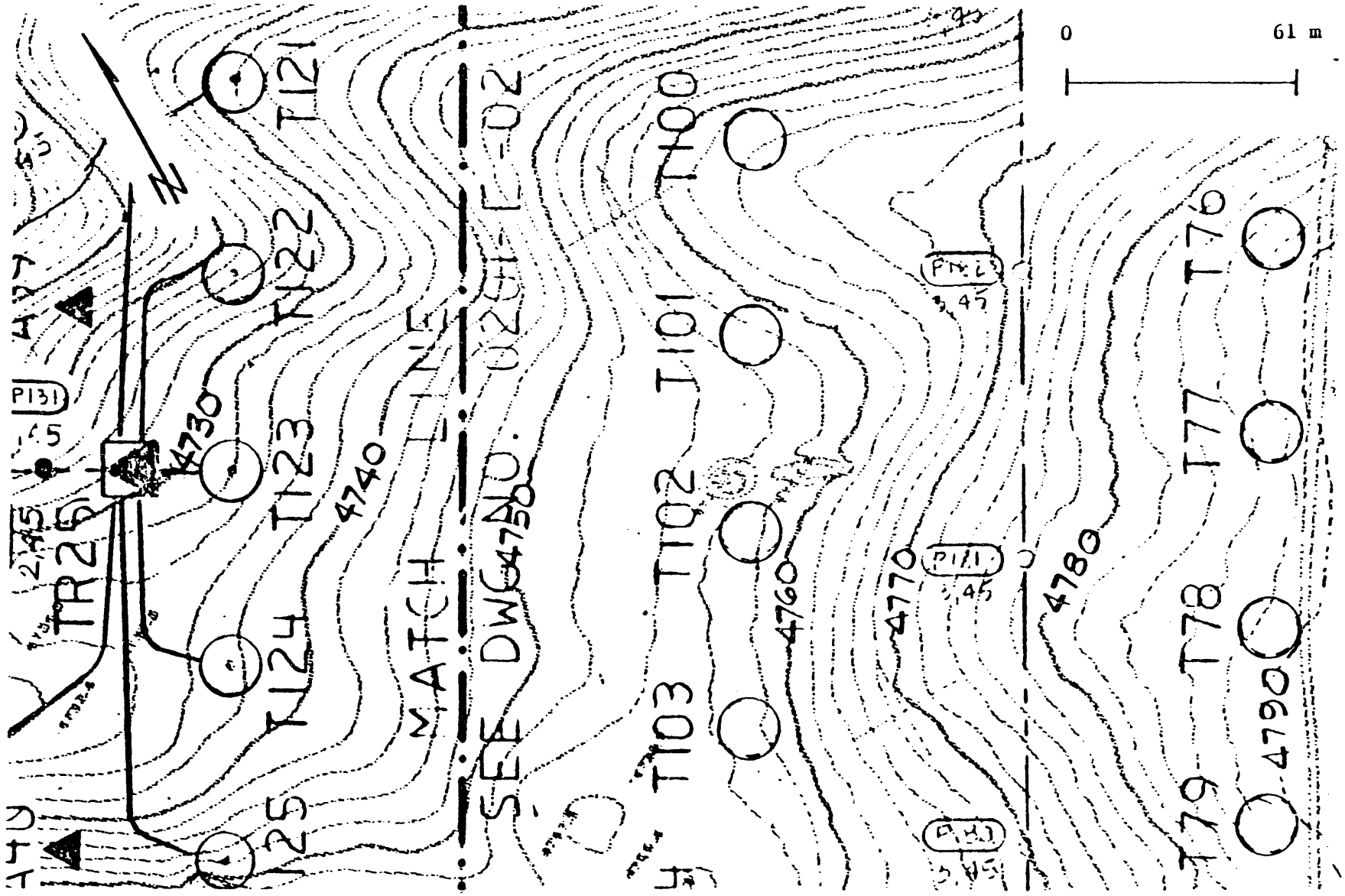

b. Topographic Map of the Test Site on Cameron Ridge, Tehachapi, California

Figure 4. Top View of the Wind Sensor Layout Within the Turbine Array.

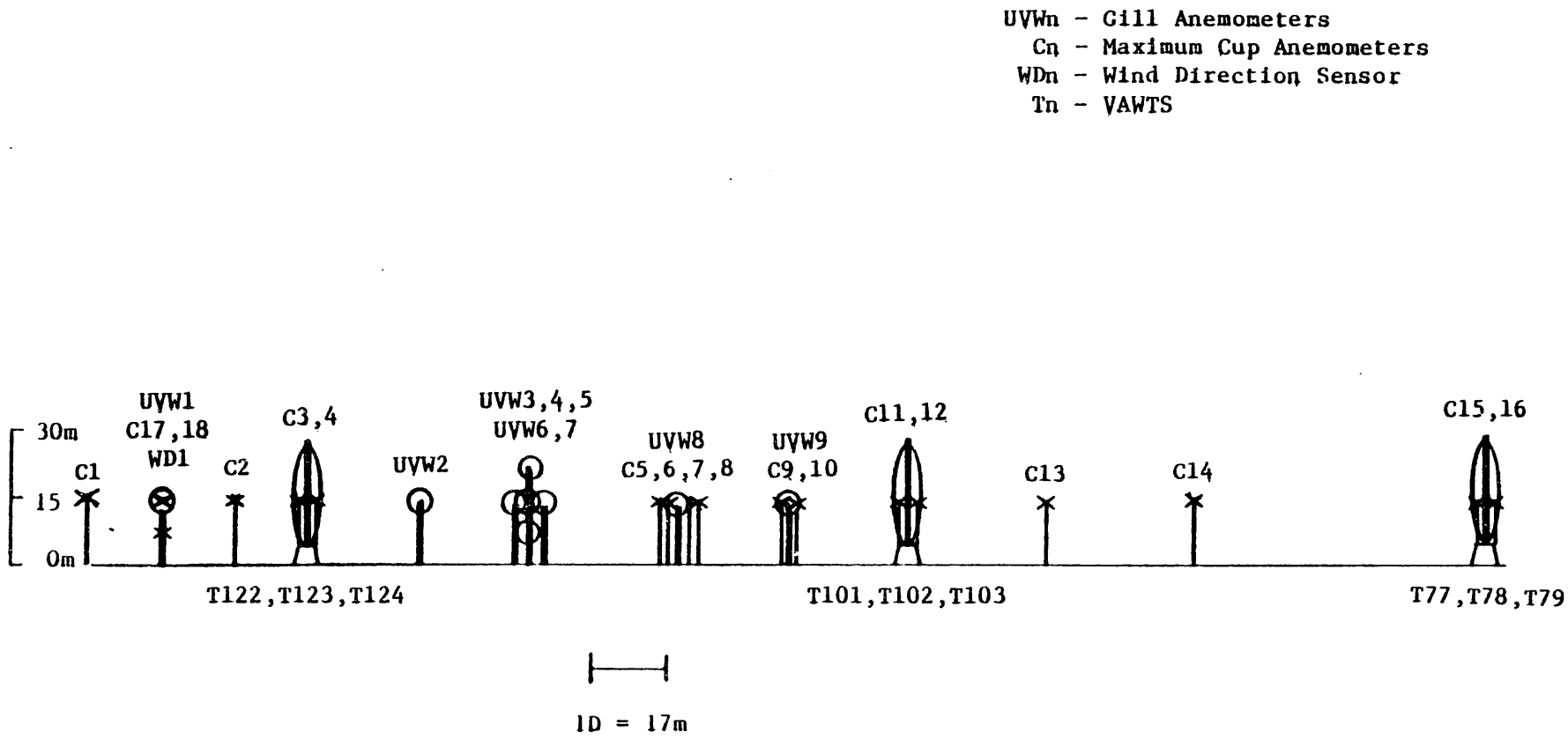

Figure 5. Side View of the Wind Sensor Layout Within the Turbine Array.

6.5D, 8D, 10D, 12D and 16D) to obtain both ambient wind and wake data. The two cup anemometers at 10D and 12D had to be shifted slightly off-axis to satisfy the safety distance of 1.5 times the tower height from a power line.

4.1.2 Test Matrix

The purpose of the field experiment was to determine the wake structure downwind of a VAWT in a windfarm array of identical turbines. To determine the site's ambient wind characteristics, we conducted a series of wind measurements with the turbines "turned off" within the wind speed range of interest. These results provided a reference for removing the "static" velocity deficit [with the upwind turbine(s) turned off] and the spatial variations of the wind field due to topographic influences.

The main thrust of the field experiment was to conduct both wind and turbine power measurements to determine the wake effects in terms of the velocity and power deficits. To assess the effects on the wake of the primary turbine in the presence of adjacent and upwind turbines, a systematic "on-off" scheme was designed and executed during the experiment.

Our strategy for a typical run was to start the wake measurements first with all the turbines on or off. After a sufficient length of steady-state data was recorded (at least 0.5 hour but preferably 1 hour), we would then start turning off or on individual turbines systematically while data continued to be recorded. Direct comparison of the above results during minimal changes in the ambient conditions would maximize our success in extracting the effects of adjacent and upwind turbines on the primary wake structure in the windfarm environment.

In reality, a steady wind speed and direction generally does not last for more than a few minutes, even in flat terrain. To account for the variability of the wind conditions, repeated runs of identical on/off patterns were conducted on different days during the field experiment. Data collected under identical wind conditions were binned to improve the statistical significance of the field results.

With the above considerations, we developed a test matrix, which was given in the final test plan (Liu, 1986a), to guide the field experiment and to document the successful completion of each of the test experiments. Our goal was to maximize the stratification of the wake data with the limited resources available to us. A revised test configuration was recommended by Dr. Peter Tu

of SERI, who was one of the members of the management team. Figure 6 illustrates the test configuration in terms of the on/off patterns of the turbines within the array. During the field experiment, we conducted most of these configurations, with a few exceptions and additions.

4.1.3 Sensor Calibration

Extensive calibration before and after the field experiment was made for various sensors. The Gill UVW anemometers were calibrated in a wind tunnel at PNL before shipment to the field. The Gill arms were first checked for bearing wear and refurbished as needed. After checking the mechanics of each Gill arm, they were individually calibrated in the PNL wind tunnel. The PNL wind tunnel is a recirculating type with a 7.6-m straight section and a 0.6 m x 7.0 m working section. Velocity profiles of the working section were measured using a Pitot tube to determine if there was wind tunnel wall interference that could affect the wind flow and, therefore, the calibration data. Only very minor differences were found, and these were determined to be insignificant.

The actual calibration procedure for each Gill arm was to insert the arm in the wind tunnel and install a generic propeller, which was used for all the arms to be consistent. The wind tunnel was then turned on and allowed to stabilize for 30 seconds. The speed in the wind tunnel was set by a potentiometer dial that was calibrated with a Pitot tube in the workng section of the tunnel. Once the tunnel speed was stabilized, data from the Gill arm were collected for one minute, and then the air flow was increased again and another one minute of data was collected. The three wind speed levels used in the tunnel were 4.5, 13.4 and 22.4 m/s (10, 30 and 50 mph). About 5 minutes of data was collected for each Gill arm, with a minimum of one minute of stabilized data for each wind speed level.

These data were recorded on a 9-track magnetic tape system to allow easy data transferral to FLOW's MC5600 for analysis. Average wind speeds for each Gill arm for each wind speed level were computed based on 30 seconds of data from the stabilized calibration data set. These averages were then used to compare and compensate for differences between each Gill arm used in the field experiment.

The Maximum cup anemometers were calibrated onsite by simultaneously mounting six to ten anemometers on a single test rig. The test rig consisted of a series of 3-m-high masts oriented in a row perpendicular to the wind

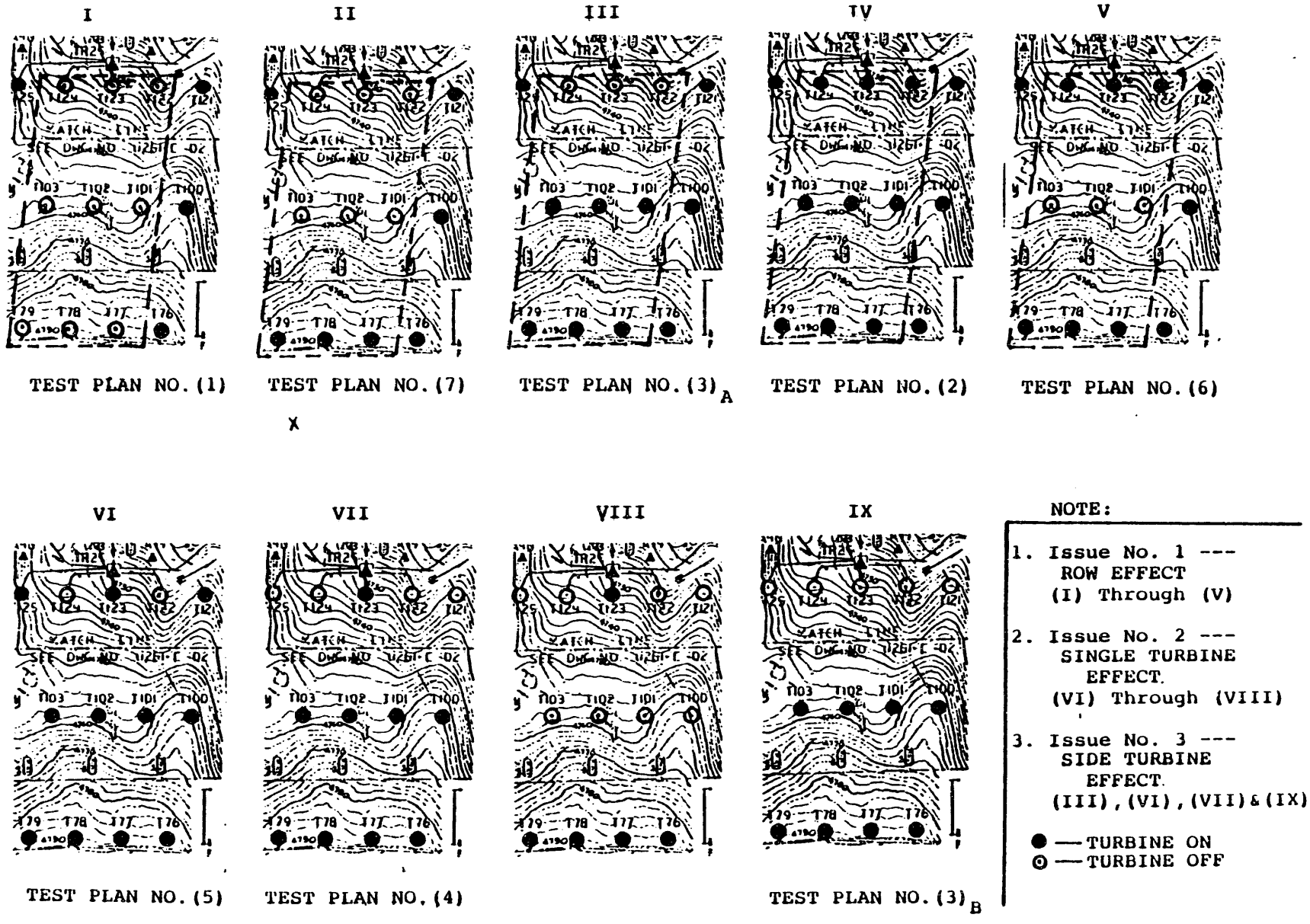

Figure 6. Test Configurations for the Field Experiment (Recommended by Dr. Peter Tu of SERI).

direction, each mast being approximately 1 m from its neighbor. The local terrain was selected to be reasonably regular, both downwind and crosswind.

The anemometers to be calibrated were monitored against a reference anemometer traceable to a National Bureau of Standards (NBS) calibration. Tthe data format was 7.5-minute averages. One of the Gill anemometers was mounted side-by-side with the cup anemometers during the pretest period. During pre-test calibration, each sensor was run for 5 hours or more, and during post-test calibration, each sensor was run for 50 hours or more.

During the field experiment, a cup anemometer (2017) and a Gill anemometer (UVW1) were mounted side-by-side at the reference tower (-2D upwind and at a height of 13.7 m). Comparison of the two outputs was available most of the time during the field experiment.

The power or watt transducers (Ohio Semitronics EW5-6B) were referenced to an NBS traceable EW5-6B watt transducer used for performance testing of FloWind's turbine T151. The transducers were installed in two groups (one being a group of four, and the other a group of five) in turbine T151 with their respective current transformers from the host turbines. They were connnected to an HP 1000 data acquisition system and monitored consecutively with the NBS traceable unit while the turbine operated in varying wind speeds and weather conditions. The data were sampled at a rate of 1 Hz and stored as a time series file. This was done for both groups of watt transducers.

To determine the accuracy of each of the transducers relative to the NBS traceable unit, the data were binned and then plotted as power of the NBS unit versus power of the wake machine unit. This resulted in a linear relationship for each of the transducers measured in the study. This was not a calibration (all transducers are factory calibrated and have a superior record of signal integrity) but rather a comparison to an NBS traceable transducer.

4.1.4 On-Site Preparation

On-site preparation included marking the locations of the towers according to the experimental setup, preparing the site for erecting the towers, receiving and shipping equipment to and from the site, installing and furnishing the research trailer, setting up the instrumentation and the data acquisition system, calibrating the instruments and other related work. The site preparation was conducted by the onsite FloWind O&M crews and several FloWind research engineers and meteorologists, with technical assistance by PNL personnel.

Site Survey

A site survey was conducted to mark the exact locations for the towers on the test site before their actual installation. During the survey, a safety check was made to ensure that a minimum distance of 1.5 times the tower height was kept between the towers to be installed and the turbines or power lines.

Installation of Towers and Sensors

Prior to the first test period, two PNL technicians visited the test site to erect the stack-up towers and to mount and align the Gill anemometers and the wind direction sensor. Each anemometer was carefully checked electronically before mounting to screen out units damaged during shipping. Signal cables of individual anemometers were brought to the research trailer and connected to the data acquisition system. During the first test period, we observed several towers undergoing a twisting motion in the wind, especially the tall tower at 3D. Stablizers were subsequently added on the tops of these towers to suppress the twisting motion. The portable towers and cup anemometers/data loggers were installed by FloWind meteorologists and O&M crews. Power transducers were installed on the nine turbines by FloWind research engineers.

4.2 Execution of Field Experiment

4.2.1 Test Schedule

From the review of the historical wind data, we found that the wind conditions became less favorable after July (except in 1985). We decided to carry out the field experiment during the May and June time frame. The field experiment was divided into two periods, the first period was conducted during April 28 through May 10, 1986. This period was dedicated to testing and checking the instruments and equipment and conducting preliminary measurements for evaluating the performance of various aspects of the field setup. In addition, we conducted measrurements of the ambient wind field (with all turbines turned off) to establish the reference conditions for the wake measurements to be conducted in the second test period. The objectives of the first test period were successfully achieved. A review meeting of the preliminary data was held on June 2 at FLOW's Headquarters in Kent, Washington. Several recommendations from the management team were considered and subsequently implemented into the test plan.

Originally, we had scheduled the second test period to commence in mid-June. During the first test period, however, it was discovered that a number of F-17s in the test array had developed cracks on the inserts that bolted the blades together. A remedy was implemented by reinforcing the joints with a thin doubler. The installation of the doublers on the turbines in question was completed by mid-July. We conducted the second test period from July 15 through August 9, 1986. All systems worked well until about two weeks into the test, when the HP computer system developed an intermittent problem probably due to overheating of one of the electronic components. After July 30, only limited velocity measurements with the Gill UVW anemometers were made. However, velocity measurements with the cup anemometers and power measurements continued until the end of the test period. The HP-computer-based data acquisition system was removed from the site on August 2. The CR21X was rewired and reprogrammed to add in the U and W components of the UVW1 Gill anemometer and the wind vane anemometer output.

4.2.2 Test Procedure

The normal procedure was to arrive at the test site in the morning, at which time the wind was often below the cut-in speed of 5.4 m/s. We then had a few hours to transfer data recorded on the HP hard disks to cassette tapes, to review the data, to document preliminary results, and to plan and prepare for the test series to be conducted that day. Preparation included setting up the data acquisition system and data loggers for measuring the wind field and the turbine power, checking the conditions of the turbines, instruments and equipment and other related tasks.

Cup Anemometer Measurements

The Windwatch 3 squirrel on which the cup data were recorded had a 12-day capacity when configured for 7.5-minute averages. To synchronize with the other data systems, we adopted a special initialization procedure. Normally, we had two to three operators working simultaneously to replace the squirrels in the recorder with blanks. We started the process on the hour and replaced one squirrel every 7.5 minutes. It took exactly one hour to replace all 18 stations with two operators working together. Appropriate information in terms of in/out time (PST) and station numbers (2001 through 2018) was recorded on each squirrel. Wind data recorded on the squirrels were retrieved with the

squirrel reader. The reader transferred the squirrel data onto a floppy disk in the Compaq computer via the RS232 port. The raw data were then converted into physical units by running a program (SQFL075) provided by Atmospheric Research & Technology. The squirrels were then cleaned magnetically for reuse. The 7.5-minute data in engineering units were readily imported into the LOTUS 123 spreadsheet for further analysis.

Turbine Power Measurements

The turbine power from the power transducer was recorded with the CR21X data loggers. One CR21X was used to record the power of all three turbines on the same row. The internal clock of each CR21X was synchronized with that of the HP-9826. The CR21X was run on six D-size batteries; it was essential that the voltage of the batteries was not lower than 9.5 volts. Instructions were input into the microprocessor to set up the data logger for a variety of sampling conditions. Typically, we used sampling/averaging rates of 0.1 s/10 s. Slower or faster sampling/averaging rates could be implemented readily by simply modifying the instructions via the input key pad on the top of the CR21X. In addition, calibration coefficients were included in the instructions so that the recorded data were in engineering units. To protect the CR21X from weathering and dirt, we enclosed the data logger inside a polystyrene cooler.

Under normal practice, we retrieved and reloaded the cassette tapes every morning. Meanwhile, we checked the battery voltage and reset the time to that of the internal clock of the HP-9826. Appropriate information in terms of the row number and in/out date and time was written on each tape. The data on the cassette tape were retrieved and transferred to the Compaq computer via a C-20 cassette interface by Campbell Scientific. The data were readily imported to the LOTUS sheet for further analysis.

Gill Anemometer Measurements

The HP computer-based system was used to record the signals of the Gill propeller anemometers and the wind direction sensor. There were a total of 27 input channels for the nine Gill anemometers, one channel for each of the three components and one channel for the wind direction sensor. A total of 34 channels were used for connections to the HP-9826. These were dedicated as follows: the power output from T123 (channel 1); the signal from the wind direction

sensor (channels 2 and 3); the crosswind components (channels 5 through 14); the downwind components (channels 15 through 24); and the vertical components (channels 25 through 34). Duplicate or dummy channels were also used to ensure sufficient signal isolation whenever a change in sensor type took place.

Manually driven data acquisition programs were installed in the computer for setting up runs of various sampling conditions. A regular run referred to that with a sampling rate of 1 Hz. Once the run parameters in terms of channel number, starting time/date and duration were entered, the computer checked for available storage space, and data sampling began. During sampling, the computer printed out 10- or 7.5-minute averages of the voltage signals for the U and V components for a record. Such records were reviewed periodically by the operators to detect potential problems with the data acquisiton system and the sensors. For sampling rates other than 1 Hz (up to 8 Hz), a different program had to be recalled for setting up the runs. No 10-minute averages were printed out in this case.

The data were temporarily stored on the hard disk, which has the capacity (20 megabytes) of storing several 12-hour runs with a sampling rate of 1 Hz. Programs were developed to calculate the mean wind speed, direction and velocity deficit from the raw data for onsite inspection of the field results. No corrections for the cosine law, however, were included in these programs. The results could be plotted with the printer to aid in the inspection.

4.2.3 Turbine Operation

During the field experiments, individual turbines were turned on and off according to the test matrix. On/off switches for a group of five turbines were located at a nearby control panel. Once familiarized with the system, the field test personnel were permitted to perform these maneuvers. In the absence of test personnel, the O&M operator on duty assisted in turning on and off the turbines according to a schedule prepared in advance. The status of the turbines in terms of the on/off time, accumulated electricity production and number of stops was recorded during each on/off operation.

4.2.4 Data Reduction

To convert the raw data to physical results with proper engineering units, we first applied the calibration coefficients and then included corrections resulting from limitations of the sensor performance. Other corrections due

to external factors, such as terrain effects, were also made according to the findings derived from the ambient wind field (Section 5.1).

For the Gill anemometer data, the maximum errors estimated from the wind tunnel calibration were less than 2.2% for wind speeds greater than 4.5 m/s (Section 4.1.3). Therefore, no corrections were made to the Gill anemometer data. As pointed out by the manufacturer (R. M. Young Company), the propeller has a slight deviation from the cosine response. Corrections were made according to the values recommended by the manufacturer. The wind speed and direction were then calculated after the above corrections were made to the raw data.

Post-calibration of the cup anemometers showed less than 2 to 3% deviations in individual sensors from the reference sensor (2017) for wind speeds greater than 4.5 m/s. However, it is well known that the cup anemometers tend to overspeed in the presence of an upward velocity component and turbulence (MacCready, 1966). Due to the upslope terrain features at the test site, the Gill anemometers measured an upward velocity component that was about 10 to 15% of the wind speed. In addition, we anticipated that the approaching wind was reasonably turbulent, even though an internal boundary layer developed as the wind passed the plateau on the top of Cameron Ridge. Figure 7 shows a comparison of the wind speed measured with a Gill anemometer (UVW1) and a cup anemometer (2017), both mounted at the same level on the upwind reference tower, for the period form May 5 to 9, 1986. The wind speed for all wind directions was binned in 1 m/s increments. The solid line represents a third-degree polynomial best-fit curve for speeds greater than 3.5 m/s. Corrections were applied to all cup data according to the best-fit curve. Figure 8 replots the same results of Figure 7 in terms of the ratio of the wind speed measured with the Gill anemometer to that with the cup anemometer. The data were the 7.5-minute averages without binning. It is evident that the correction factor is wind-speed dependent. At wind speeds below 6 m/s, the relatively high friction of the cup anemometer results in a ratio greater than one, as anticipated. For speeds exceeding 6 m/s, the effects of the upward velocity component and turbulence become increasingly important. Finally, the ratio levels off around 0.97 for speeds greater than 15 m/s.

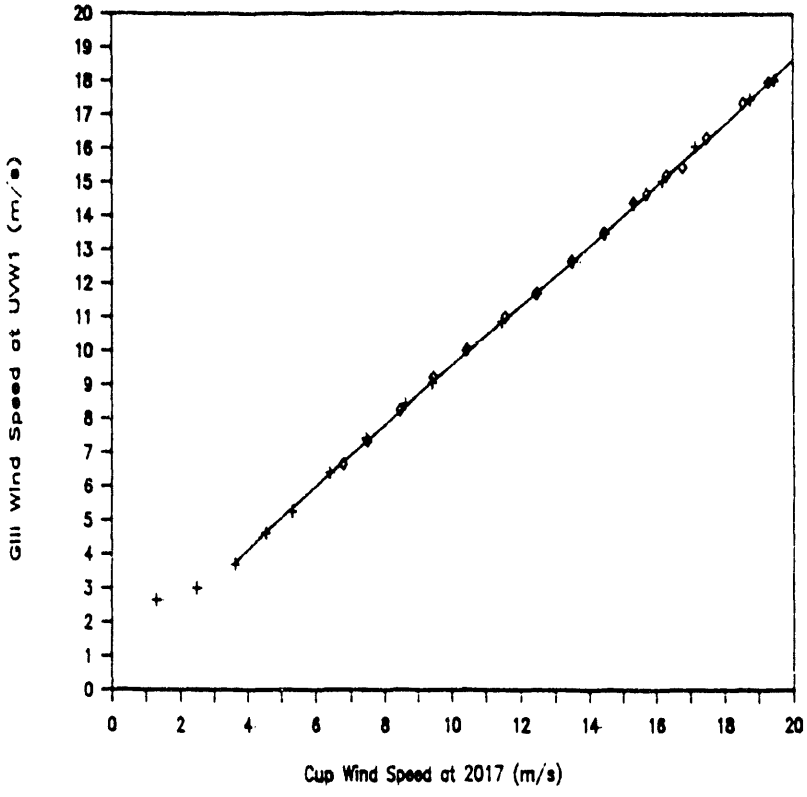

Figure 7. Comparison of Wind Speeds Measured with a Gill Anemometer (UVW1) and a Maximum Cup Anemometer (2017) Mounted on the Reference Tower.

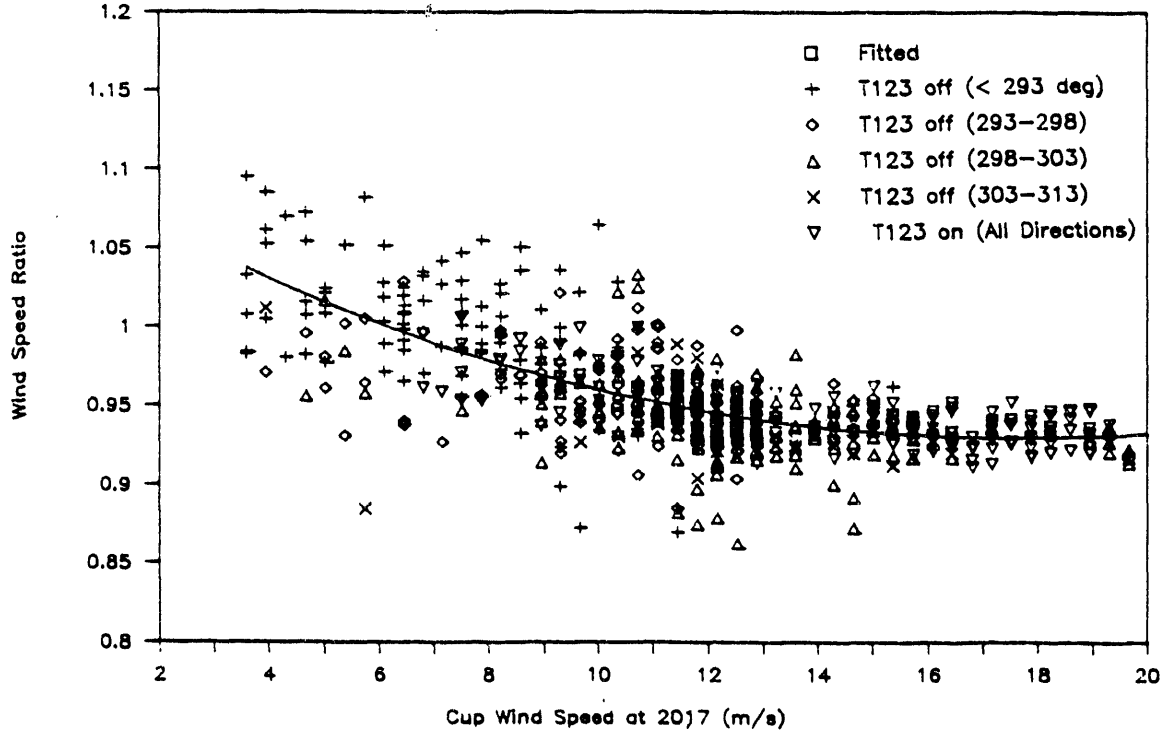

Figure 8. Ratio of Wind Speeds Measured with a Gill Anemometer and a Maximum Cup Anemometer as a Function of the Wind Speed.

5. RESULTS OF FIELD EXPERIMENT

5.1 Ambient Wind Field

As discussed in Section 2.1, the wind field during the primary season from April to August at Cameron Ridge is basically thermally driven. Figure 9 shows typical wind speed time series for August 4 (pluses) and 6 (triangles), with the former and latter representing, respectively, the wind patterns in the presence and absence of a weak high-pressure system east of the mountains. In the absence of such a system, the wind speed generally displays two troughs at about 6:00 and 11:00. The first trough occurred just before sunrise, when the temperature gradient on the two side of the mountains is at a minimum. The "hump" between the two troughs was believed due to local effects, whose nature is not known at present. Often, the wind speed inbetween the two troughs was quite low, not much higher than the cut-in speed. As the desert temperature rose and the temperature difference on the two sides of the mountains increased, the wind speed picked up in early afternoon and reached a maximum just before sunset. It is interesting to note that there was often a small "dip" in the wind speed right after sunset. The wind speed generally remained reasonably high well after midnight. In the presence of a high-pressure system off the Pacific coast, the wind blew all day long with speeds exceeding that of the cut-in value. The thermal effects were traceable but became secondary, as demonstrated by the pluses.

The corresponding wind direction time series are shown in Figure 10. In general, the wind direction correlated well with the wind speed with few exceptions. For example, the second trough in the wind direction was not as pronounced as that in the wind speed, and there appeared to be a phase reversal at 20:00.

Figures 11 and 12 show the histograms of the wind speed and direction for the period from August 3 through 7, with the wind speed exceeding the cut-in value for the 7.5-minute averages. It is clear that the wind speed distribution is quite scattered. The frequency of occurrence was between 7 and 12% and 3.5 and 6% for wind speeds between 10 and 13 m/s and, outside that window, between 6 and 15 m/s. The wind direction distribution displayed a single peak at 300.7 deg, with a 22% frequency of occurrence.

Next, we examine the terrain effects on the ambient wind field. Although the terrain features at which the selected turbine array was located were relatively regular in comparison with other locations at Cameron Ridge, there

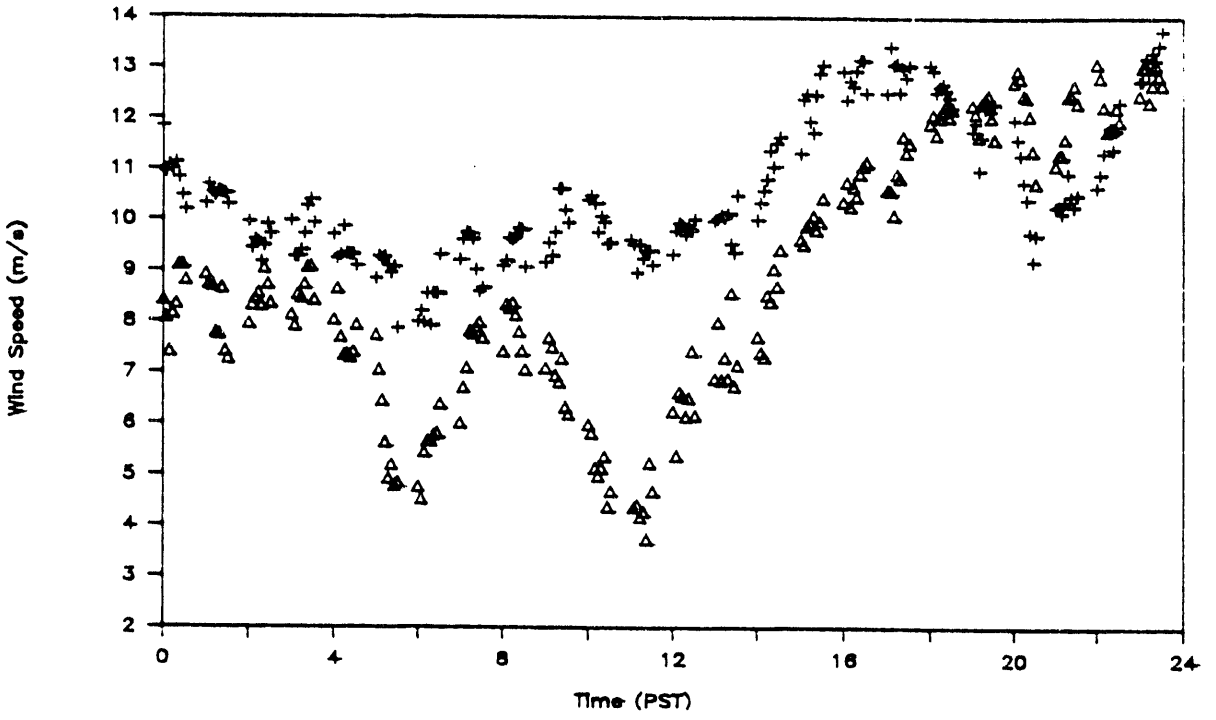

Figure 9. Typical Time Series of 7.5-Minute-Averaged Wind Speeds.

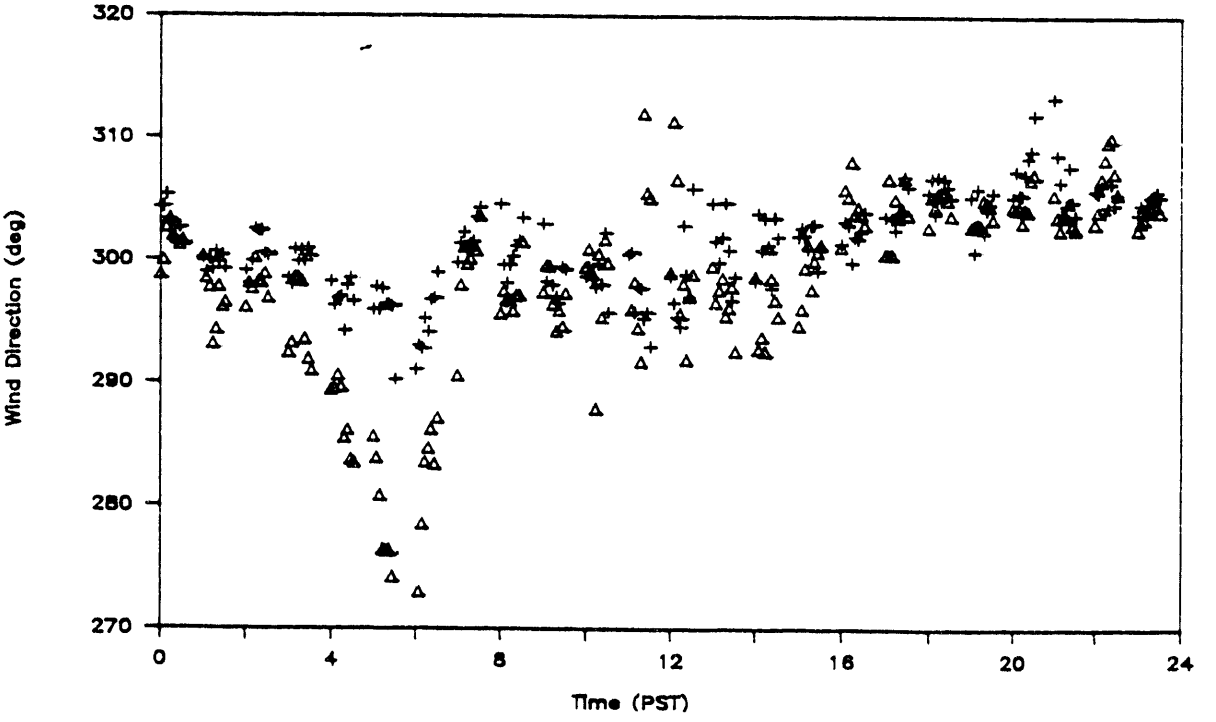

Figure 10. Typical Time Series of 7.5-Minute-Averaged Wind Directions.

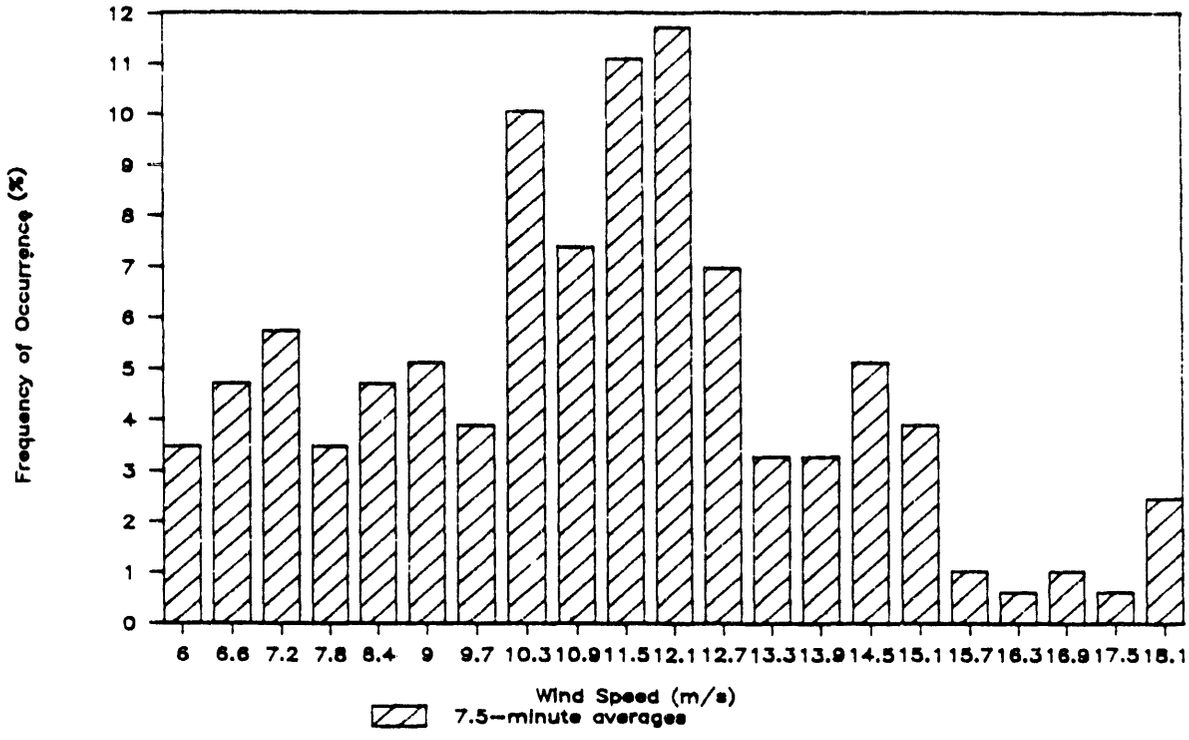

Figure 11. Histogram of the Wind Speed from August 3 through August 7, 1986.

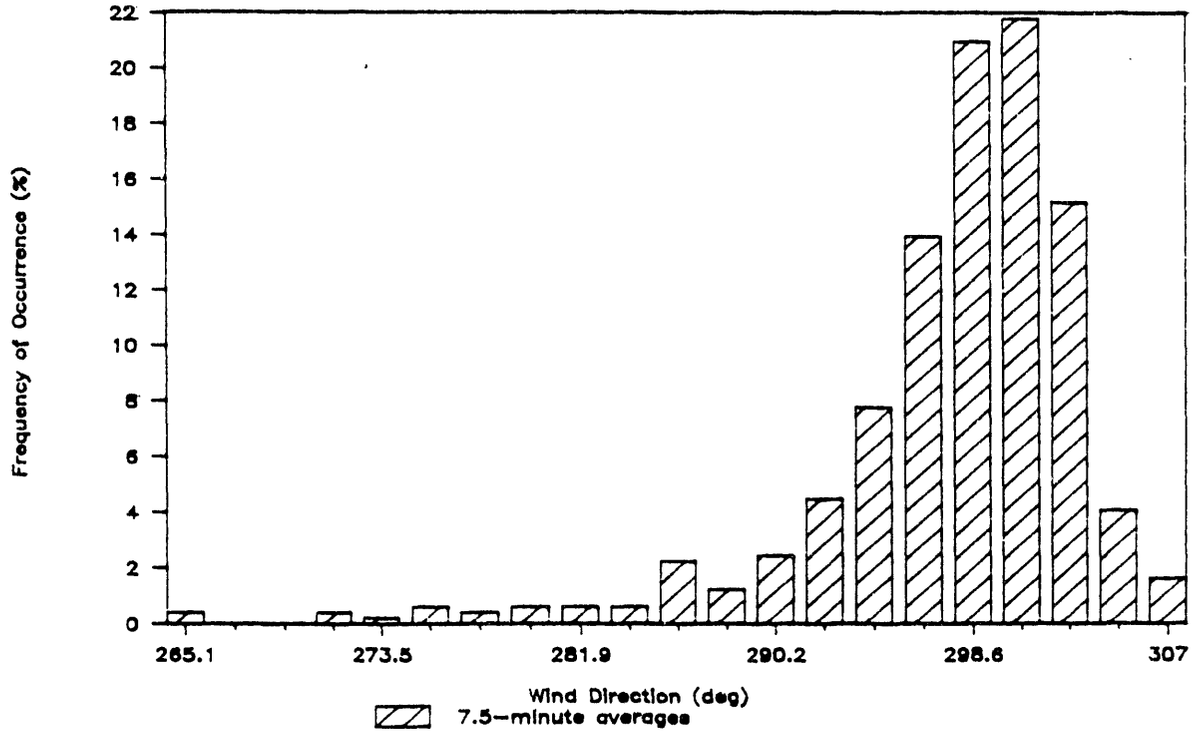

Figure 12. Histogram of the Wind Direction from August 3 through August 7, 1986.

was a general upslope trend toward the downwind direction together with local variations in the slope (see Figure 4b). Figure 13 shows the 5-day-averaged wind speed measured with cup anemometers at 16 stations for the period between May 5 and 9, during which all turbines were turned off. We observed a low-speed zone at the vicinity of row 2 (stations 2011 and 2012) with a speed ratio (with respect to that of the upwind anemometer at station 2017) of 0.93 to 0.9. Careful examination indicates that the speed ratio is wind speed dependent, as shown in Figure 14 in which the ratios of three stations (2010 through 2012) are plotted. The line represents an 8-degree polynomial fit of the data. Corrections were subsequently made using the cup data to determine the power curve and deficit. The above observation depends intimately on the recovering process of a developing boundary layer, which will be discussed below.

Figure 15 shows the vertical profiles of the mean wind speed measured at three levels above the ground, 6.1, 13.7 and 21.3 m (enclosed by solid curves). Only the data within the wind direction range from 298 to 308 deg are presented. The wind speed data were binned for a 2-m/s increment (with reference to the wind speed measured at the upwind stack-up tower). The abscissa and ordinate are, respectively, the wind speed ratio (with respect to the speed measured at 21.3 m) and the vertical distance in meters from the ground. A general trend of decreasing vertical shear with the increase in the wind speed is established, indicating that the boundary layer flow becomes more turbulent as the wind speed increases. The boundary layer thickness appears to reduce as the wind speed increases.

As the air flow rises from the valley floor and reaches the ridge top, we anticipate an overspeed zone near the leading edge of the ridge. For flow over a bluff, a recirculating and low-speed zone may even exist at the leading edge, as demonstrated by Walker and Wade (1987). In this case, the upwind terrain slope is not extremely steep as compared to that of a bluff. We did not experience any flow reversal at any part of the upslope region upwind of the turbine/tower array. To demonstrate the evolution of the recovery process in the developing boundary layer, we present in Figure 15 the vertical profiles measured at the reference tower at the 13.7- and 6.1-m levels (dashed curves). For comparison with the profiles measured at $x = 3D$, we made an assumption that the averaged speed ratio of the wind speed at 13.7 and 21.3 m was 0.99 due to lack of measurements at the highest level at -2D. It is evident that the vertical shear below $z = 13.7$ m at $x = -2D$ is markedly weaker than that at

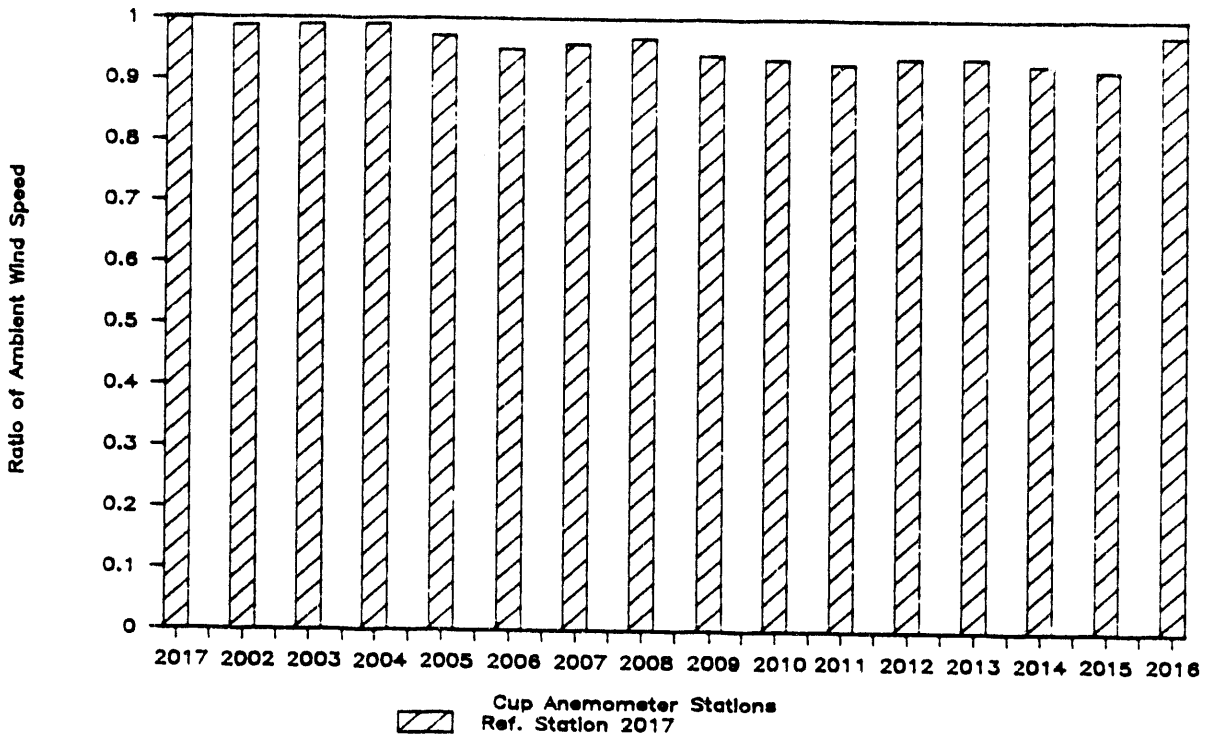

Figure 13. Ratio of Ambient Wind Speeds at Cup Anemometer Stations. The wind data are 5-day averages beginning May 9, 1986.

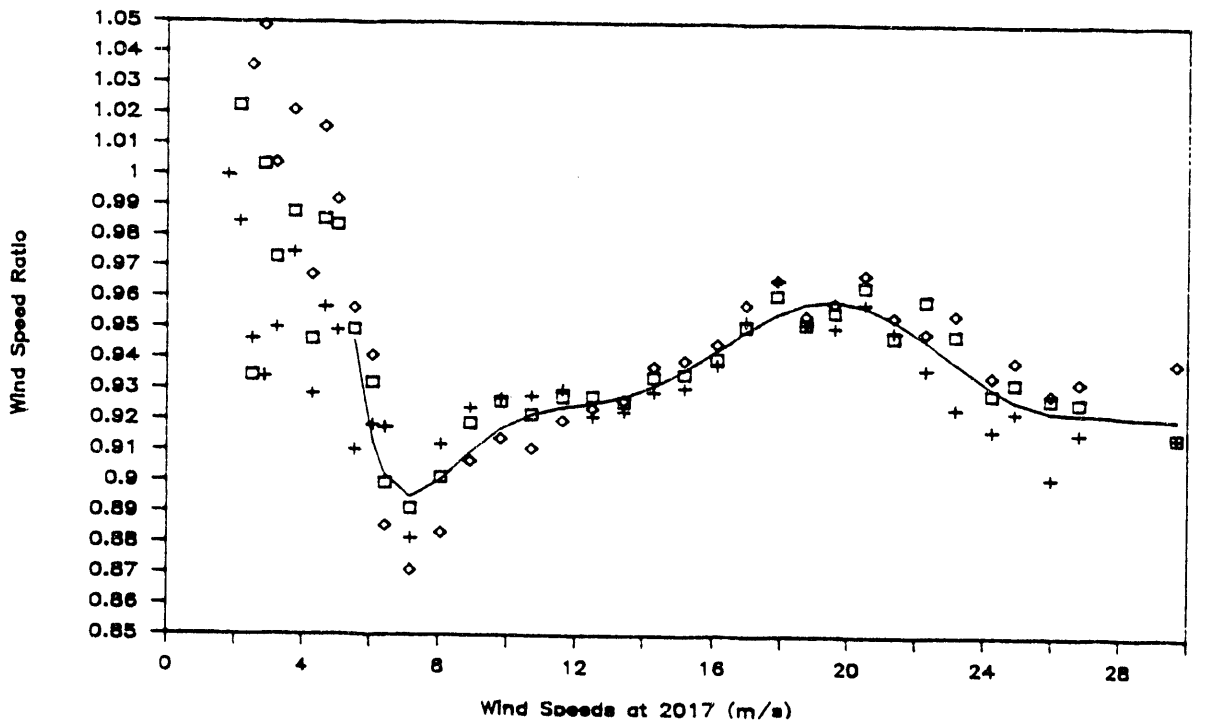

Figure 14. Ratio of Ambient Wind Speeds as a Function of the Wind Speed at Stations in the Vicinity of the Second Row of Turbines.

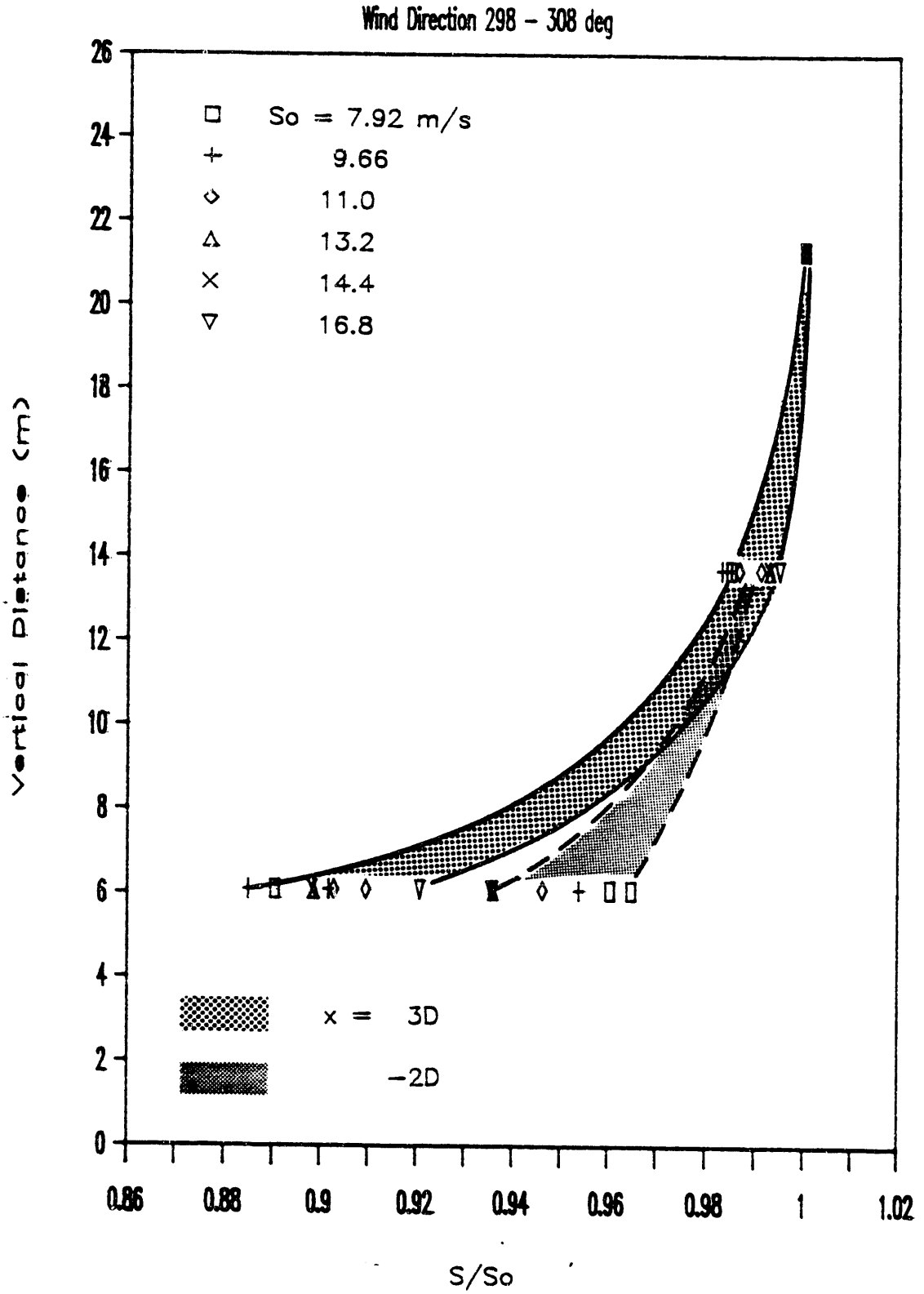

Figure 15. Vertical Profiles of the Wind Speed Measured at x = -2D and 3D. The presence of a strong wind shear in the developing boundary layer is evident.

x = 3D, which is typical of a developing boundary layer. Careful examination of the shear profiles reveals that the shear increases with increasing wind speed at x = -2D, whereas the trend reverses at x = 3D. Consequently, the difference in the shear between the two locations decreases with increasing wind speed, indicating the recovery requires a shorter fetch to complete when the wind speed increases. The above observation is physically consistent in that the intensity of terrain-generated turbulence increases with the wind speed, which helps hasten the recovery of a developing boundary layer. We anticipate that the characteristics of the boundary layer profiles would have some impact on the performance of the turbines.

5.2 Velocity Deficit

The velocity deficit was estimated based on the following equation

$$V_d = (S_o - S_{x/D})/S_o - (V_d)_o \qquad (1)$$

where $(V_d)_o$ is the background velocity deficit measured with the upwind turbines turned off and S is the wind speed. To establish the velocity deficit in the wakes of a single turbine and of the turbines in the upwind row, we first measured the ambient wind at all the stations with all the turbines turned off. These measurements enabled us to estimate the background velocity deficit. Subsequently, we applied the above equation to derive the velocity deficit for various turbine configurations as illustrated in the test matrix.

5.2.1 Background Velocity Deficit

Figure 16 displays the 7.5-minute averaged background velocity deficit at x = 1.5D (UVW2), 3D (UVW4), 5D (UVW8), 6.5D (UVW9), and 8D (2012). The background velocity deficit is created in the presence of the wake of the stationary turbine and modified by the local terrain features. The deficit depends on the orientation of the turbine blades, with a maximum value when the two blades are aligned with the wind and with the downwind anemometer. This correlation was clearly observed from the wind data measured at 1.5D. At such a close distance, the orientation changes not only the drag force but also the effective distance between the turbine and the anemometer (a maximum of 0.5D difference). Subsequently, we made an effort to orient the blades perpendicular to the wind direction whenever the turbine was turned off.

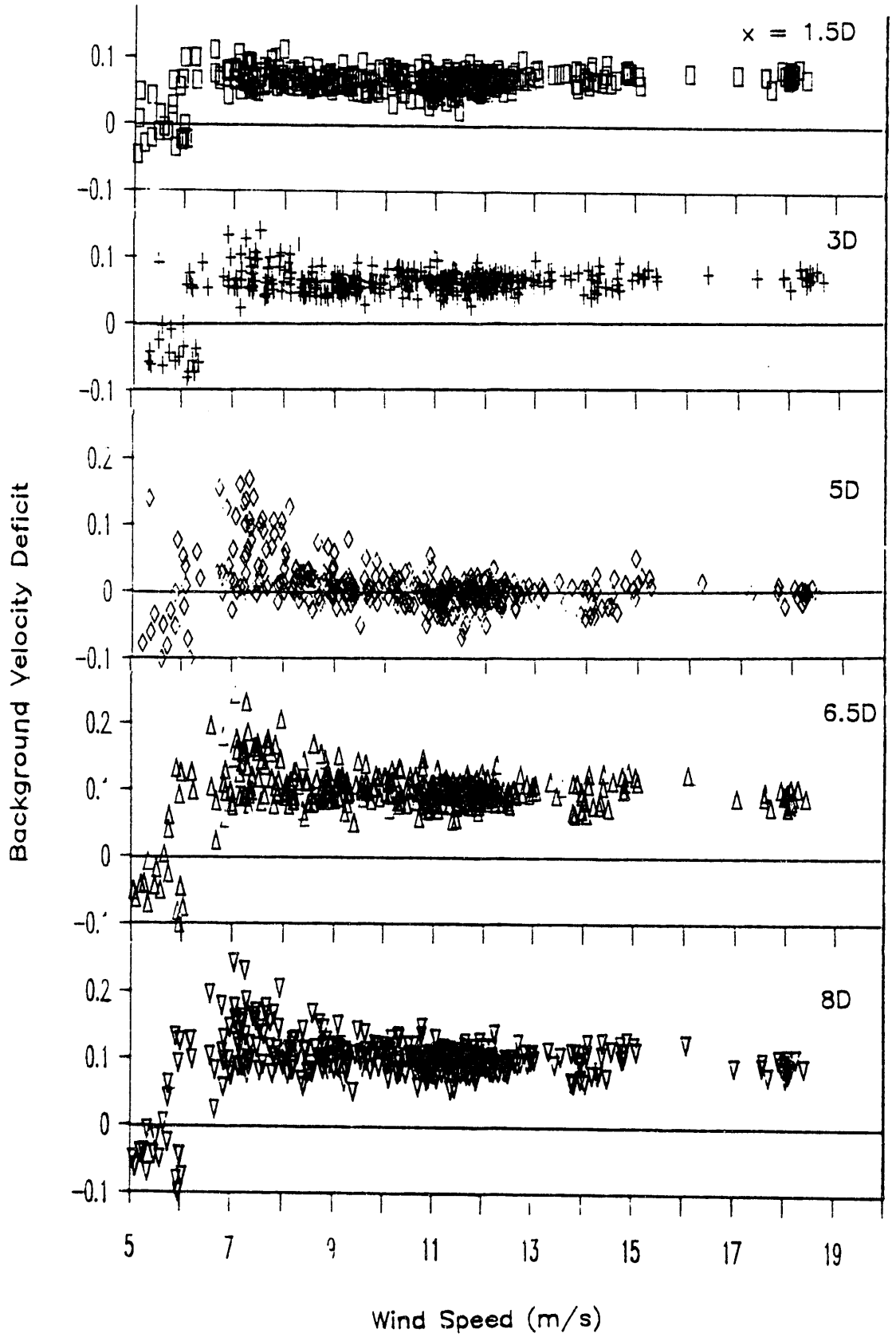

Figure 16. Background Velocity Deficits Measured at x = 1.5D, 3D, 5D, 6.5D, and 8D. The trend of the data changes at wind speeds below 7 m/s.

Figure 17 shows an example of the background velocity deficit (x = 3D) binned into several wind direction ranges. The data were sorted into 2-m/s speed intervals and binned into 5-deg wind direction increments within each wind speed interval. As shown in Figure 17, the scatter in each symbol group respresents the variations due to differences in the wind direction. It is clearly demonstrated that the background velocity deficit is essentially wind-speed dependent. The solid curves are the polynomial fits through the data points. The best-fit values were used in the above equation for removal of the background velocit deficit from the data.

There is a significant change in the trend of the background velocity deficit for speeds below 7 m/s, as shown in Figures 16 and 17. Apparently, the ambient flow tends to be strongly affected by the local terrain features at low wind speeds. For wind speeds below 7 m/s, the turbines often operated in a transition state between the modes of generating and motoring, especially when the wind field was highly fluctuating. The velocity and power deficits measured within this low-wind-speed regime do not generally represent the actual values due to the mode-switching situation. Interpretation of the results measured in this wind regime should be made with discretion.

5.2.2 On-Axis Velocity Deficit

Next, we examine the effects of wind speed and wind direction on the velocity deficit derived from wind data measured at stations along the major axis of the turbine and tower array (308 deg). The effects of the turbines adjacent to the primary turbine (T123) are also assesed. Figures 18 through 22 illustrate the velocity deficit measured at 1.5D (UVW2), 3D (UVW4), 5D (UVW8), 6.5D (UVW9) and 8D (2011) when T123 was on and its adjacent turbines were off. The cup anemometer at Station 2011 was 1D off the 308-deg orientation, which resulted in an orientation 7.1 deg off the major axis (see Figure 4). The abscissa and ordinate are, respectively, the velocity deficit and wind speed. Except for x = 8D, the velocity deficits for all speeds reach their maximum values for wind direction between 298 and 303 deg, which is about 5 deg below the direction of the major axis of the turbine and tower array. The velocity deficits for wind directions between 303 and 308 deg were only slightly below those between 298 and 303 deg, with the former occurring much less frequently than the latter. A 5-deg offset is, however, within the accuracy allowed in aligning the Gill and/or vane anemometer. The 7.1-deg offset

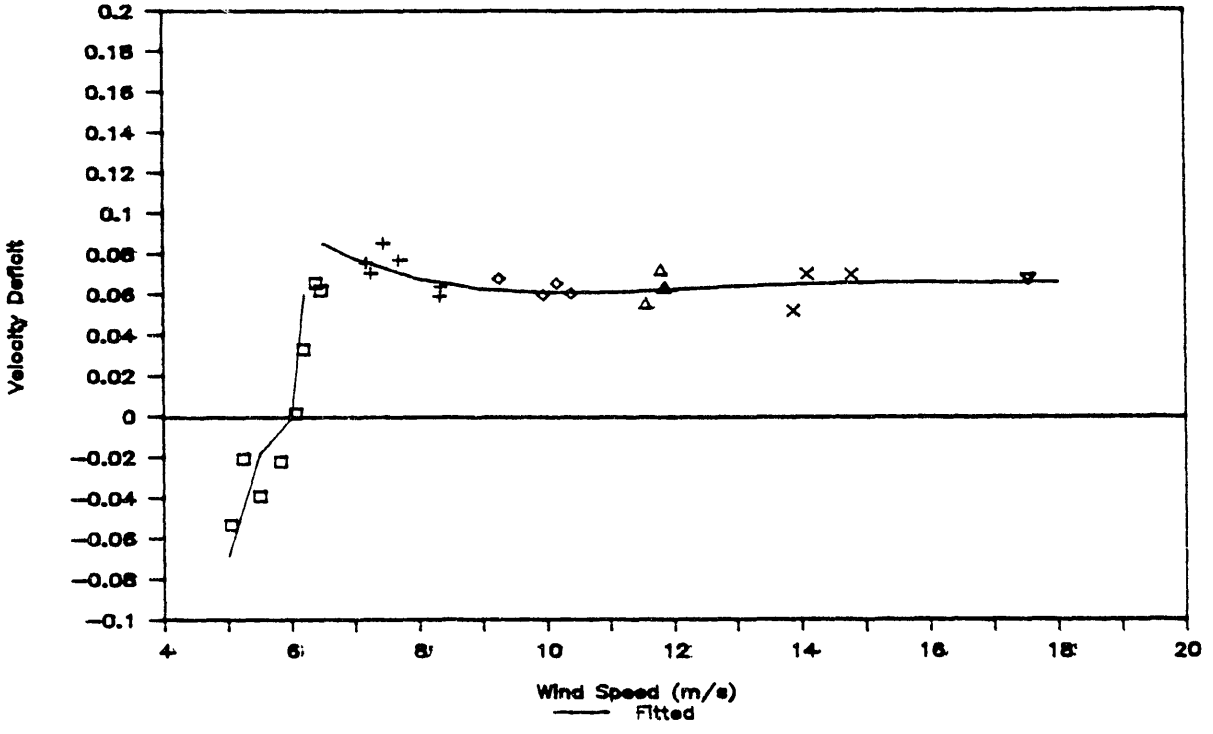

Figure 17. Background Velocity Deficits Binned in 5-deg Increments at x = 3D. The solid curves are polynomial best fits of the data.

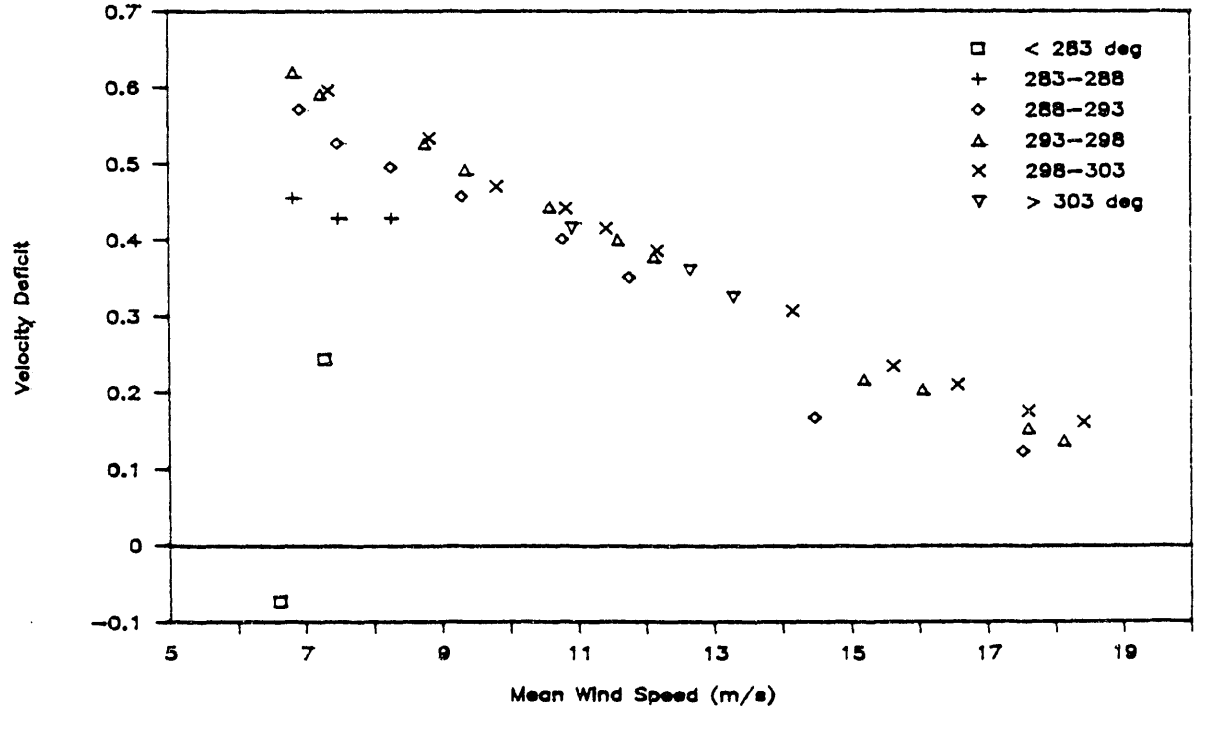

Figure 18. Velocity Deficit Measured at z = 13.7 m and x = 1.5D (UVW2) on Major Axis of Turbine Array when T123 Was On. The data were sorted into 5-deg intervals and binned over 1-m/s increments.

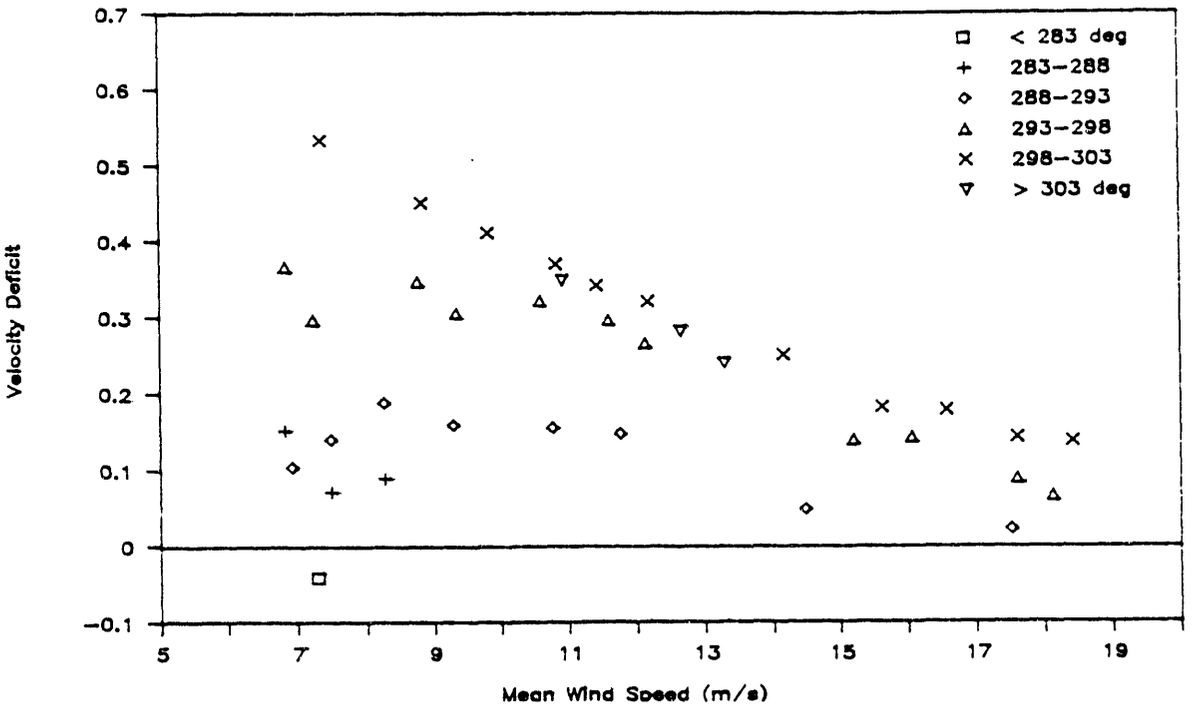

Figure 19. Velocity Deficit Measured at z = 13.7 m and x = 3D (UVW4) on Major Axis of Turbine Array when T123 Was On.

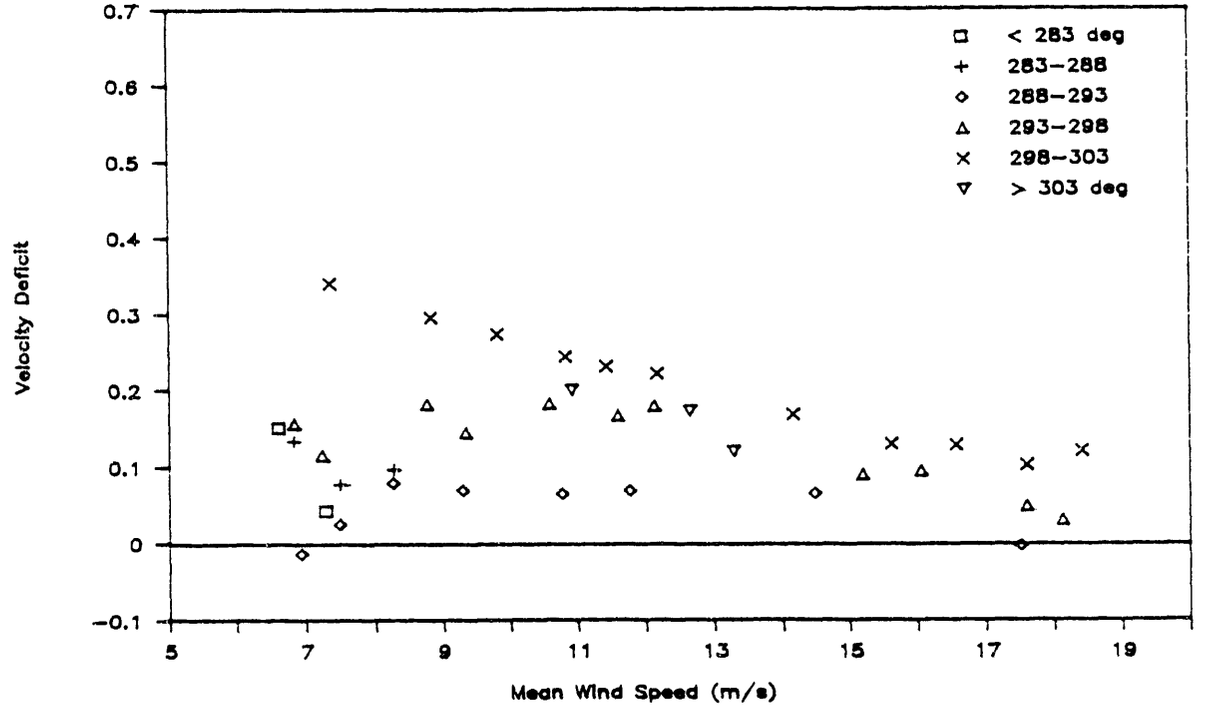

Figure 20. Velocity Deficit Measured at z = 13.7 m and x = 5D (UVW8) on Major Axis of Turbine Array when T123 Was On.

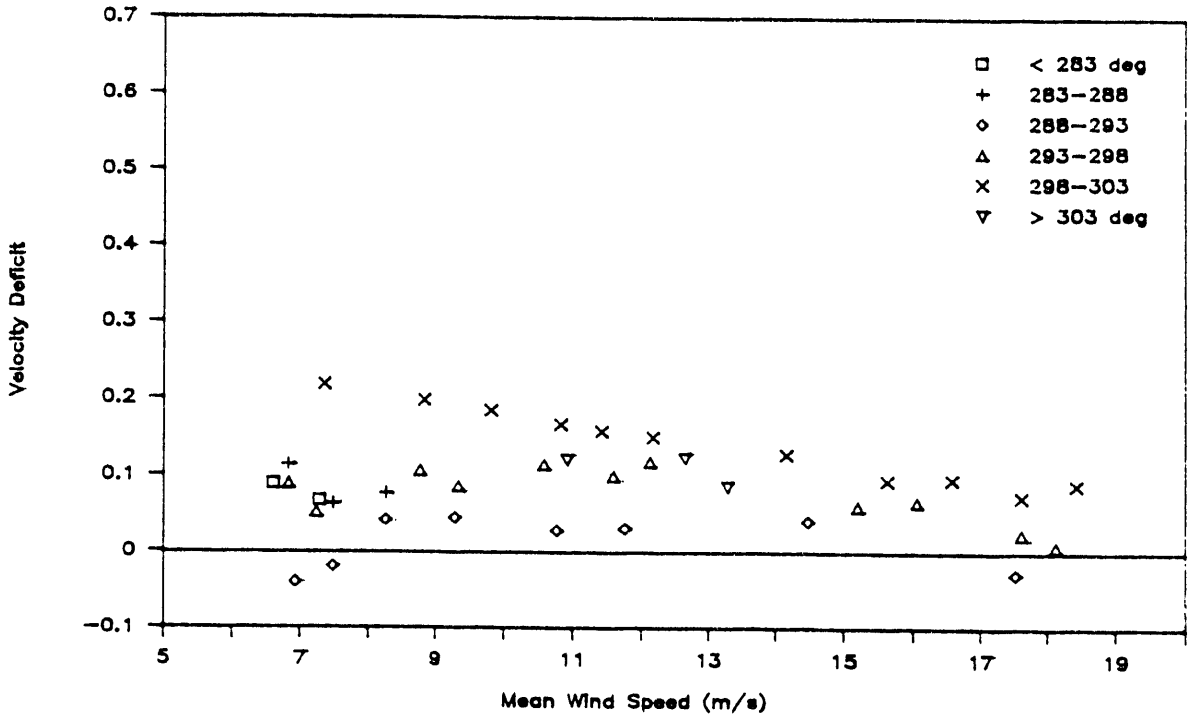

Figure 21. Velocity Deficit Measured at z = 13.7 m and x = 6.5D (UVW9) on Major Axis of Turbine Array when T123 Was On.

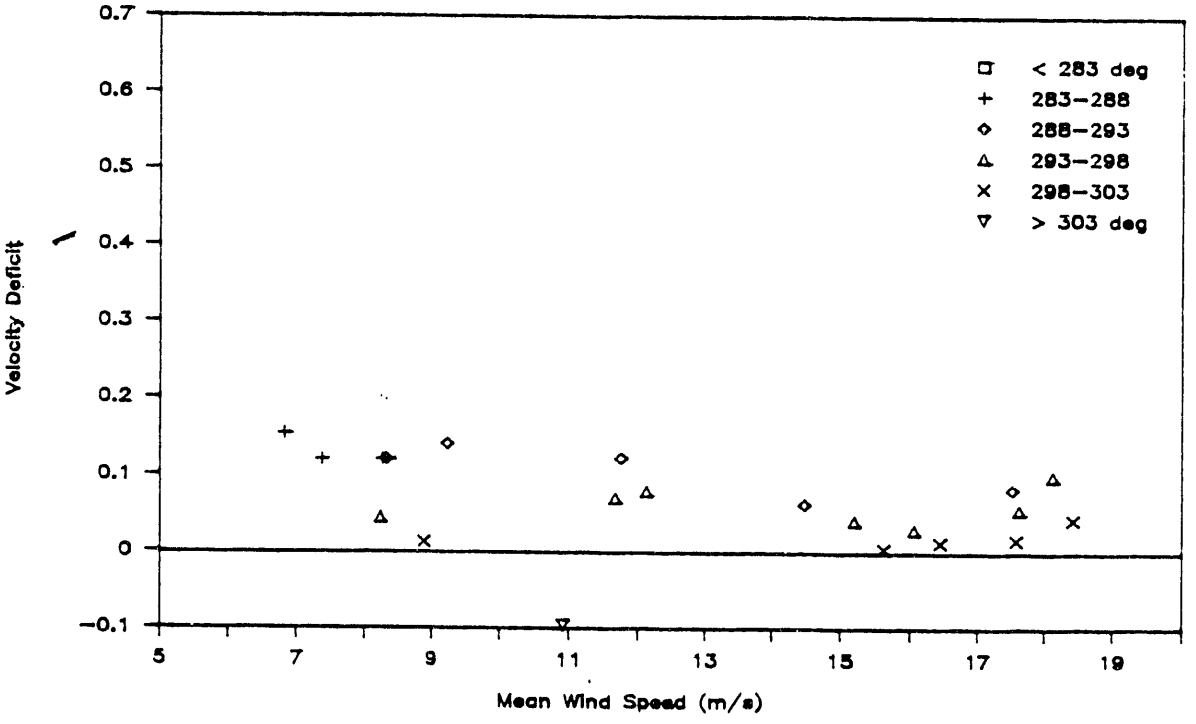

Figure 22. Velocity Deficit Measured at z = 13.7 m and x = 8D (2011) +7.1 deg Off Major Axis of Turbine Array when T123 Was On.

in the location of the cup anemometer at 8D (2011) causes a shift in the wind direction range in which the maximum deficit occurs. In addition, the maximum velocity deficit shifts to a higher wind direction range with increasing wind speed. However, the relatively large data scatter at 8D might have smeared the data trend to a degree. As the wind direction deviates more than 10 deg from 308 deg (or 301 deg for 2011), the velocity deficit as a function of wind speed differs significantly from that within 10 deg from 308 deg.

The maximum velocity deficit tends to decrease with increasing wind speed:

$$V_d \sim S^{-n} \tag{2}$$

where n equals unity for low speeds and decreases with increasing speed. Extrapolation of the data indicates that the maximum velocity deficit decreases asymptotically to zero as the wind speed increases. To establish the dependence of the maximum deficit on the wind speed and downwind distance, we present in Figure 23 a summary of the maximum deficit for the five downwind locations.

Figures 24 and 25 illustrate the velocity deficits measured at the levels z = 6.1 and 21.3 m. Note that the velocity deficits at z = 6.1 m are significantly lower than those at z = 13.7 and 21.3 m, which differ only slightly. As shown in Figure 15, there is a strong shear below the equator height. We anticipated that the turbulence intensity would be higher below the equator height than above. Evidently, the relatively high turbulence near the ground increases mixing and entrainment in the wake, which in turn reduces the velocity deficit inside the wake. In Figure 26, we compare the maximum deficit at the three levels for all the wind speed regimes encountered. The gradient of the deficit above z = 13.7 m is considerably lower than that below that level.

To investigate the effects of the adjacent turbines (T122 and T124) by the primary VAWT (T123), we present in Figures 27 through 31 the velocity deficits with all three upwind turbines on, corresponding to those shown in Figures 18 through 22 with only T123 on. Comparison of these two sets of figures depicts one noticeable difference. Except for x = 1.5D and perhaps 8D, the trend of an increase in the maximum deficit with increasing wind speed reverses at the low-wind-speed end. This reversal in the trend is clearly demonstrated in Figure 32, in which we have plotted the maximum deficits from Figures 27 through 31 at the five downwind locations. This is an indirect effect, as the

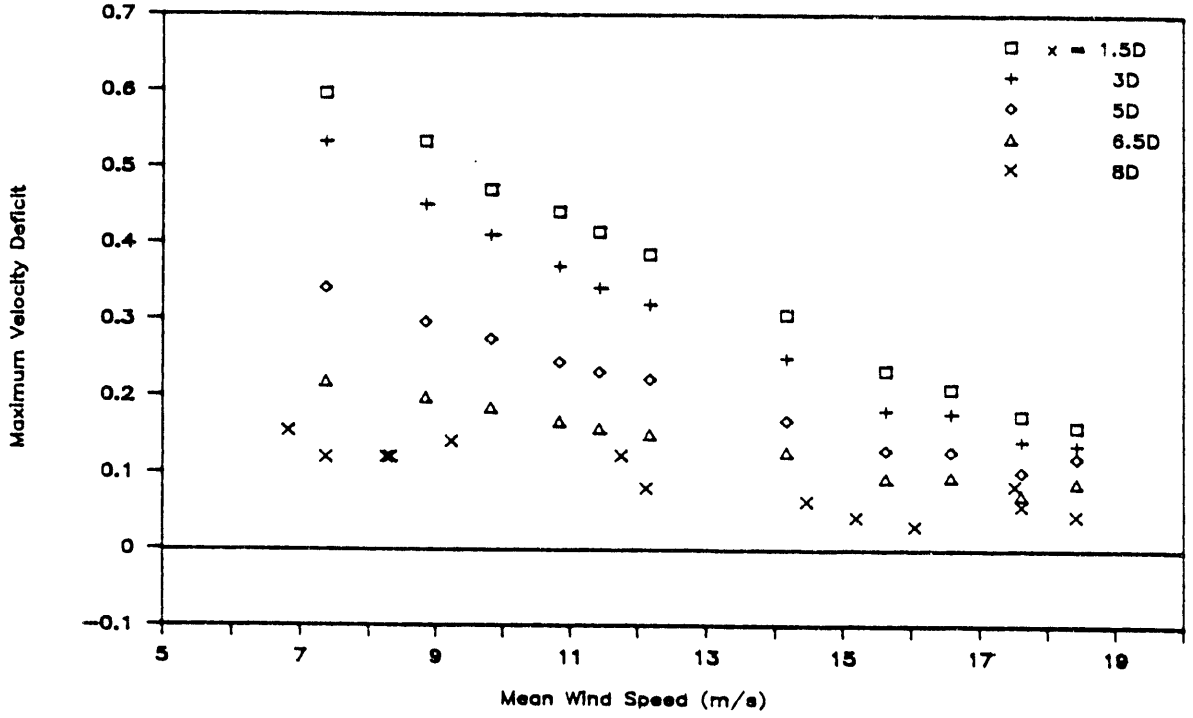

Figure 23. Maximum Velocity Deficits at x = 1.5D, 3D, 5D, 6.5D and 8D when T123 Was On.

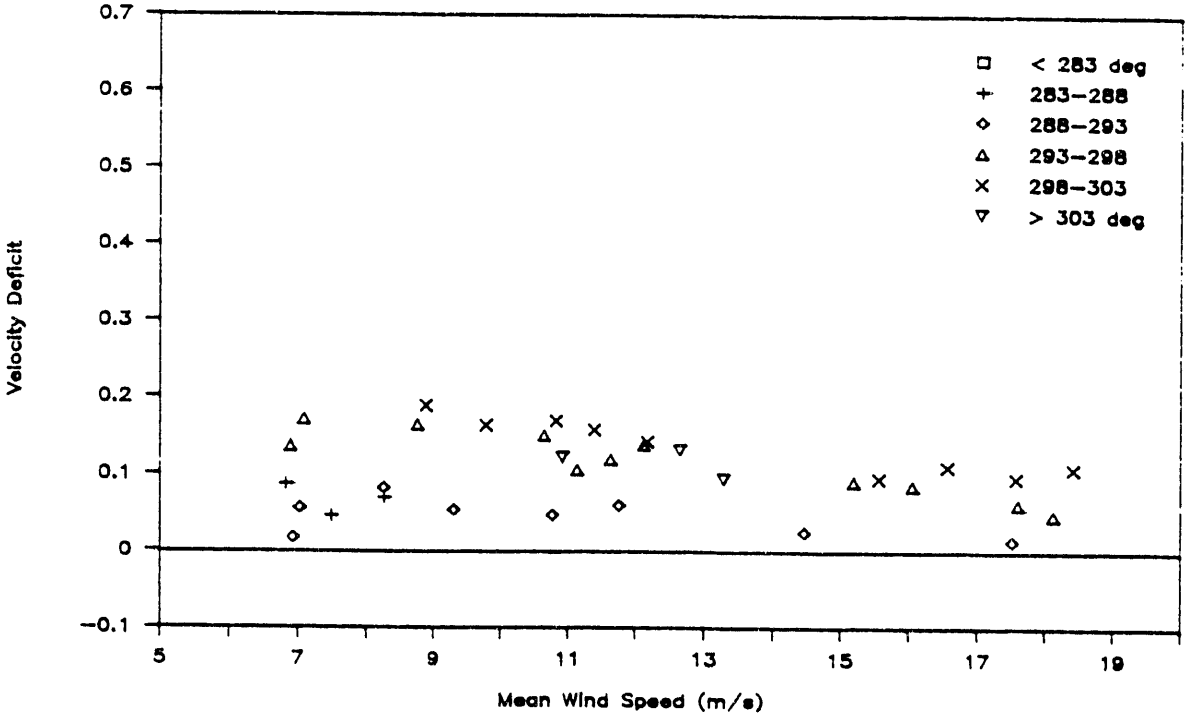

Figure 24. Velocity Deficit Measured at z = 6.1 m and x = 3D (UVW5) on Major Axis of Turbine Array when T123 Was On.

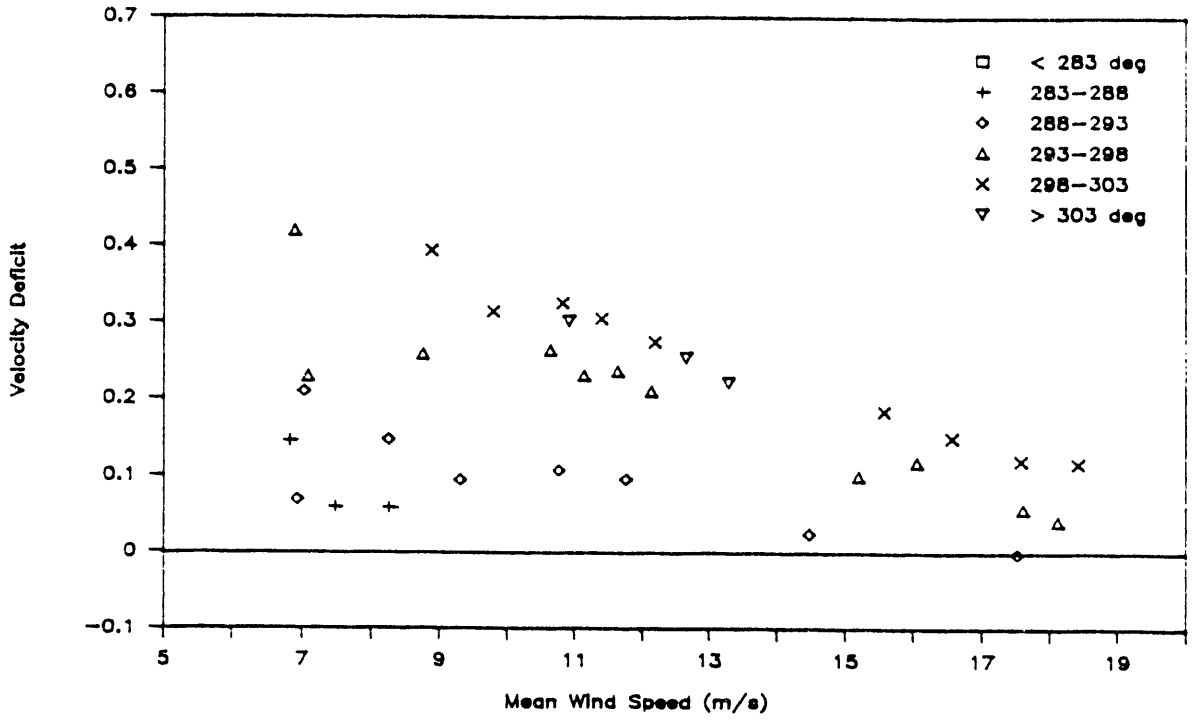

Figure 25. Velocity Deficit Measured at z = 21.3 m and x = 3D (UVW3) on Major Axis of Turbine Array when T123 Was On.

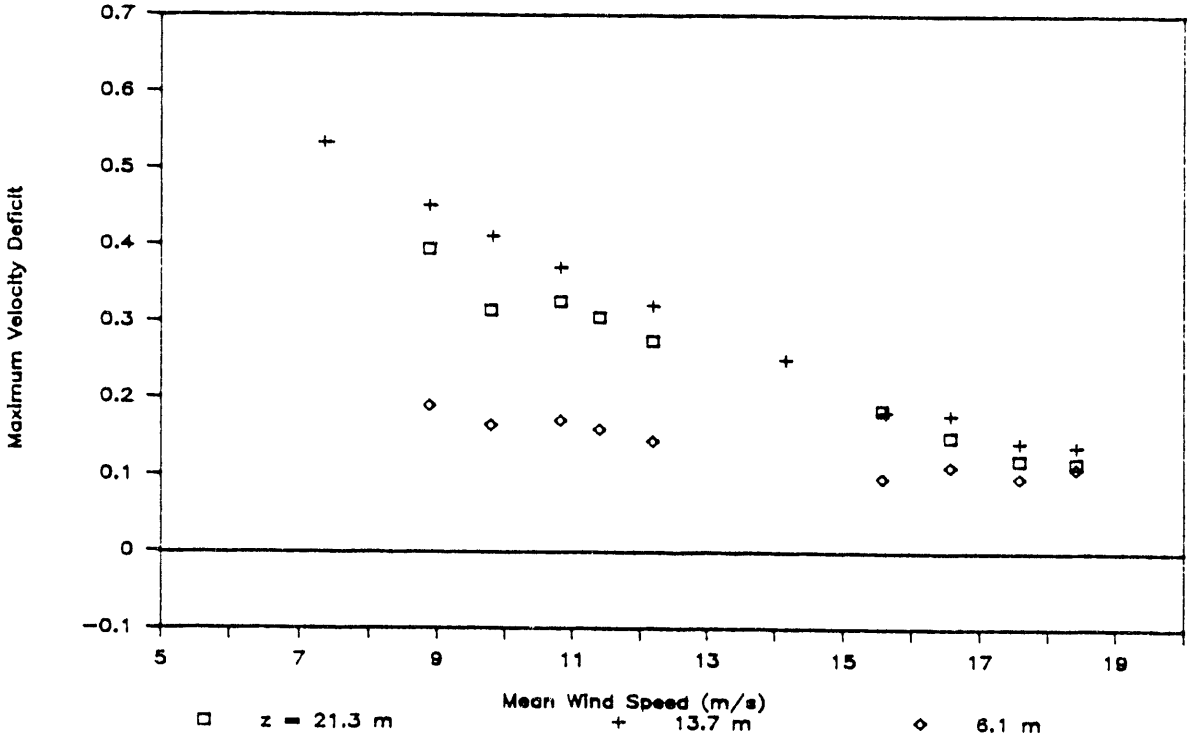

Figure 26. Maximum Velocity Deficits at z = 6.1, 13.7 and 21.3 m and x = 3D on Major Axis of Turbine Array when T123 Was On.

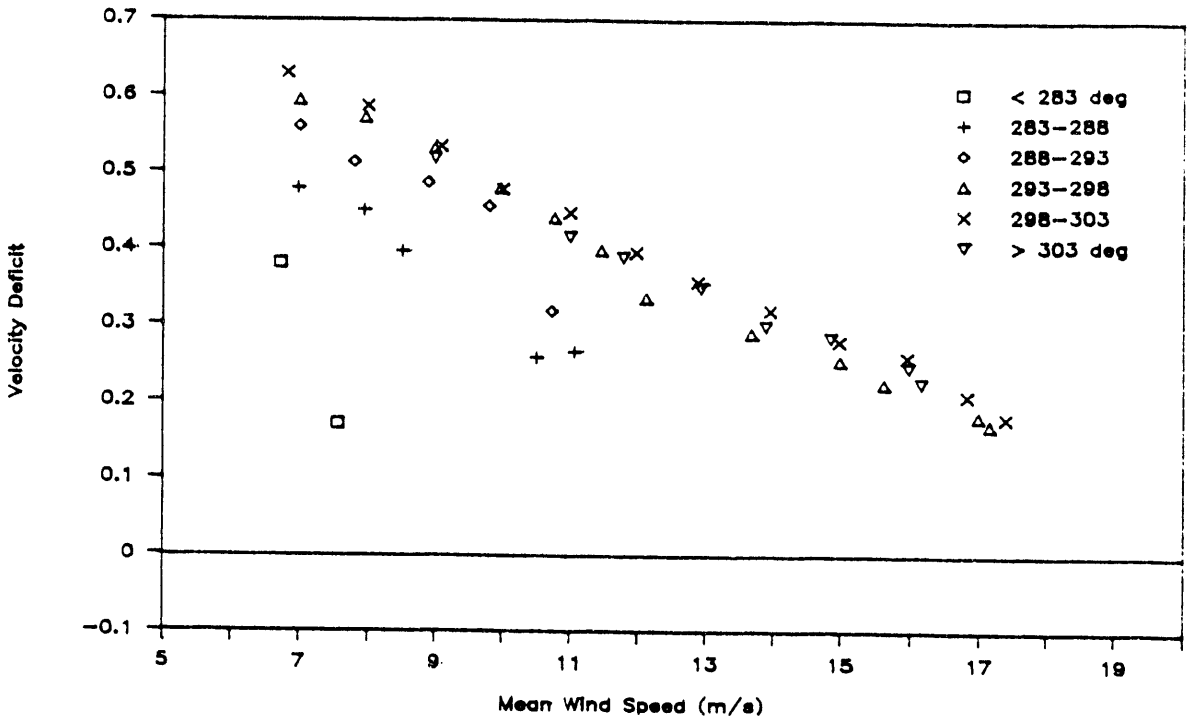

Figure 27. Velocity Deficit Measured at z = 13.7 m and x = 1.5D (UVW2) on Major Axis of Turbine Array when T122 Through T124 Were On.

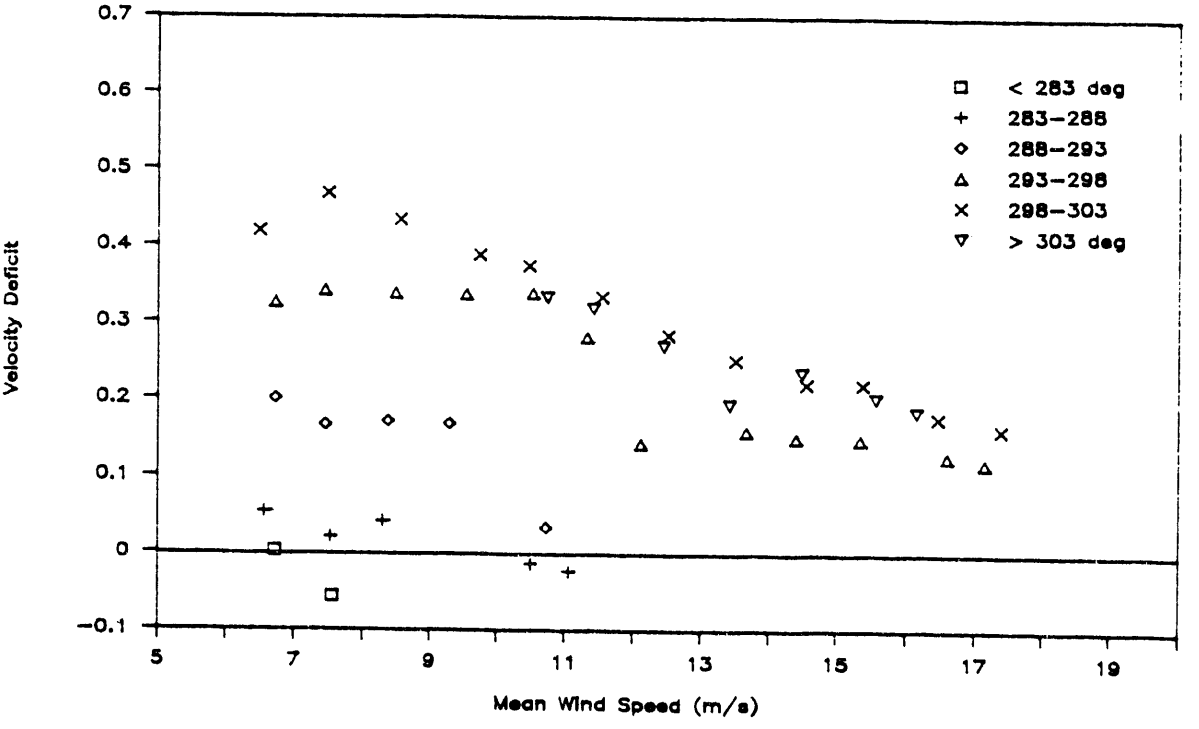

Figure 28. Velocity Deficit Measured at z = 13.7 m and x = 3D (UVW4) on Major Axis of Turbine Array when T122 Through T124 Were On.

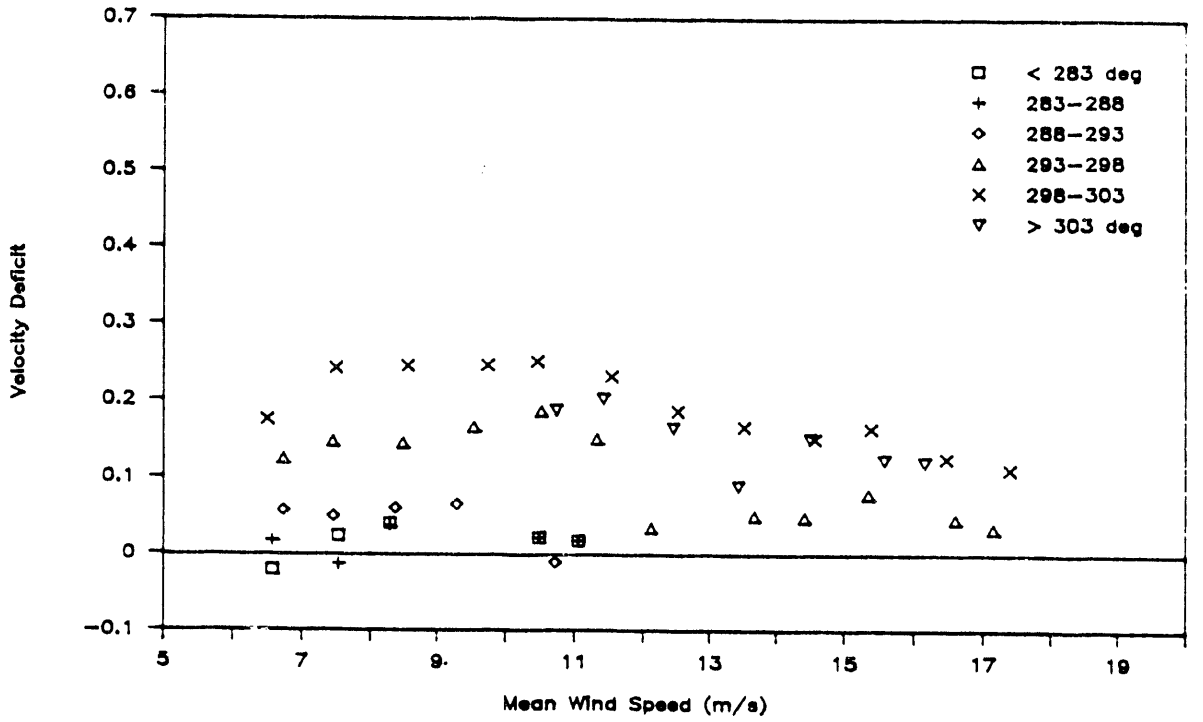

Figure 29. Velocity Deficit Measured at z = 13.7 m and x = 5D (UVW8) on Major Axis of Turbine Array when T122 Through T124 Were On.

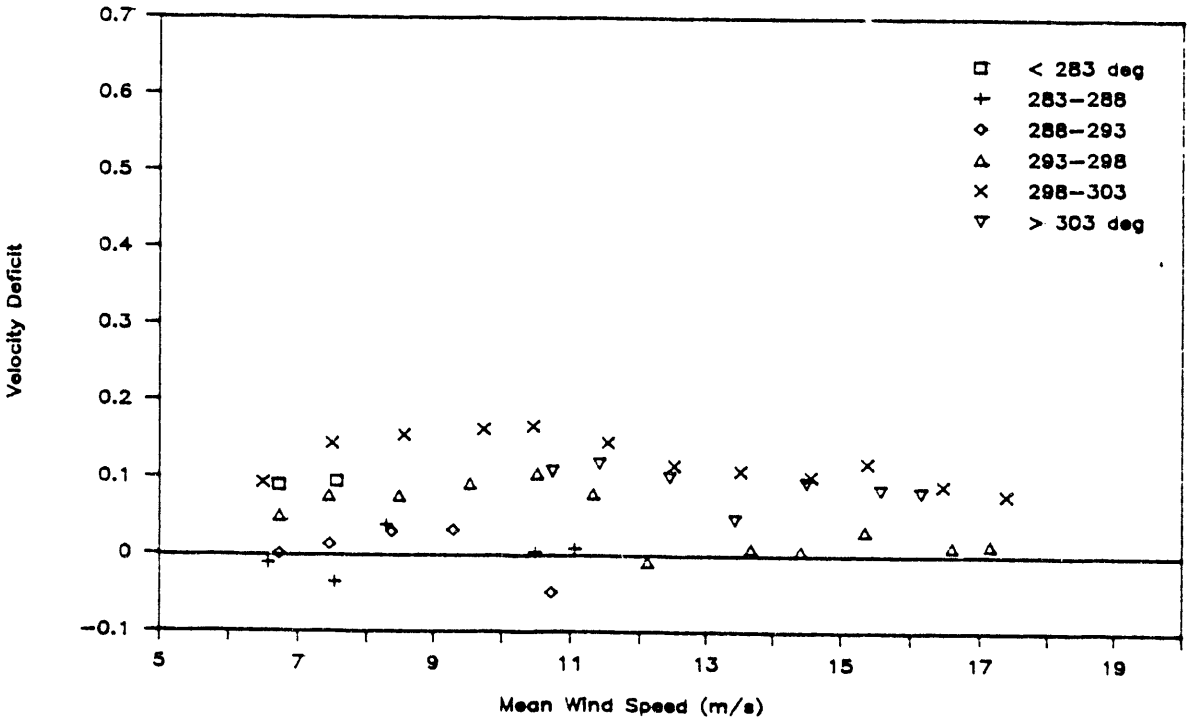

Figure 30. Velocity Deficit Measured at z = 13.7 m and x = 6.5D (UVW9) on Major Axis of Turbine Array when T122 Through T124 Were On.

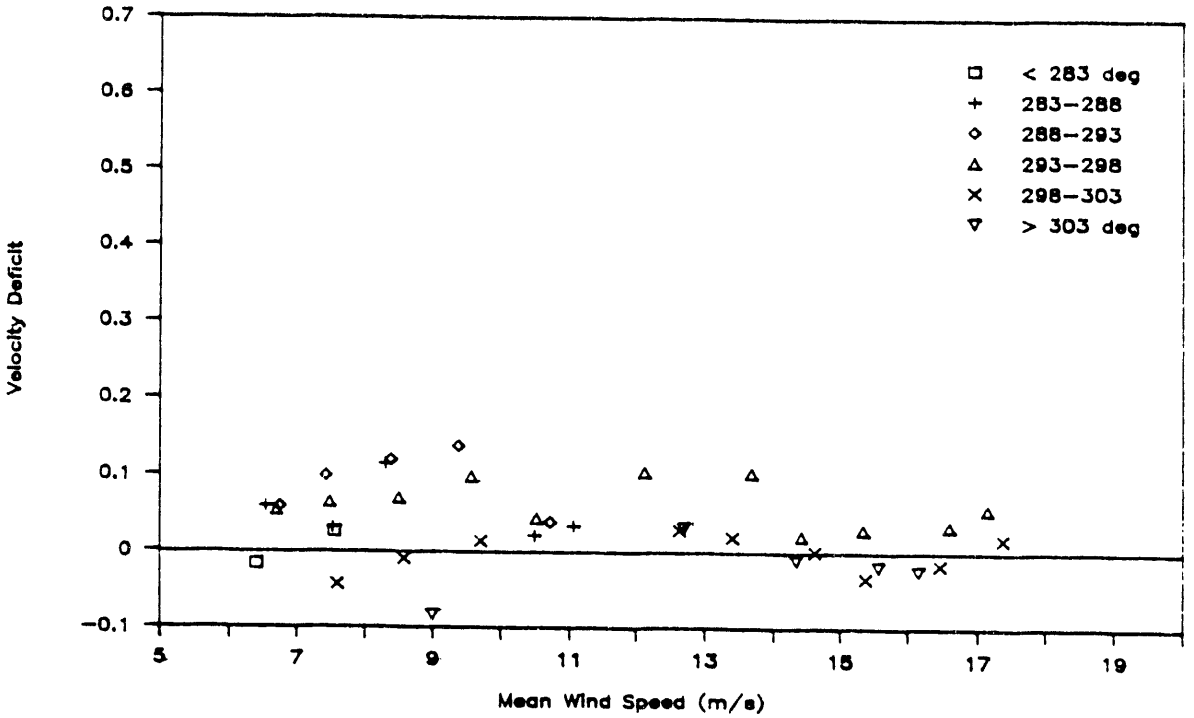

Figure 31. Velocity Deficit Measured at z = 13.7 m and x = 8D (2011) +7.1 deg Off the Major Axis of the Turbine Array when T122 Through T124 Were On.

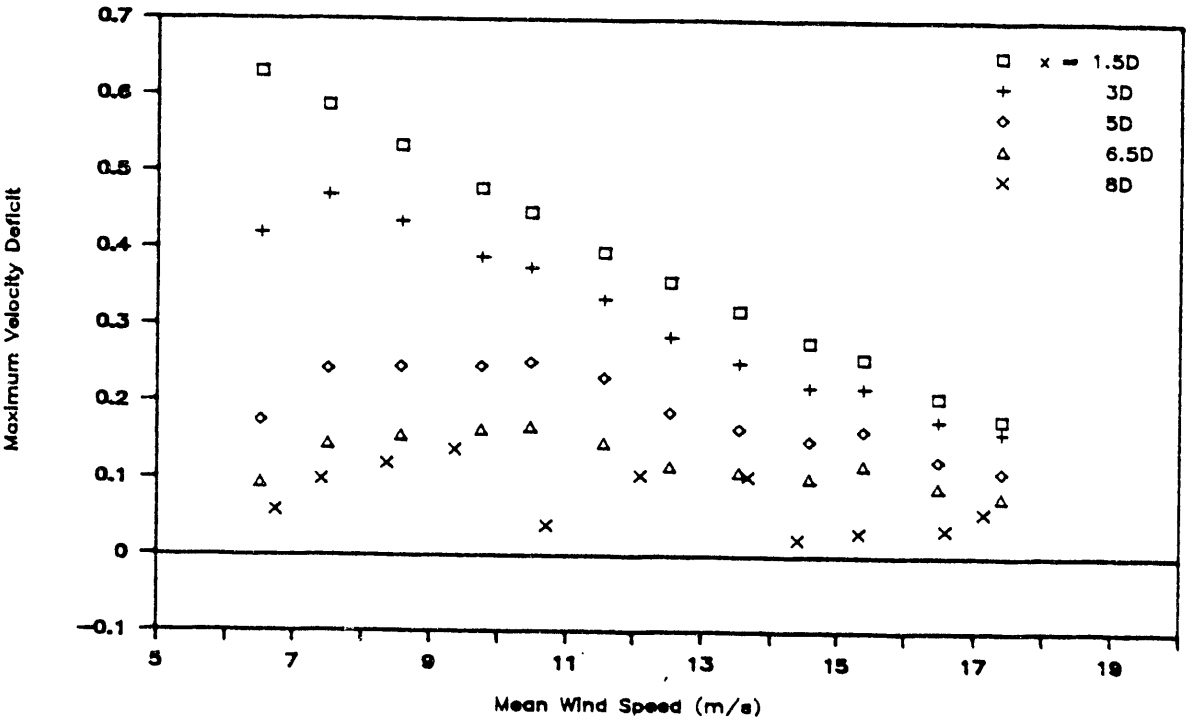

Figure 32. Maximum Velocity Deficits at x = 1.5D, 3D, 5D, 6.5D and 8D when T122 Through T124 Were On.

presence of the adjacent wakes may have induced additional unsteadiness (shedding of vortices) or turbulence in the ambient flow between the two wakes. Stronger mixing and entrainment result and, consequently, reduce the velocity deficit in the individual wakes, especially for the low-speed regime where the ambient turbulence level is low. As the speed or Reynolds number increases, the ambient turbulence becomes stronger, which in turn reduces the effectiveness of the induced turbulence. The above observation is consistent with the prediction of a shorter near-wake length by Lissaman et al. (1982), especially at low wind speeds.

At x = 5D and 6.5D, we find that the reversal of the trend ceases at about 10 m/s, beyond which the two sets of data may be considered identical within the accuracy of the experiment. In the very near wake (e.g., x = 1.5D), however, the induced turbulence has little time to affect the wake structure because the advection time is short. In particular, the profiles of the maximum deficits for the two cases are essentially identical, as observed from Figures 23 and 32. In other words, the wake at this short distance is well within the potential core, which is not affected by the presence of the adjacent wakes.

Except for the reversal in trend discussed above, the vertical variations of the velocity deficit do not show noticeable deviations from those with T123 on. Figure 33 summarizes the maximum deficit at the three levels z = 6.1, 13.7 and 21.3 m. The reversal in trend and the deficit reduction at low wind speeds when the two adjacent turbines were turned on can be seen by comparing the results in Figures 26 and 33.

5.2.3 Cross-Wake Velocity Deficit Profiles

From the profiles of the maximum velocity deficit up to x = 8D, an excessive velocity deficit is not distinguishable from the data scatter except at low wind speeds, when the two adjacent turbines were turned on. One explanation is that the individual wakes have not yet merged sufficiently up to that distance to generate a large excess deficit. Note that the 3D-by-8D spacing would require a half-angle of 20 deg before the edge of an adjacent wake (e.g., T122) brushes the turbine (T102) directly downwind of the primary turbine (T123). To confirm that this is the case, we present a set of cross-wake profiles of velocity deficits using both the measurements of the Gill and cup anemometers downwind of the primary turbines. Combinations of these results

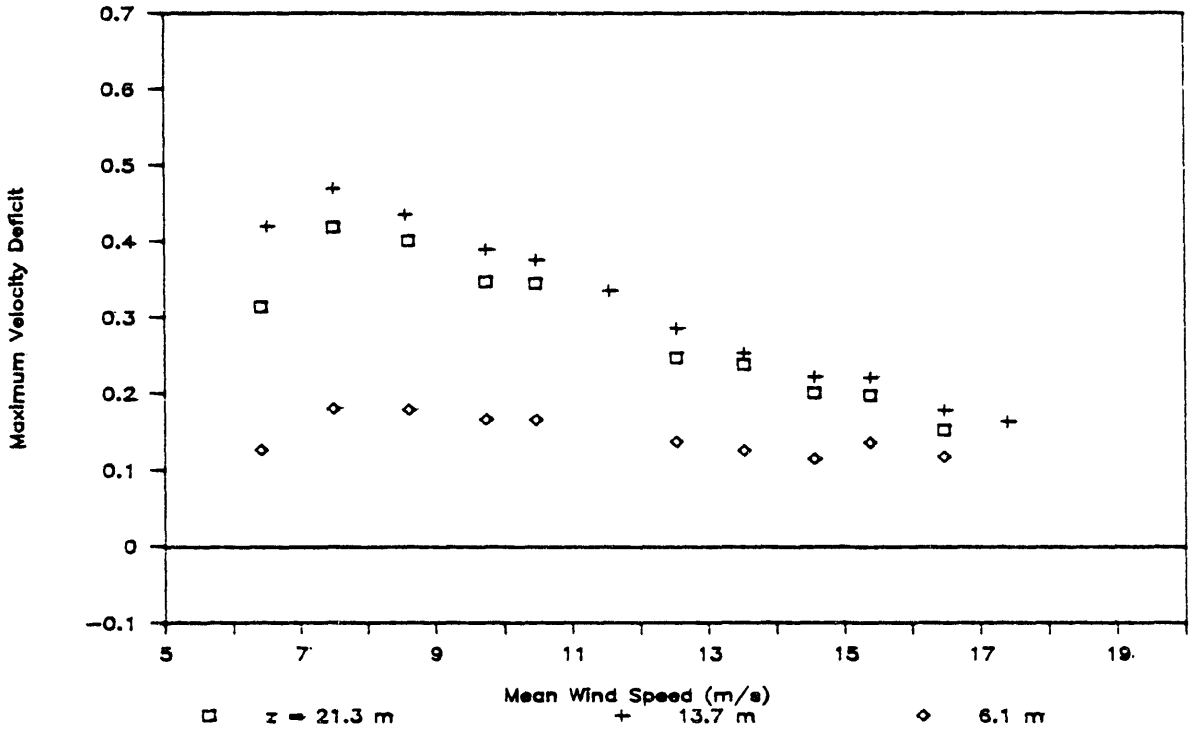

Figure 33. Maximum Velocity Deficits at z = 6.1, 13.7 and 21.3 m and x = 3D on Major Axis of Turbine Array when T122 Through T124 Were On.

were made by plotting the velocity deficit versus the wind direction. For the off-axis anemometers, an offset value of the wind direction is added depending on the lateral displacement of the anemometer from the major axis of the turbine/tower array. Conversion of the width of the wake from angular units to length units may be made by multiplying the downwind distance by the tangent of the 308 - θ, where θ is the wind direction..

Figures 34 through 38 present cross-wake profiles of the velocity deficit at 1.5D, 3D, 5D, 6.5D, and 8D when the primary turbine (T123) was on. The results were sorted into 2-m/s intervals in wind speed and binned over 5-deg increments in wind direction. For the 1.5D measurements, only one anemometer was installed (UVW2). The variations in wind direction were not sufficiently large to enclose the entire cross-wind wake profile. The method of binning the data over a wide range of atmospheric conditions, in terms of turbulence intensity, ambient stability and shear, tends to smear the sharpness of the wake edge, as compared to the visual results of a wake experiment in which a full-scale MOD-2 turbine wake was traced by smoke trails (Liu et al., 1983). The decrease in the velocity deficit with increasing wind speed is evident. One particular trend that becomes clear at 3D is the shift in the wake and its center to lower angles; the lower the wind speed, the larger the shift. At 1.5D and 3D, the shift can be as much as 10 deg or larger (deviation from 308 deg), which is also observable when T122 through T124 were on (Figures 39 and 40). The shift is induced by the counter-clockwise rotation (looking down) of the blades, which creates a side force due to the asymmetry of the wake flow. By analogy to flow past a rotating cylinder (Rauscher, 1953), the blade-to-wind speed ratio governs the degree of induced asymmetry and, thus, the shift in the wake's center. The rotating speed of the blades at 53 rpm is 60.5 m/s at the equator height. At wind speeds of 7 and 15 m/s, the blade-to-wind-speed ratios are 8.6 and 4.0, respectively. As the wake is being advected downwind, turbulence mixing and entrainment cause the wake to grow and tend to mask the above shift. At 5D and beyond (Figures 36 through 38), the relative shift in the wake and its center as a function of the wind speed becomes less pronounced. There is, however, a mean shift of about 5 deg in reference to the major axis of the turbine array, resulting from the initial shift of the wake.

At 3D, the wake width in the near wake reduces with increasing wind speed, indicating that advection dominates entrainment as the wind speed increases. The wake width in linear dimension increases with the downwind distance but at

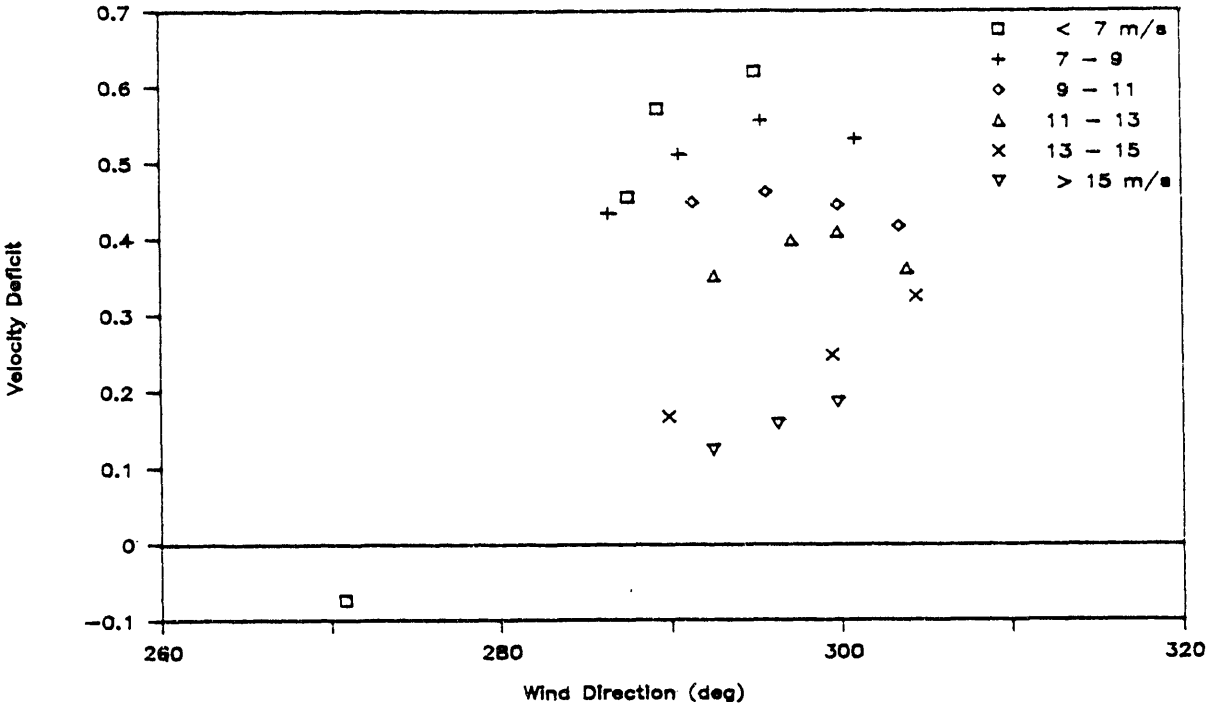

Figure 34. Cross-Wake Profiles of Velocity Deficit at z = 13.7 m and x = 1.5D when T123 Was On.

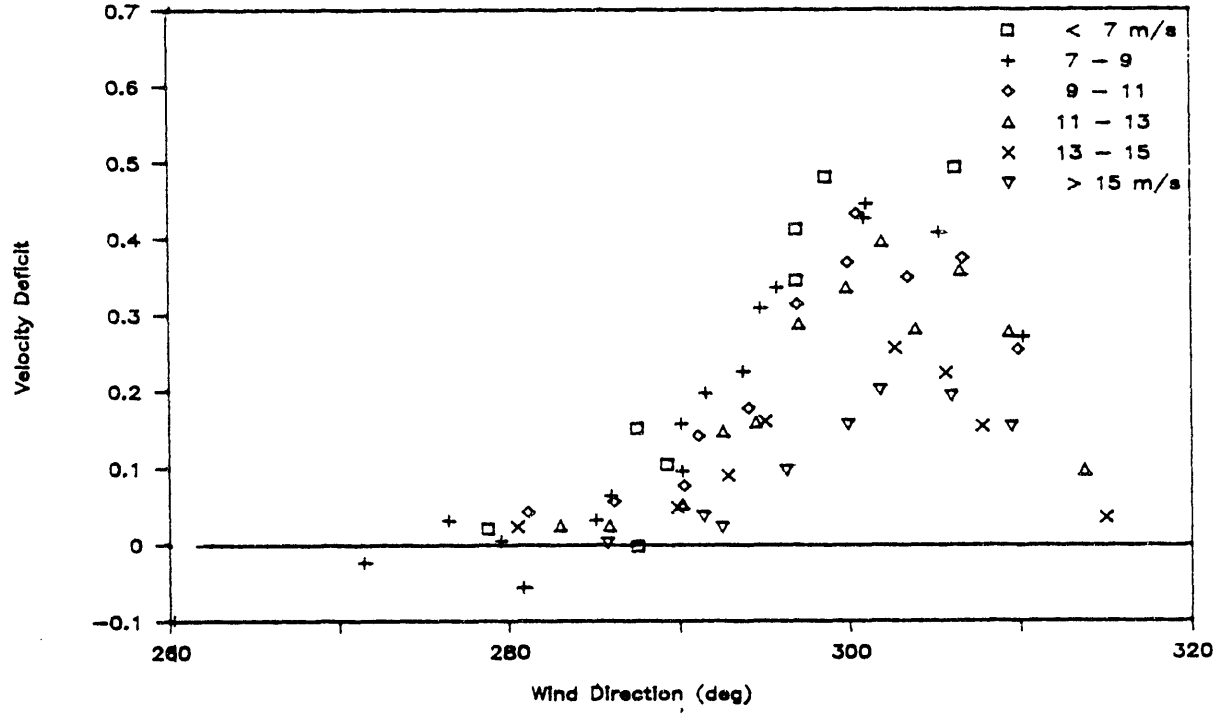

Figure 35. Cross-Wake Profiles of Velocity Deficit at z = 13.7 m and x = 3D when T123 Was On.

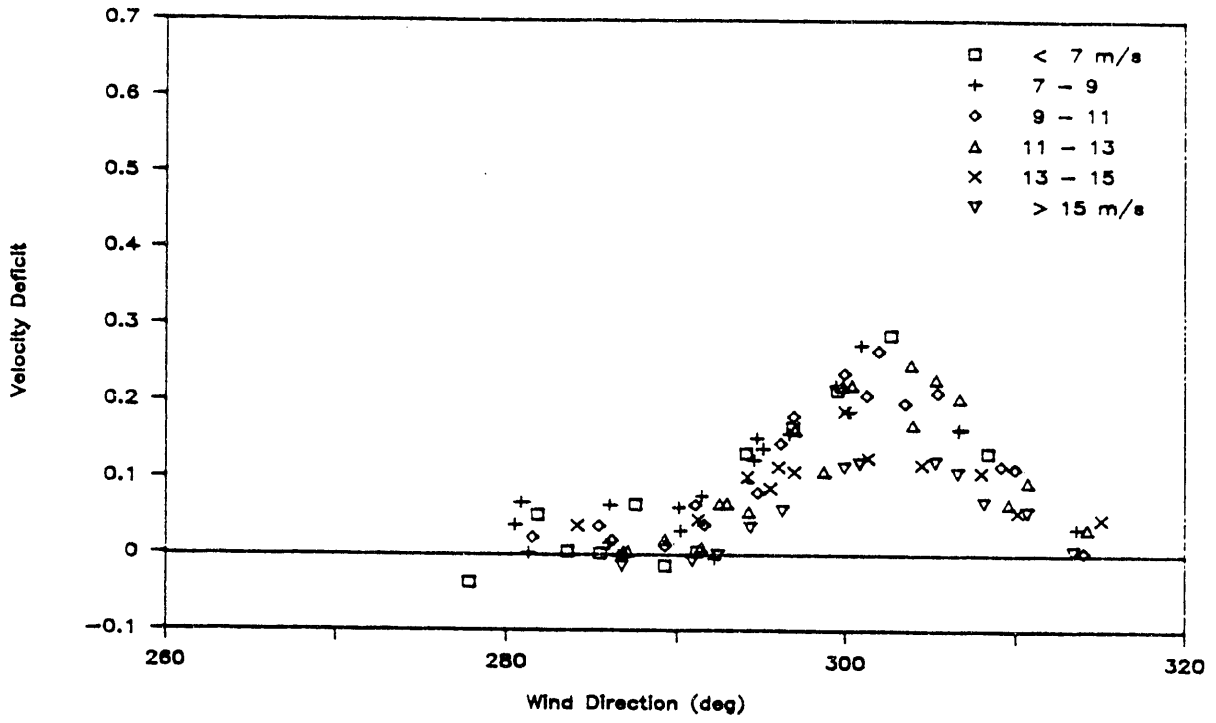

Figure 36. Cross-Wake Profiles of Velocity Deficit at z = 13.7 m and x = 5D when T123 Was On.

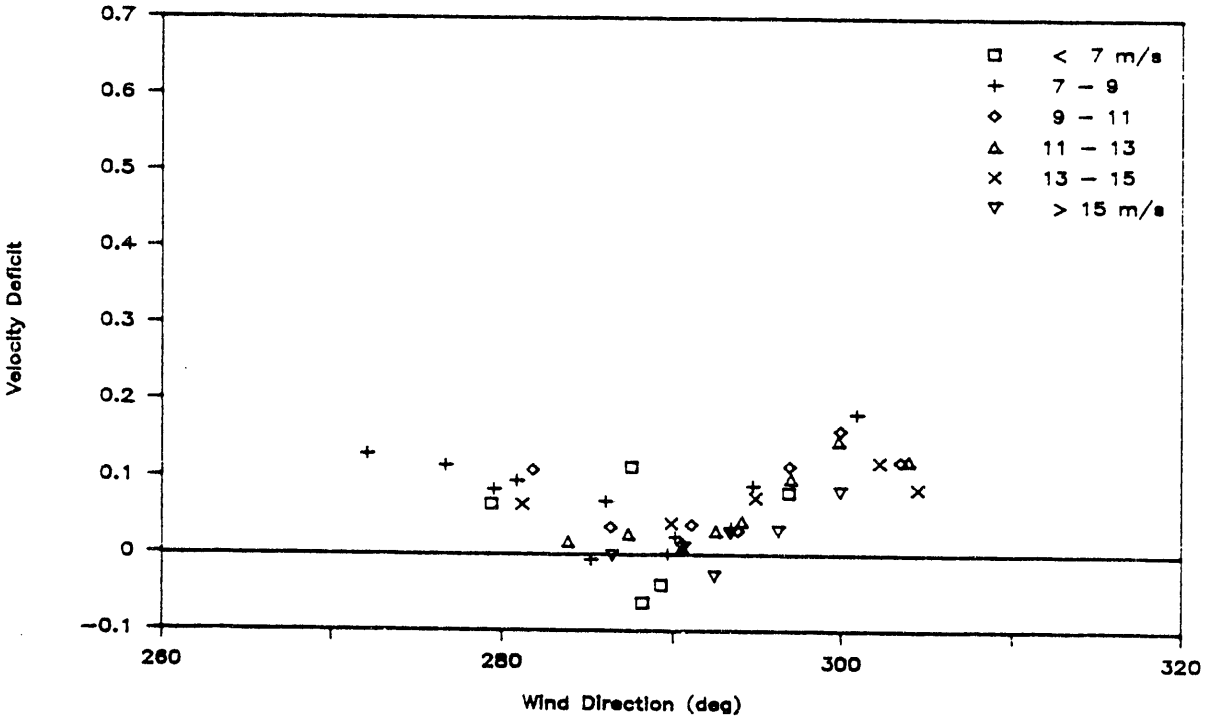

Figure 37. Cross-Wake Profiles of Velocity Deficit at z = 13.7 m and x = 6.5D when T123 Was On.

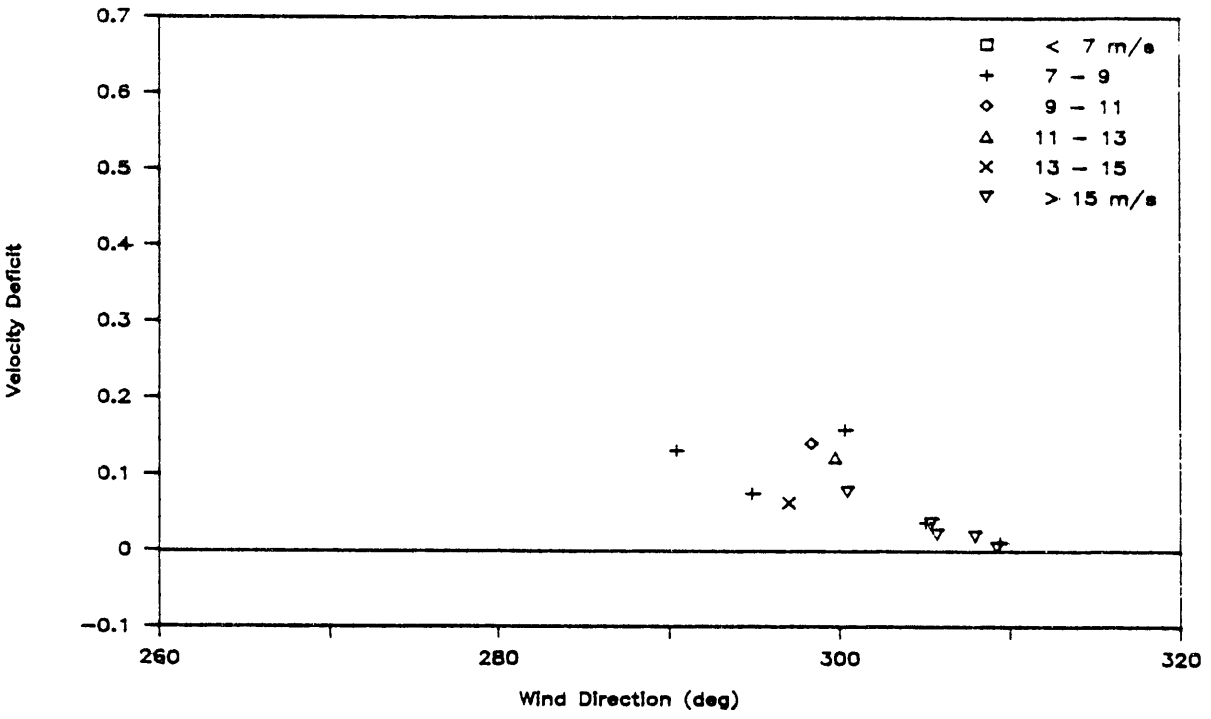

Figure 38. Cross-Wake Profiles of Velocity Deficit at z = 13.7 m and x = 8D when T123 Was On.

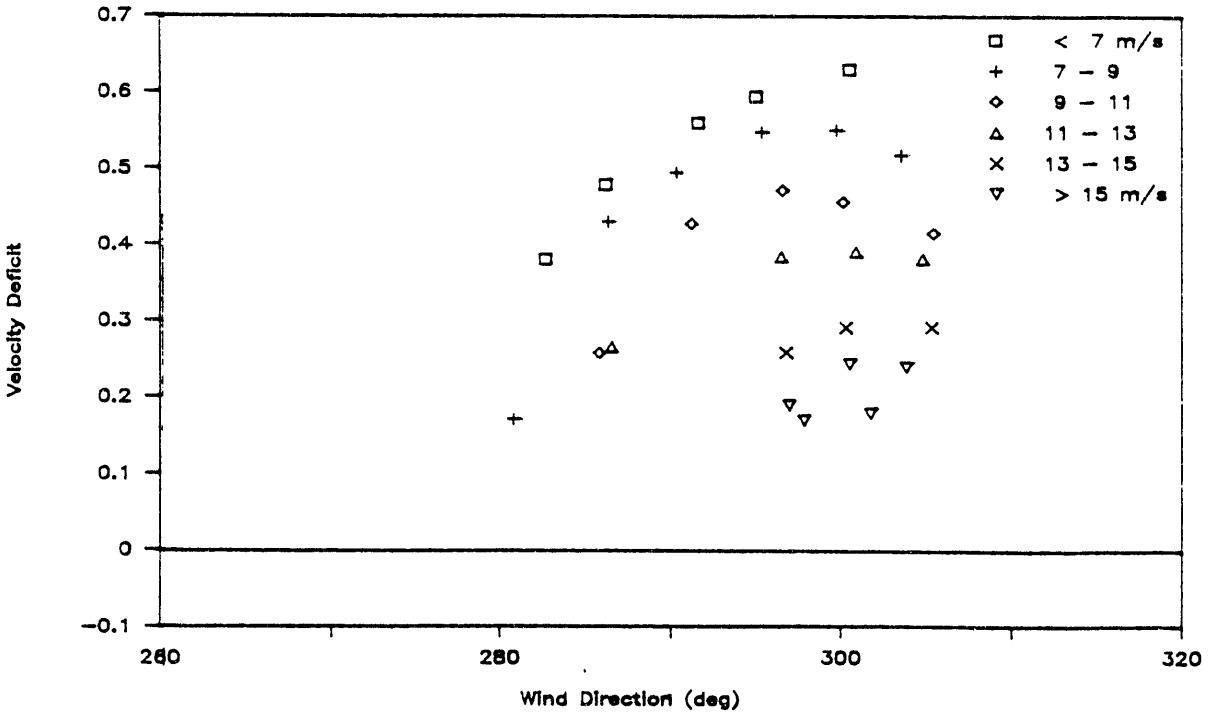

Figure 39. Cross-Wake Profiles of Velocity Deficit at z = 13.7 m and x = 1.5D when T122 Through T124 Were On.

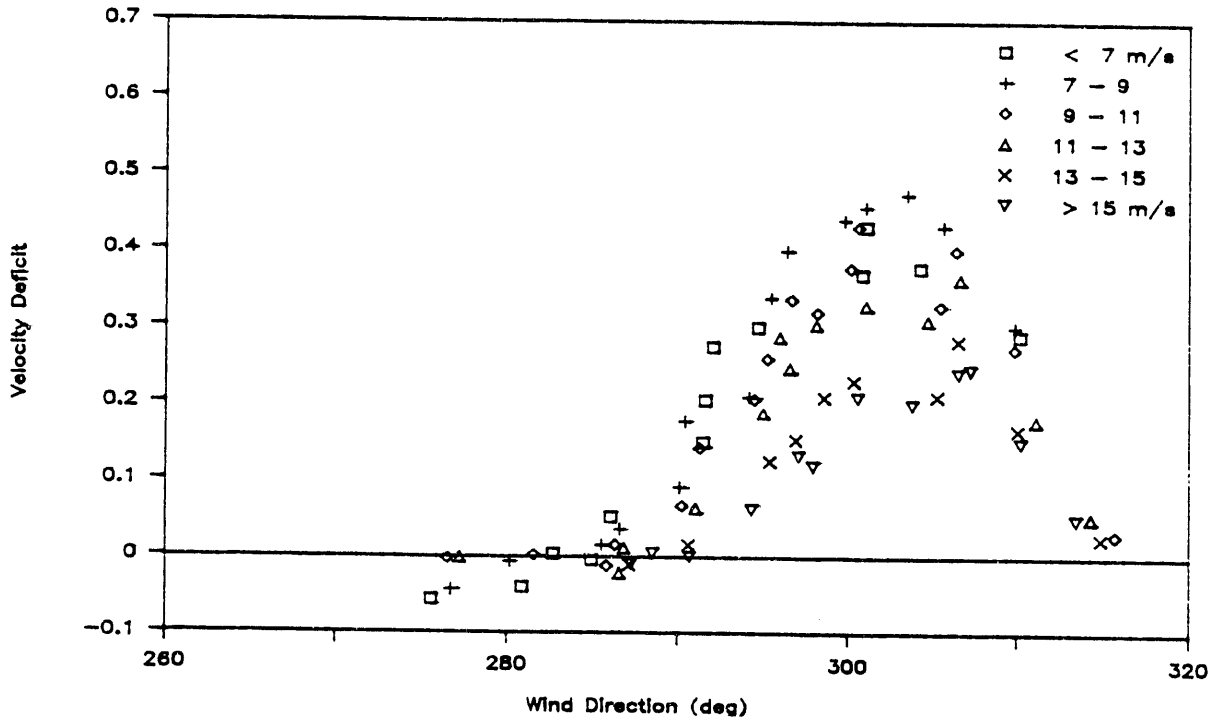

Figure 40. Cross-Wake Profiles of Velocity Deficit at z = 13.7 m and x = 3D when T122 Through T124 Were On.

a rate below that of a constant-angle spread. At and beyond 6.5D, the ambient wind field deviates from the normal pattern for wind directions below 290 deg, resulting in an abnormally high apparent velocity deficit. Examination of the local topography indicates that, for wind directions below 290 deg, several anemometer stations (e.g., 2010, 1012, and 2013 through 2016) are in the shadow of the terrain feature (with its gradient perpendicular to the predominant wind direction) in the vicinity of T125. We excluded those data points in the absence of an appropriate means for correcting the above anomaly.

From the cross-wake profiles, we see that an accelerating region exists outside the wake, as depicted by a negative velocity deficit. This is especially clear when we plot the 7.5-min data rather than the binned data. Such a region was also observed in the smoke trail visualization results from a wake study of a MOD 2 HAWT at the Goldendale Test Site (Liu et al., 1983).

The cross-wake profiles of the velocity deficit when T122 through T124 were on are shown in Figures 39 through 43. At 1.5D (Figure 39), the presence of the adjacent wakes has no observable effect on the primary wake. The shift in the wake and its center is clearly demonstrated because of a better coverage of the wake by the variations in the wind direction. The trend of reversal of decreasing deficit with increasing wind speed, as discussed above (i.e., Figures 23 and 32), becomes evident from 3D to 6.5D (Figures 40 and 42). At 6.5D, one of the cup anemometers (2009) operated only intermittently; thus, its results were excluded. As a result, we did not have full coverage of the entire wake. Except for the trend reversal of the velocity deficit at low wind speeds, comparison of the cross-wake deficit profiles with the primary turbines on and with the upwind three turbines on does not show any other systematic deviations. In other words, any effects would have to be less than 3 to 5%, which is within the data scatter of the velocity deficit. Instead of using the binned data, one may resolve some of the effects by comparing results from back-to-back series of experiments with different turbine operating configurations. By so doing, we would reduce significantly the variations in the ambient conditions as compared to those in the binning data.

To further examine the array effects, we present in Figures 44 to 46 the cross-wake velocity deficit profiles at 3D, 5D, and 6.5D when all five upwind turbines were on. No systematic deviation was observed between the velocity deficit profiles generated by an isolated turbine and a row of five upwind turbines, except perhaps at 6.5D. At that distance, the velocity deficit near

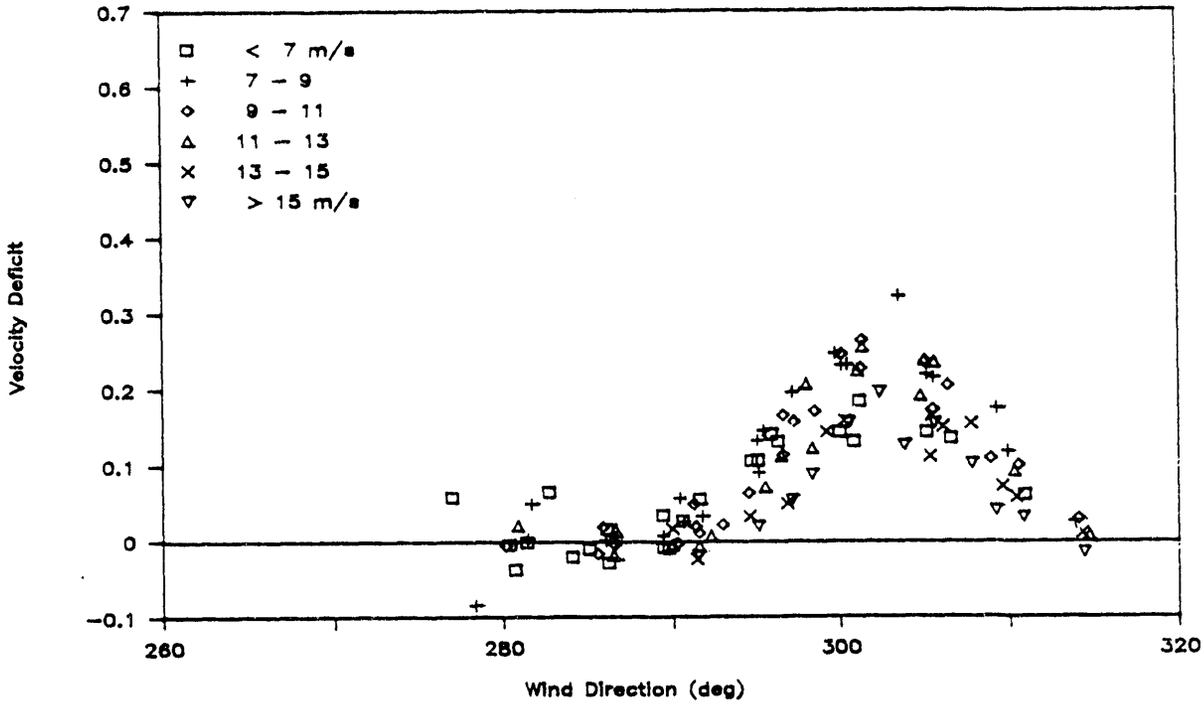

Figure 41. Cross-Wake Profiles of Velocity Deficit at z = 13.7 m and x = 5D when T122 Through T124 Were On.

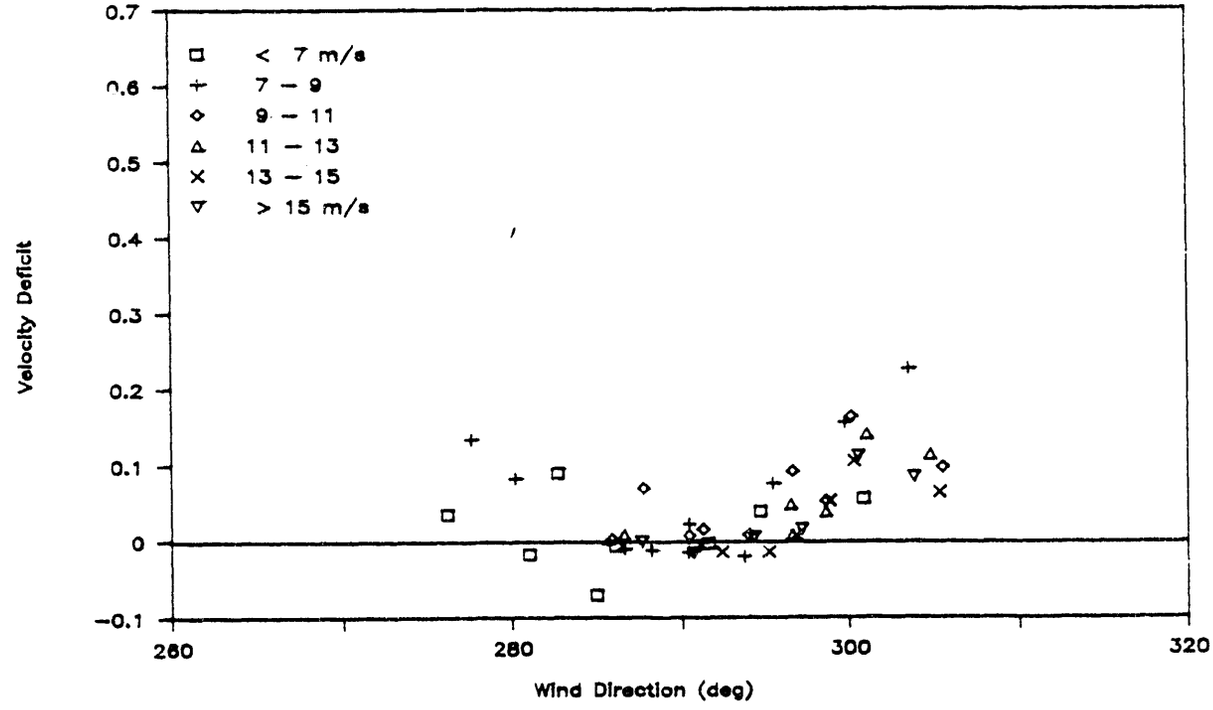

Figure 42. Cross-Wake Profiles of Velocity Deficit at z = 13.7 m and x = 6.5D when T122 Through T124 Were On.

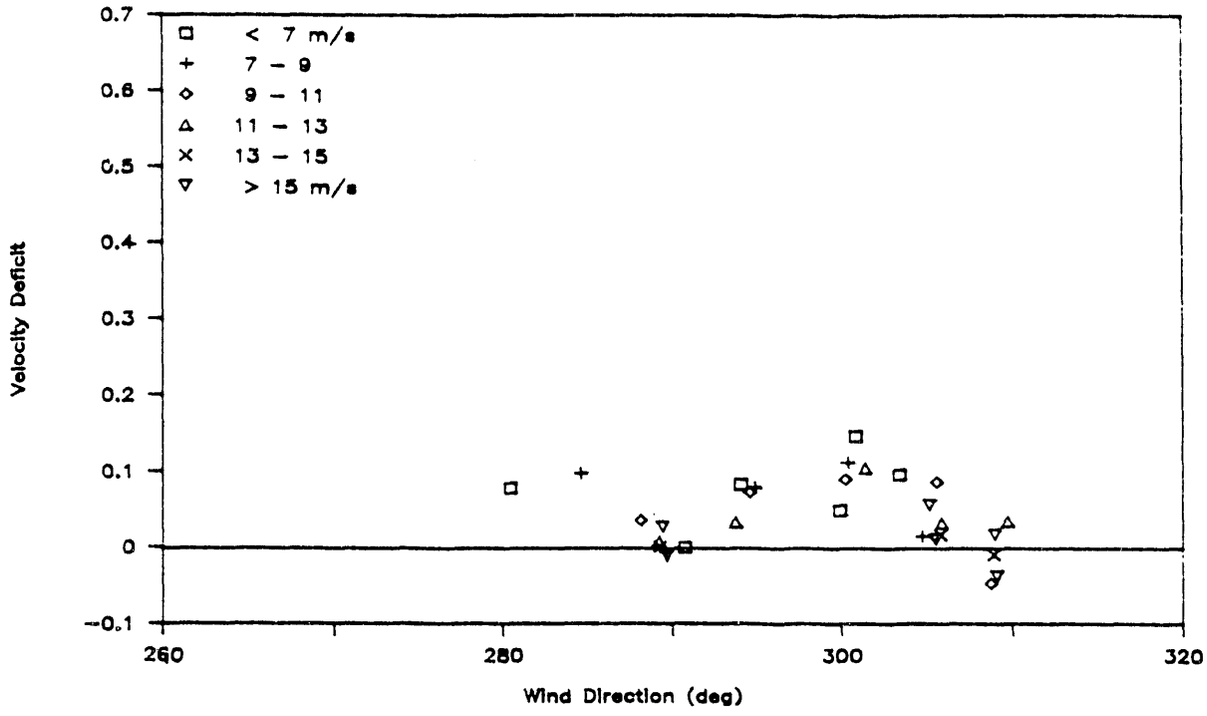

Figure 43. Cross-Wake Profiles of Velocity Deficit at z = 13.7 m and x = 8D when T122 Through T124 Were On.

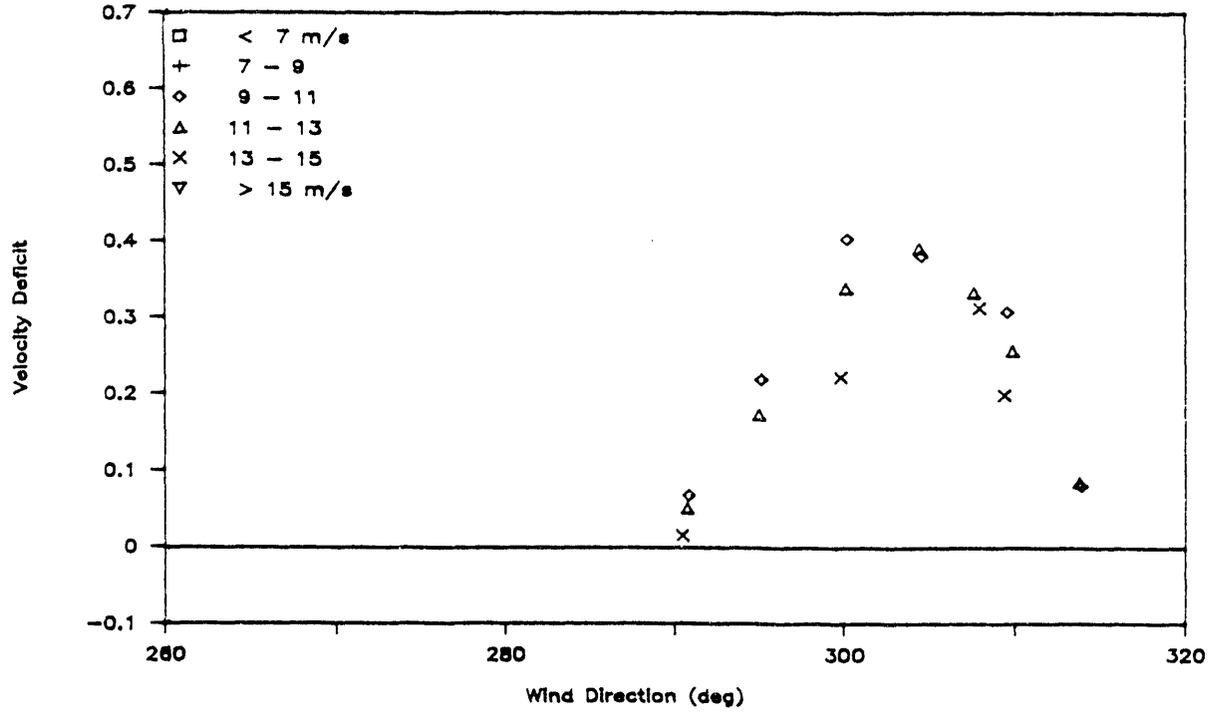

Figure 44. Cross-Wake Profiles of Velocity Deficit at z = 13.7 m and x = 3D when T121 Through T125 Were On.

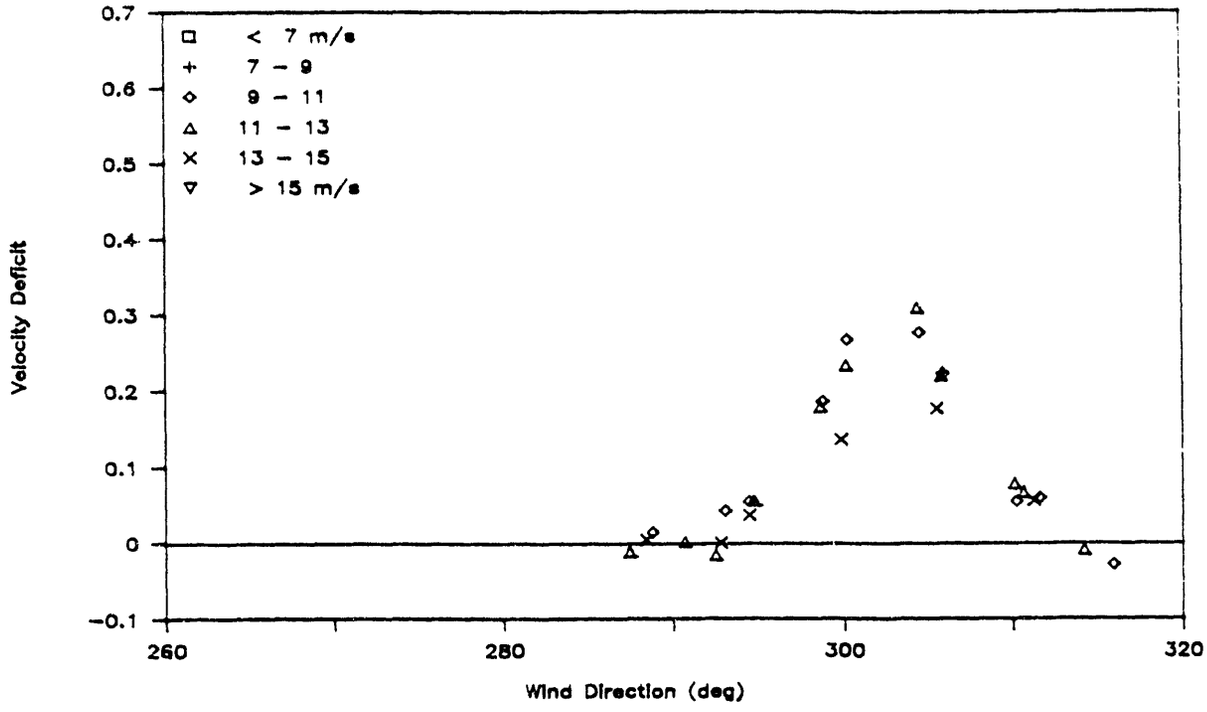

Figure 45. Cross-Wake Profiles of Velocity Deficit at z = 13.7 m and x = 5D when T121 Through T125 Were On.

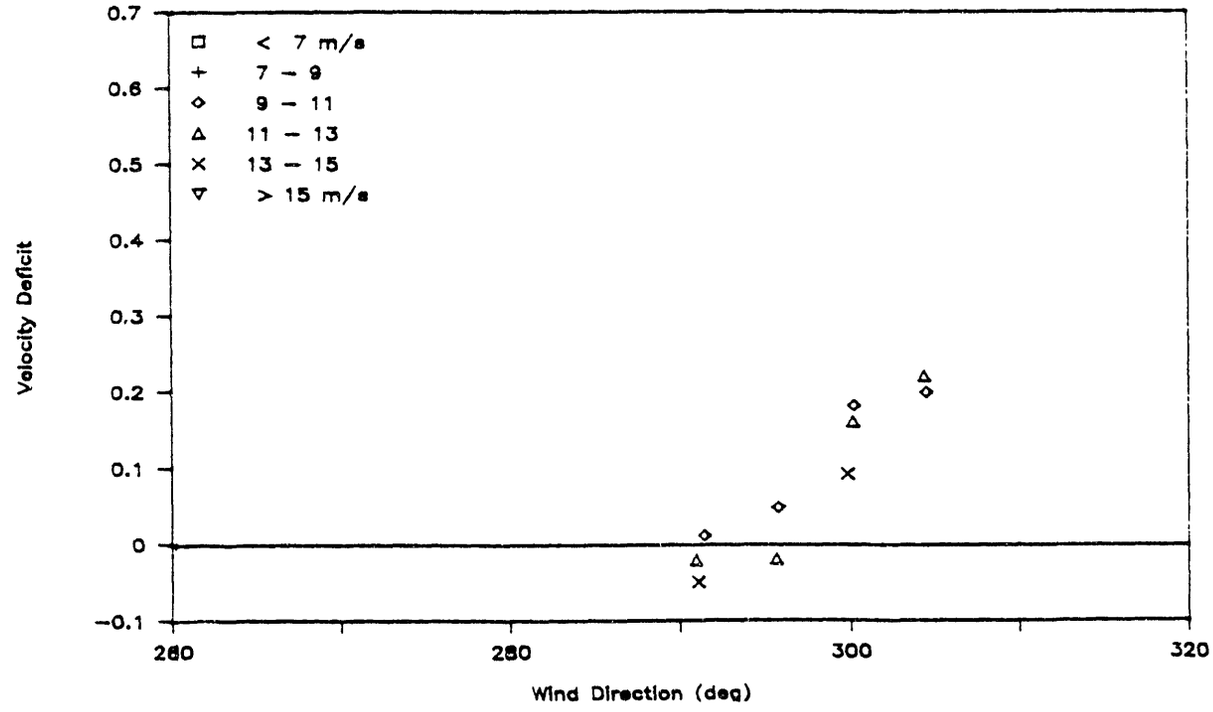

Figure 46. Cross-Wake Profiles of Velocity Deficit at z = 13.7 m and x = 6.5D when T121 Through T125 Were On.

the wake center tends to be higher when a row of five turbines is on than when the primary turbine is on. No data, however, were available at 8D to confirm such a trend.

5.3 Power Deficit

As discussed in the last subsection, the array effects on the performance of downwind turbines cannot be determined based on the velocity deficit due to the relatively large amount of scatter in the wind speed data. Further, since the wind field was measured at limited, fixed points downwind, to assess the array effects on downwind turbines, we need to integrate the wind data measured at these points via interpolation and/or extrapolation. As a result, the integrity of the information derived from the velocity deficit is degraded considerably through the processing of the data. On the other hand, the turbine power is a direct measure of the performance of the turbine under a given wind condition. Any effects from the presence of upwind wakes should be reflected in the power loss. Moreover, the turbine power is proportional to S^3; thus, we anticipate that the turbine power would be a much more sensitive barometer to the array effects.

5.3.1 F-17 Power Curves

Prior to the investigation of the power deficit under various turbine on/off configurations, power measurements were made to determine the performance of all the nine turbines within the array in the absence of upwind wakes. The power curve for each turbine was derived to serve as a reference and compare with the published values provided by FloWind. The measured turbine power was adjusted to the sea level equivalent under the conditions $T = 15°C$, $P = 1013.25$ mbar. The adjustment was made by multiplying the measured power with the density ratio at sea level and at the site. The mean temperature and pressure at the site were recorded on a computer twice a day at a nearby FloWind research trailer. Additional manual readings were made to fill in the gaps and when the computer was not operating. The atmospheric pressure varied within a narrow range from 850 to 857 mB for the entire field experiment, which introduced an error of less than 1% even if no adjustment was made. The temperature, on the other hand, could vary by as much as 16°C in one diurnal cycle. A 10-deg variation in temperature would result in an error of about 3% in the turbine power if not corrected for. To improve the

accuracy in interpolating the temperature for each diurnal cycle, we also incorporated measurements made at the Tehachapi Fire Department (at 14:00 PST) in the City of Tehachapi. Comparison of the temperature readings between the two locations shows good correlation with a maximum deviation of less than $\pm$3.5 deg, which would result in a maximum error of about $\pm$1.1%.

Figure 47 shows the power curves for the primary turbine (T123). The abscissa and ordinate are, respectively, the mean wind speed in meters per second and the turbine power in kilowatts. The solid curve corresponds to the data published by FloWind. The symbols are measurements sorted every 5 deg in wind direction and binned over 1-m/s increments in wind speed (see description in the figure legend). The wind speed was measured at the upwind reference tower at x = -2D and z = 13.7 m. Also included is a set of measurements without the wind direction information (inverted triangles); these measurements were taken when the reference wind speed was being measured with the cup anemometer (2017). For wind speeds up to 15 m/s, the measured and published data agreed fairly well, with a trend of slightly lower values for the former than for the latter. Such a small discrepancy could be caused by a slight wind speed difference at the anemometer and turbine locations in the developing internal boundary layer as the upslope wind approached the ridge top (see Figure 15). The data scatter is surprisingly small, indicating a high correlation of the wind speeds at the two locations.

For wind speeds beyond 15 m/s, the measured power levels off and is noticeably lower than the published data. Initially, we speculated that the doubler plates attached to the joints might have caused the reduction in power. Such a speculation was soon resolved, however, as another turbine (T124) without doubler plates showed the same feature (see Figure 48). With a set of theoretical assumptions, it was estimated that the maximum power loss due to the presence of the plates would be about 3 kW. Apparently the dynamic stall characteristics of the airfoil section probably played the most important role in the behavior of the VAWT at high wind speeds.

The dynamic stall is one of the least understood aerodynamic phenomena that significantly affects the performance of wings at high angles of attack. When an airfoil undergoes oscillatory motions, i.e., pitching or plunging, several dramatic phenomena that deviate greatly from the static situation take place. As discussed by Ho (1983) and demonstrated by McCroskey (1981), the excursion of the aerodynamic properties from that of the static case depends

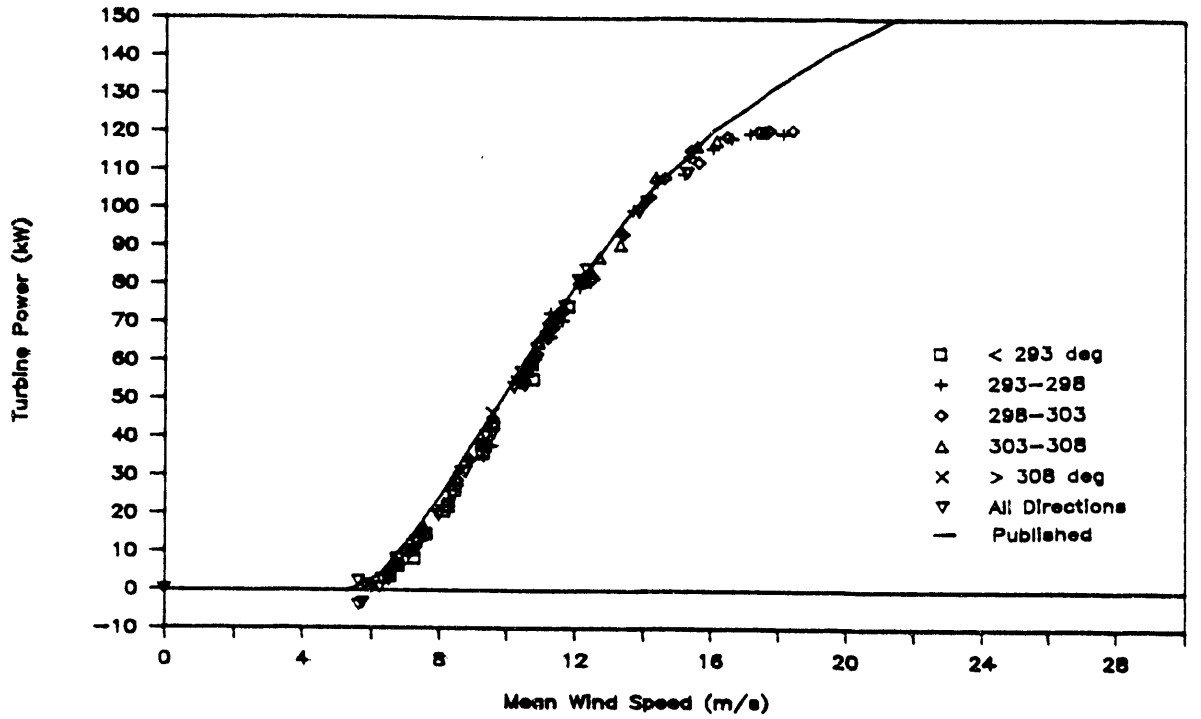

Figure 47. Power Curves of the Primary Turbine T123 with Wind Speed Measured at z = 13.7 m and x = -2D at Reference Tower.

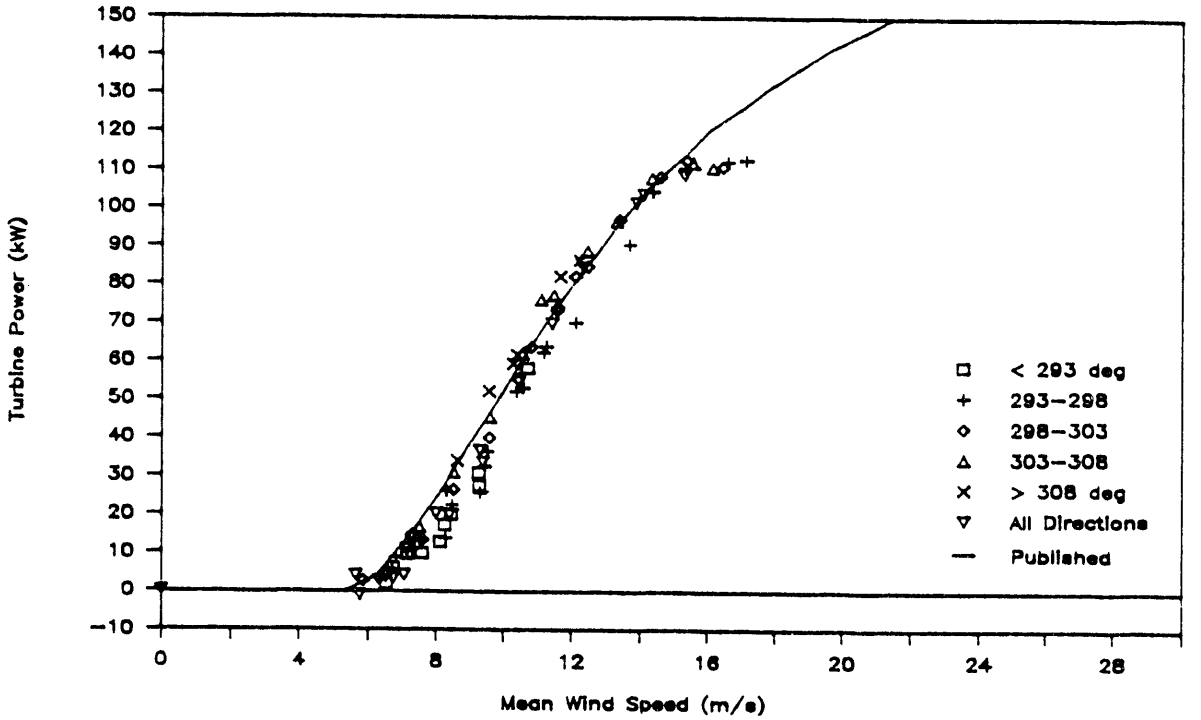

Figure 48. Power Curves of T124 with Wind Speed Measured at z = 13.7 m and x = -2D at Reference Tower.

on the operational parameter of the unsteady motion. The difference can be very pronounced if a large separation vortex occurs at the leading edge. When the angle of attack oscillates around a mean value α_o near or greater than the static-stall angle, the maximum values of the lift, drag and pitching-moment coefficients can greatly exceed their static counterparts. The higher value in the lift coefficient is generally referred to as the "lift overshoot". Such increases in C_L, C_D, and C_M cannot be reproduced even qualitatively by neglecting the unsteady motion of the airfoil. On the other hand, large hysteresis develops in the aerodynamic forces and moments with respect to the instantaneous angle. The above process is referred to as dynamic stall, which is intimately related to unsteady separation of the flow around the wing.

Recently, Liu (1986b) conducted a series of full-scale experiments to quantify the effects of turbulence and gust on the performance of a Wortmann FX 63-137 wing. A one-of-a-kind Environmental Aerodynamic Test System (EATS) (Liu et al., 1985) consisting of a full-scale Wortmann wing boom-mounted on an instrumented truck as a mobile platform was designed for the experiments. The experiments were conducted at a windy site (Ellensburg Airport, Ellensburg, Washington) by aligning the wing with the prevailing wind. The full-scale results from one of the series, with a chord Reynolds number ranging from 250,000 to 450,000, differed markedly from their wind-tunnel counterparts under steady conditions. In essence, significant lift overshoot was observed in the full-scale data, which resulted in a significant increase in the maximum lift coefficient and in the stall angle, together with a twofold reduction in the minimum drag coefficient.

For a VAWT, the dynamic stall becomes extremely complicated due to its wide range of Reynolds numbers, angles of incidence, angular acceleration of incidence, ambient turbulence, blade surface condition, etc. All the above parameters are sensitive to the dynamic stall characteristics of the VAWT. It is believed that the conditions of bug accumulation could change the dynamic stall characteristics. From the outputs of one of the F-19s at FloWind's Altamont Windfarm, as monitored by PG&E, the power curves of the same turbine measured during two consecutive weeks before and after a rain shower showed different features. The earlier one displayed features similar to those shown in Figure 47, whereas the later one followed closely the trend of the published curve. Apparently, the accumulated bugs were washed out around the leading edges of the turbine blades, restoring the proper development of the boundary

layer on the blades and allowing vigorous dynamic stall. We anticipate that, in the high-speed regime, a vigorous stall would at least match the performance of the published data; a moderate one would cause the power curve to level off; and a relatively poor one would allow it to drop off with increasing wind speed. Further investigation of dynamic stall phenomena would definitely help optimize the design and operation of VAWTs.

The power curves for the two adjacent turbines (T124 and T122) are shown in Figures 48 and 49. These figures illustrate a couple of interesting features. First, there is a noticeable increase in the data scatter that depends on the wind direction. In general, the data scatter increases with increases in the deviation of the wind direction from the 308-deg orientation. Evidently, the local topography introduces nonuniformity in the ambient wind field, an appropriate demonstration of the micrositing issue. The correlation of the wind speed between that measured at the reference tower and that sensed by the turbines deteriorates as the distance between the two locations increases. Note that the two adjacent turbines are located 3D away from the primary turbine in the crosswind direction. The elevation at the turbine bases differs about 1.6 m (between T122 and T123) and 2.7 m (between T123 and T124), as shown in Figure 4b. There are a couple of terrain features that are potential sources of the nonuniformity, although the influence of the upwind terrain to the local wind field (Section 5.1) should not be overlooked. One such feature is the relatively steep gradient at and upwind of T125, with the gradient roughly perpendicular to the predominant wind direction. The other is the presence of a small gorge next to T122, with its axis roughly parallel to the predominant wind direction. These features, with a vertical scale less than 5 m, may influence the local wind field and should not be ignored.

In addition to the difference in the data scatter, Figure 48 differs from Figures 47 and 49 in that the former displays no stalling trend at wind speeds up to 16 m/s. It should be pointed out that the same doubler plates used at T123 were also installed at T122. At present, we are unable to pinpoint the exact causes of such a difference in the stall characteristics. We believe the ambient turbulence level is one of the key factors, as we will discuss below. Whatever the causes, nevertheless, it is beneficial to promote dynamic stall to improve the energy capture of the turbines at high wind speeds.

To further demonstrate the micrositing effects, we present in Figure 50 the power curve of turbine T102, which is downwind of T123 along the major

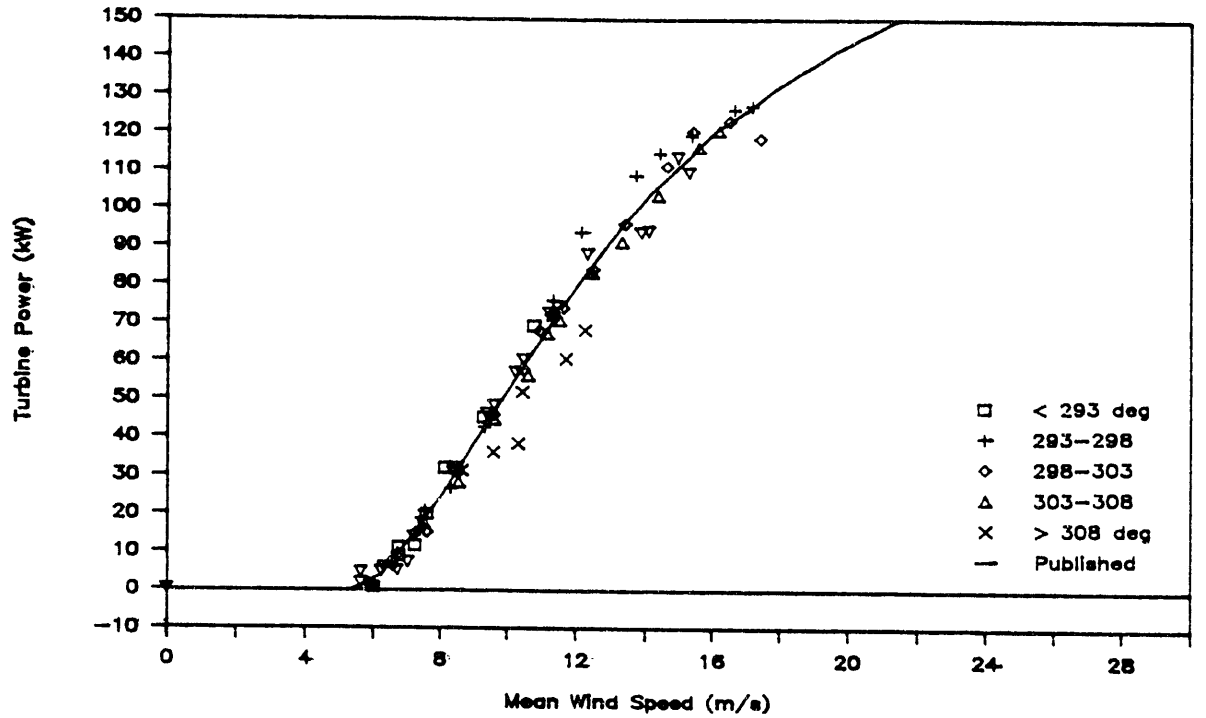

Figure 49. Power Curves of T122 with Wind Speed Measured at z = 13.7 m and x = -2D at Reference Tower.

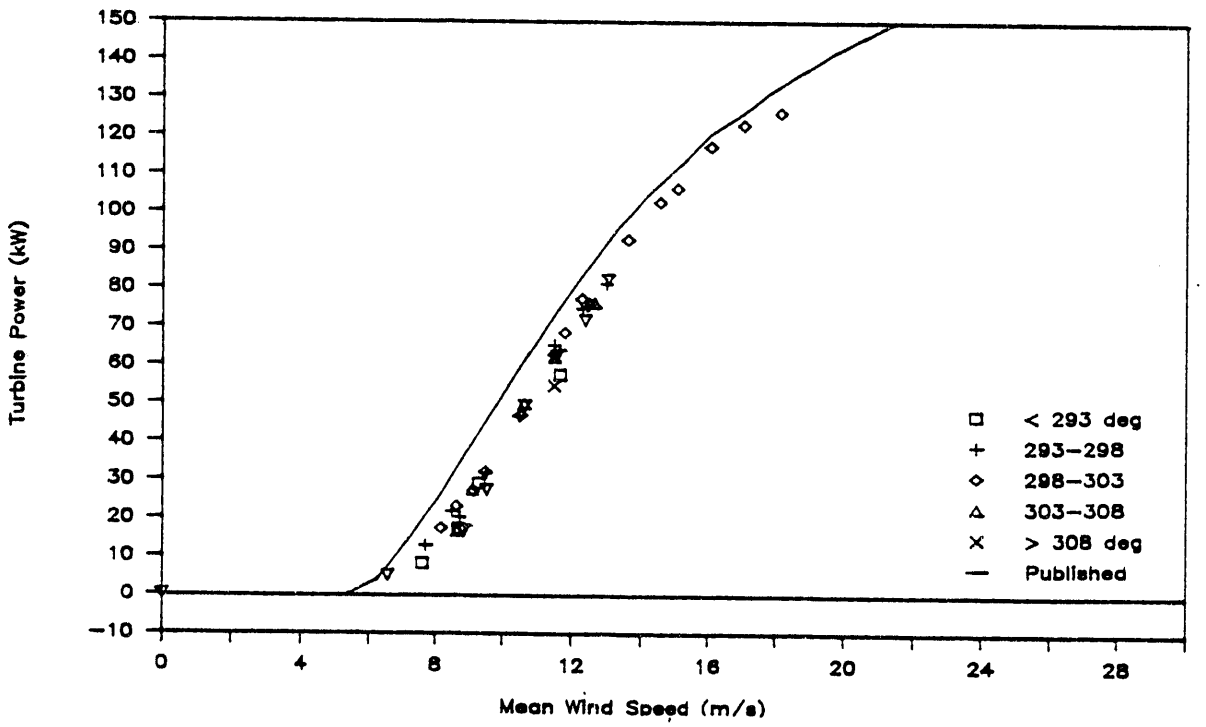

Figure 50. Power Curves of T102 with Upwind Row of Turbines Off and Wind Speed Measured at Reference Tower.

axis of the turbine/tower array. Here, we used the wind speeds measured at the same upwind tower (UVW1) to derive the power curve. At first glance, T102 appeared to be underperforming considerably compared to T122 through 124. In Section 5.1, we demonstrated that the mean wind speed meassured in the vicinity of the second row (T101 through T103) is consistently lower than that measured at the reference tower. As shown in Figure 13, the 5-day averaged mean wind speed measured at Stations 2011 and 2012 is between 6 and 7% lower than that measured at UVW1 or 2017. Figure 14 illustrates that the speed ratio at the two locations depends on the wind speed. Figure 51 replots the power curve using the adjusted wind speed based on the speed ratio. The dashed curve is a fairing to the measured data points. Now, the measured data compare reasonally well with the published curve, with data scatter comparable to that shown in Figure 47 but noticeably smaller than in Figures 48 and 49. The power curves of T103 and T101 adjacent to T102 (Figures 52 and 53) display similar features, with data scatter noticeably smaller than those of T122 and T123. This is consistent with the observation that the local topography in the vicinity of the second-row turbines is relatively flat and regular (Figure 4b). Furthermore, the correction for the wind speed that was used to general the power curves results in accurate representation of the local wind speed.

The power curves of the turbines in the second row show no trend of stalling at the high-wind-speed end. At these locations, the wind profile is recovering after rising from the valley floor. In the recovering process, the turbulent boundary layer thickens. The turbulence intensity at the equator height is expected to be higher at row 2 than at row 1. High ambient turbulence intensity is known to promote (intensify) dynamic stall, which would delay the stall to higher wind speeds (Liu, 1986a).

For the turbines in the third row, the power output from T78 did not yield the correct values, although we did not find anything wrong with the power transducer or with the circuitry. This happened after the replacement of a motor/generator during the field experiment. The power curves for T77 and T79, shown in Figures 54 and 55, are plotted using the wind speed measurements at the upwind reference tower (UVW1). An attempt was made to correct for the local terrain effects using the measurements at Stations 2015 (between T79 and T78) and 2016 (between T78 and T79), but there was too much scatter in the data. Figure 39 shows that the power output depends strongly on the wind direction. Apparently, the terrain feature at and upwind of T125, with the

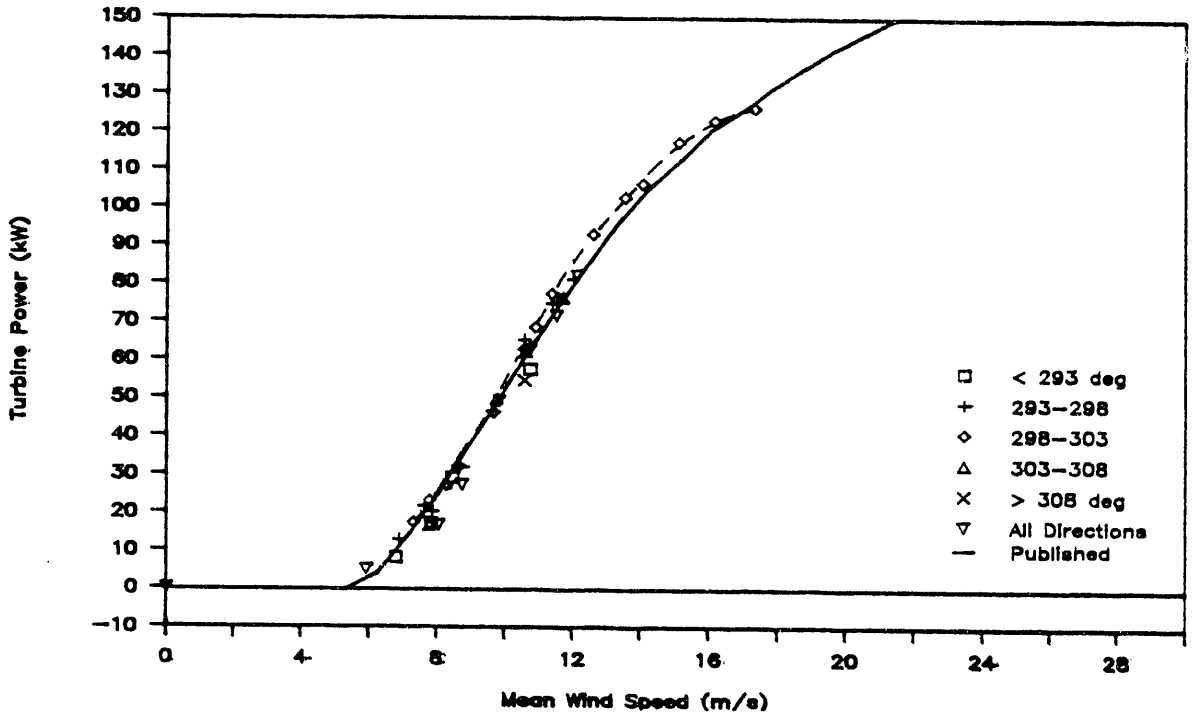

Figure 51. Power Curves of T102 with Upwind Row of Turbines Off and Wind Speed Corrected for Local Terrain Influences.

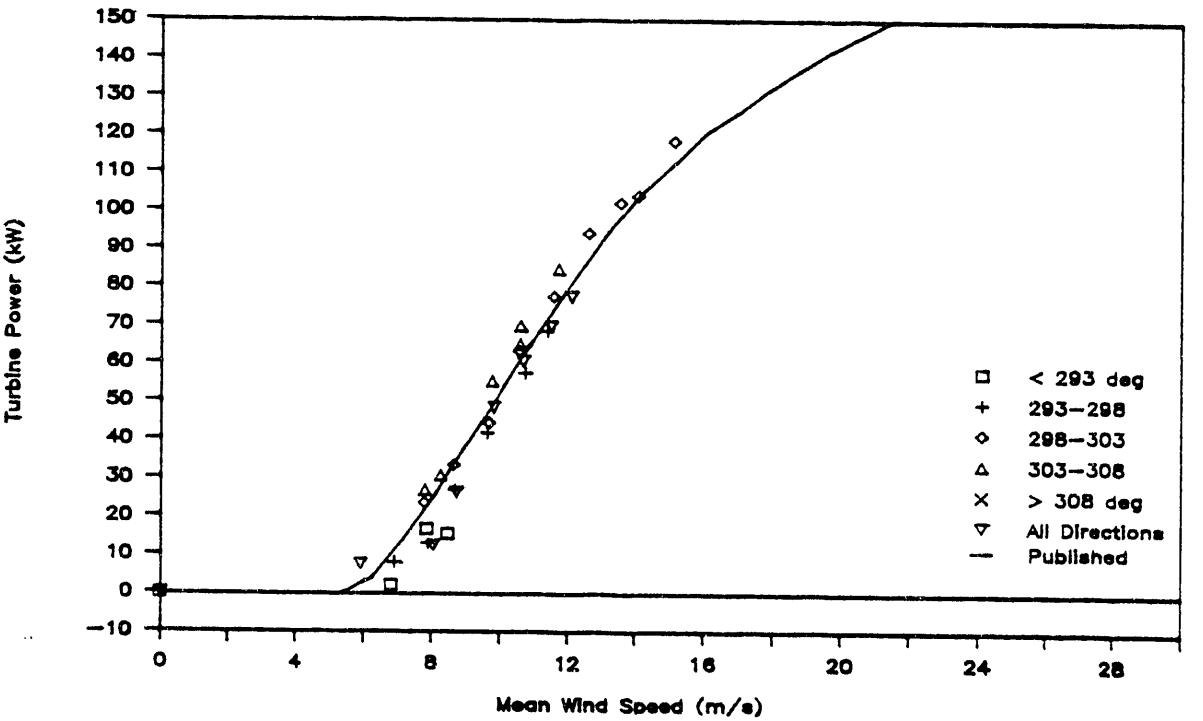

Figure 52. Power Curves of T103 with Upwind Row of Turbines Off and Wind Speed Corrected for Local Terrain Influences.

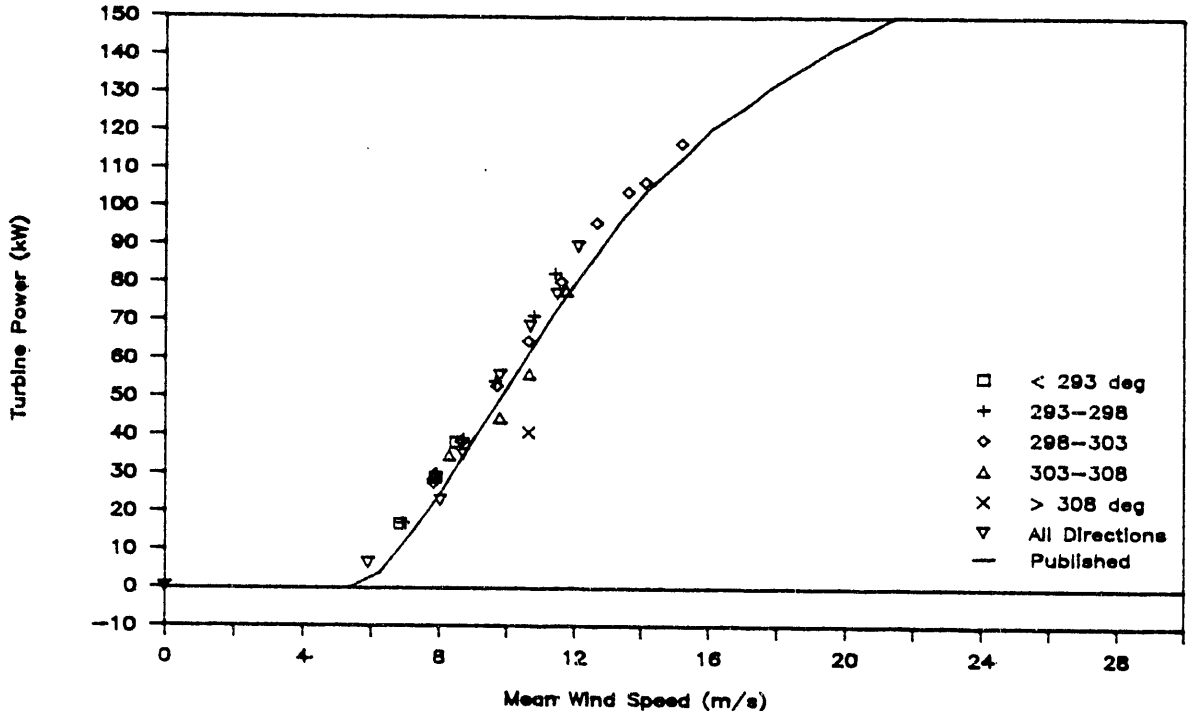

Figure 53. Power Curves of T101 with Upwind Row of Turbines Off and Wind Speed Corrected for Local Terrain Influences.

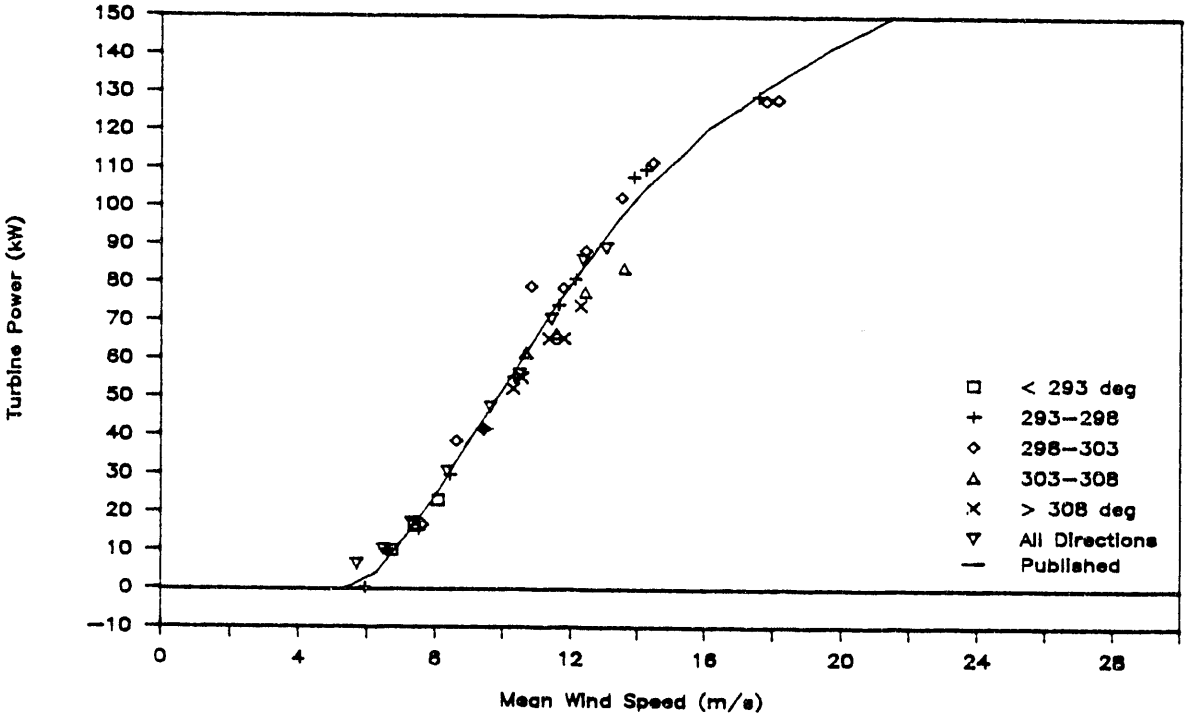

Figure 54. Power Curves of T77 with Two Upwind Rows of Turbines Off and Wind Speed Measured at Reference Tower.

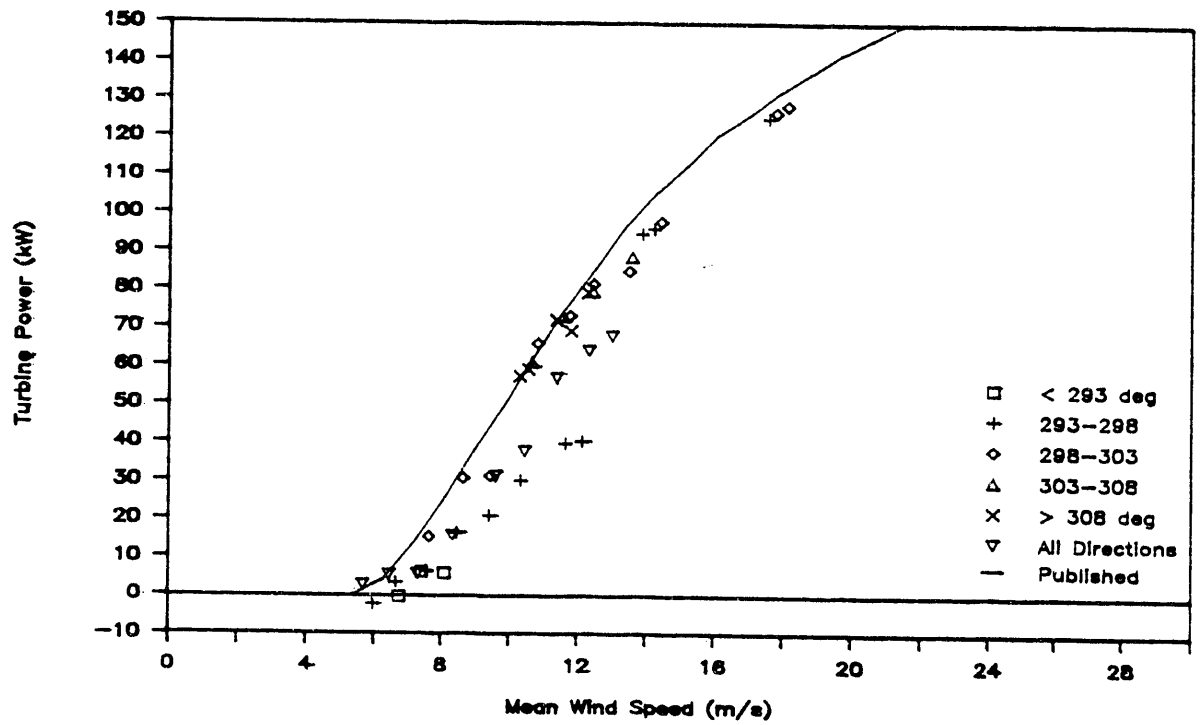

Figure 55. Power Curves of T79 with Two Upwind Rows of Turbines Off and Wind Speed Measured at Reference Tower.

gradient perpendicular to the predominant wind direction (Figure 4b), creates a shadow zone for wind directions less than 295 deg, especially at low wind speeds. This is also reflected by the data set without the wind direction measurements (inverted triangles). As a result, the data scatter is the worst of all cases presented. The power outputs from T77 compare surprisingly well with the published data, although the wind speed was measured at a distance 18D upwind. The lack of complicated terrain features along the upwind strip of this turbine is the main reason for maintaining a good spatial correlation of the mean wind speeds. For that reason and others, we chose T77 and T102 as the key turbines for assessing the array effects on the turbine performance.

5.3.2 Array Effects

Based on the performance and the relative positions of the turbines within the array, we selected T102 (second row) and T77 (third row) as the primary downwind turbines for assessing the array effects. Measurements from other turbines have been used, as needed, to confirm important findings and to illustrate potential deviations.

Power Loss or Deficit

In Figures 56 and 57, we present the power outputs from T102 with only the primary turbine (T123) and the first row of turbines (T122 through 124) turned on. These results may be compared with those shown in Figure 51 to estimate the power loss and deficit due to the presence of upwind turbine wakes. Here, we define the power loss as the difference between the power outputs in the absence and presence of upwind wakes; the power deficit, in the same sense as the velocity deficit, is defined as the power loss divided by the unobstructed power output. As anticipated, the power loss and deficit depend strongly on both the wind direction and wind speed. The maximum power loss occurs for wind directions in the range between 298 and 308 deg, which is consistent with the position of the wake and its center when the 5 deg mean shift is taken into account. The power loss tends to reduce with increasing deviation of the wind direction from that range. At the low-speed end, the trend of the data shows that the cut-in speed increases in the presence of upwind wakes. In practice, the cut-in wind speed should be modified to account for the power loss depending on the position of the turbines within the array. Otherwise, the turbines would be in the motoring mode, which would not only reduce the

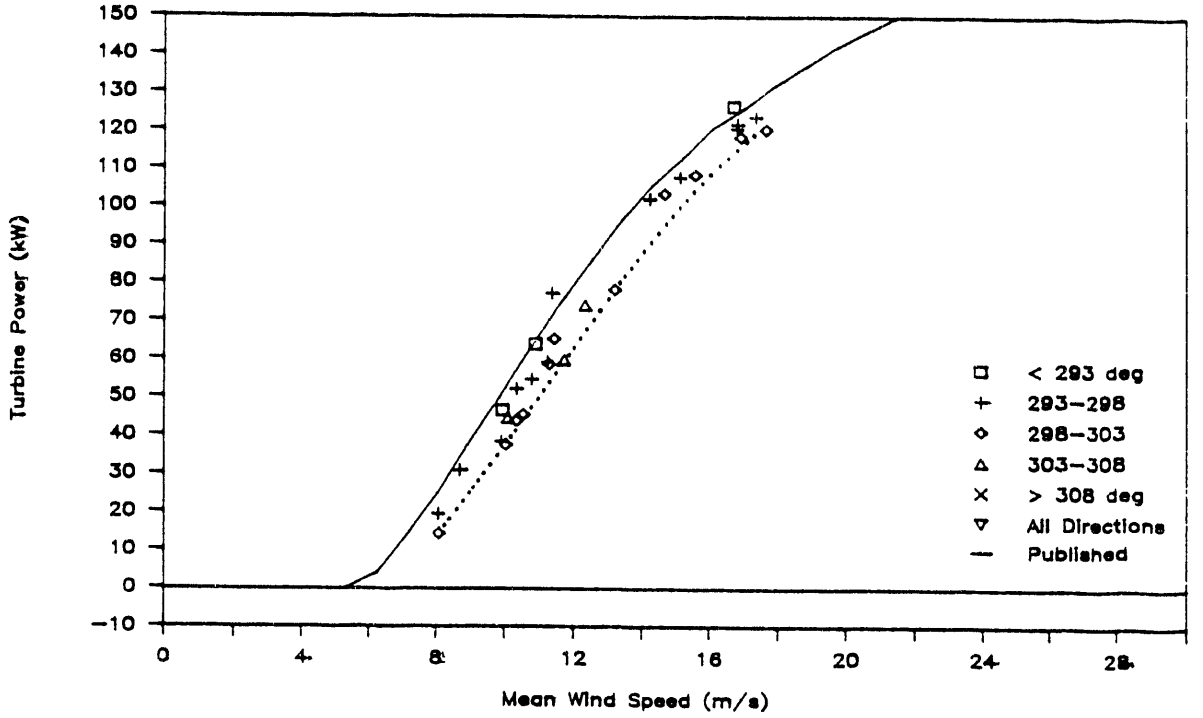

Figure 56. Power Curves of T102 with T123 On. The turbine power was sorted into 5-deg intervals and binned over 1-m/s increments.

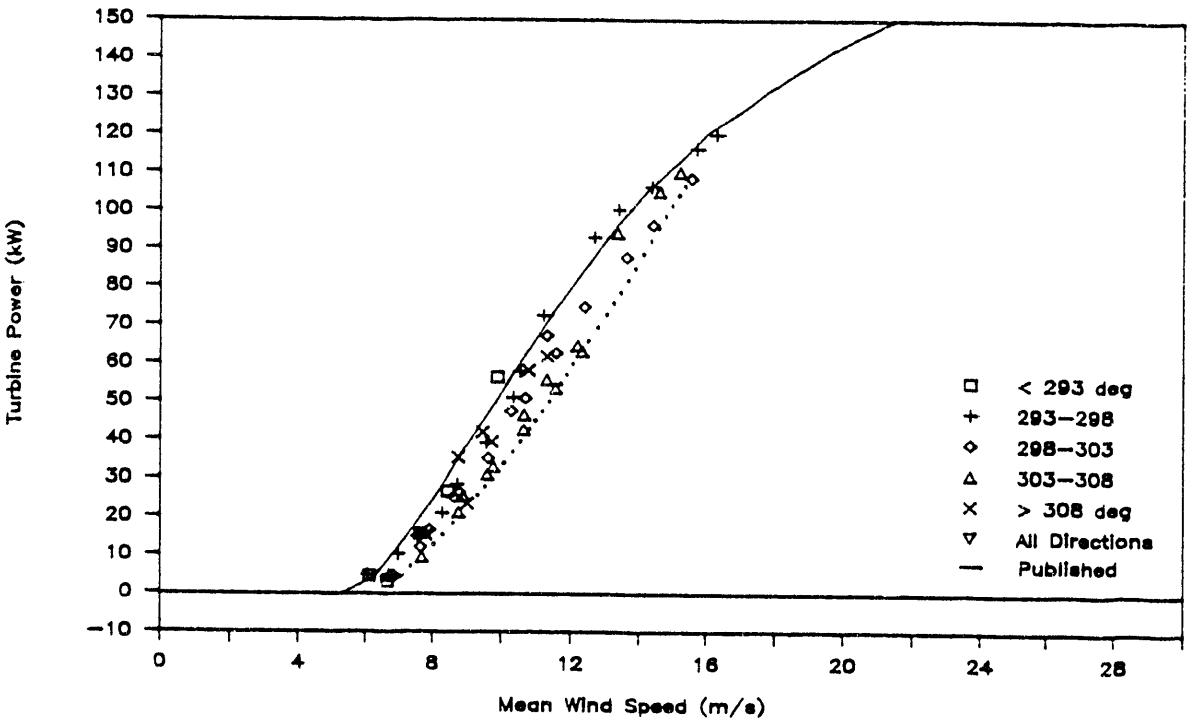

Figure 57. Power Curves of T102 with T122 Through T124 On. The turbine power was sorted into 5-deg intervals and binned over 1-m/s increments.

overall efficiency of the windfarm operation but also impose an extra burden on the control system due to the unnecessary increase in the number of on/off cycles. At the high-speed end, the power loss also tends to reduce, consistent with the decrease in the velocity deficit with increasing wind speed (Section 5.1). Consequently, the maximum power loss would be in the medium-wind-speed regime, in which the frequency of occurrence is also high. The optimum array configuration should be designed according to the predominant wind conditions.

In the figures, we have drawn a dotted curve as an envelope to show all the measured data that represent the maximum power loss. The maximum power loss is higher when T122 through T124 were on than when T123 was on alone, as expected. For example, the maximum power losses are roughly 22 and 18 kW at 12 m/s, and the corresponding power deficits are 0.27 and 0.22 for the two cases, respectively. At 15 m/s, the maximum power deficit reduced to about 7% for both cases. To estimate the average power deficit accurately, we have to incorporate the joint probability distribution of the wind direction and speed, $p(\theta, S)$, which may be constructed from the results similar to those shown in Figures 11 and 12, for a particular site:

$$\Sigma_\theta \Sigma_S \, p(\theta, S) \, P_d(\theta, S) \qquad (3)$$

where $P_d(\theta, S)$ is the measured power deficit, S is the wind speed and θ is the wind direction.

Figures 58 through 60 present the power outputs from T77 with the first row of turbines (16D), the second row (8D), and both first and second rows on, respectively. In these cases, the data stratification was a little low to cover all the regimes of wind speed and direction of interest. It is, however, sufficient for detecting the data trend to support and extend the observations made above. With the first row of turbines turned on, the power loss at T77 is about 3% due to the presence of the wakes generated 16D upwind, although there were no data available at wind speeds between 9.5 and 11.5 m/s. In this case, the orientation coincident with the alignment between T123 and T77 is 299 deg. With the second row of turbines turned on and the first row turned off, the power loss at T77 increases noticeably and displays a similar trend to that illustrated in Figure 41 for T102. The maximum loss is observed for wind directions greater than 303 deg, which indicates that the loss is due mainly

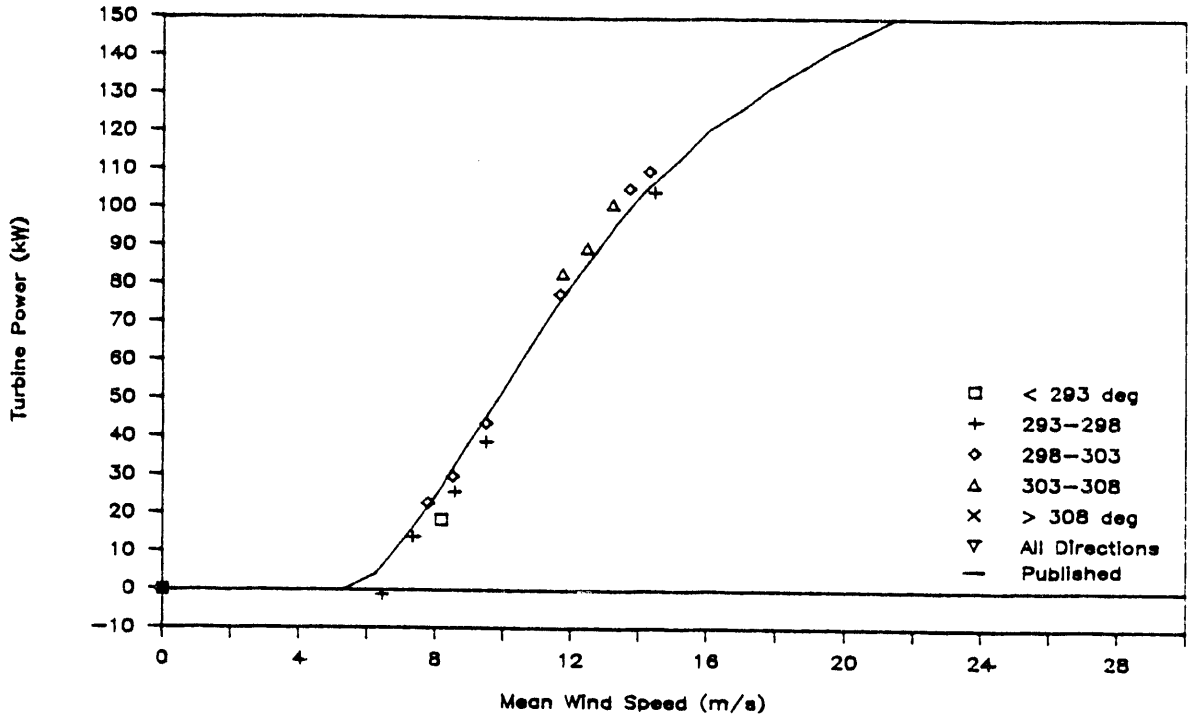

Figure 58. Power Curves of T77 with T122 Through T124 On (16D Upwind).

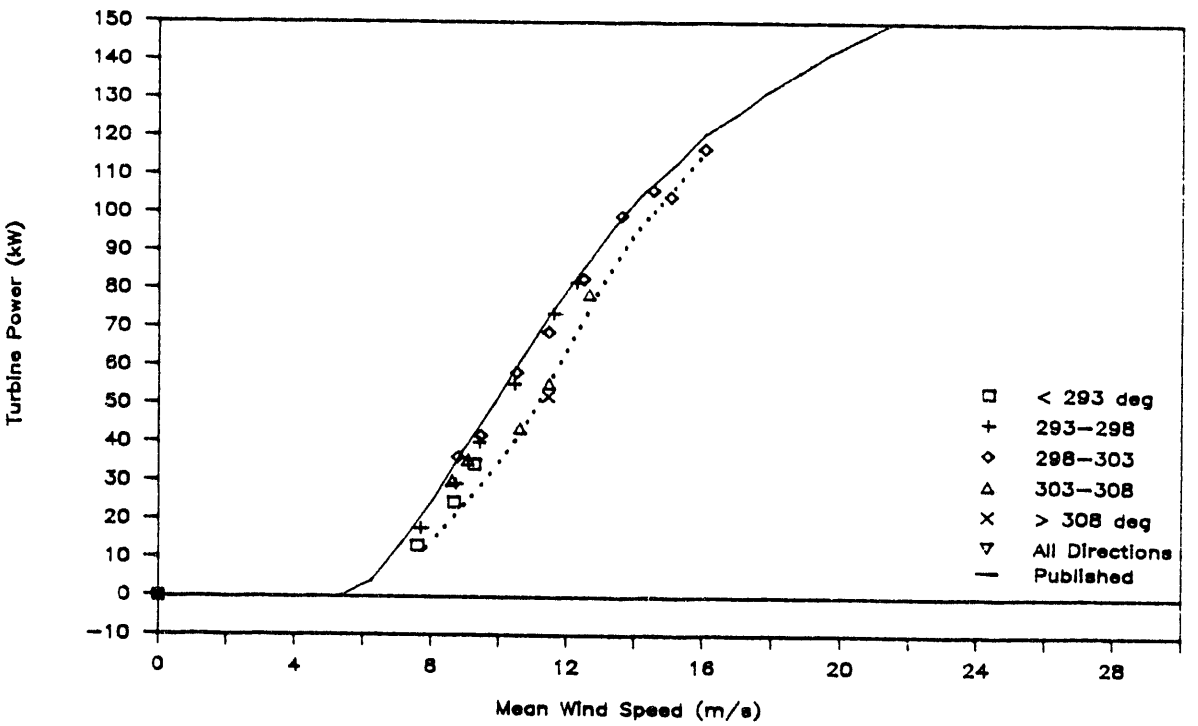

Figure 59. Power Curves of T77 with T102 Through T103 On (8D Upwind).

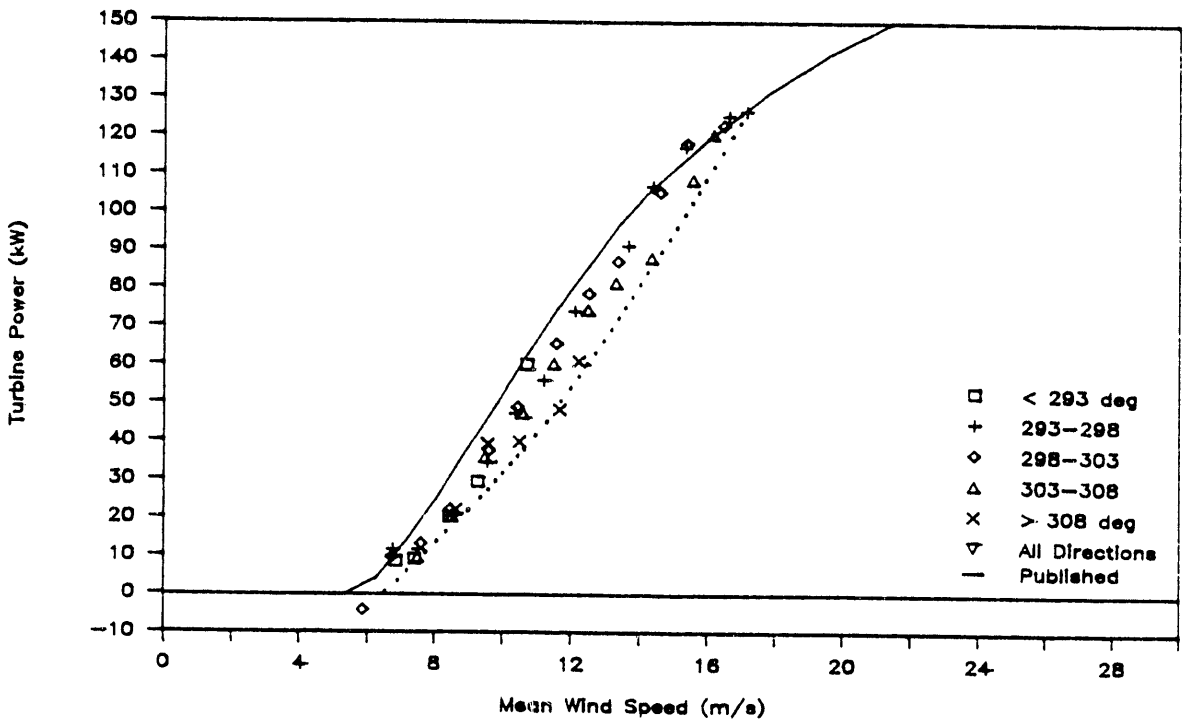

Figure 60. Power Curves of T77 with T122 Through T124 and T102 Through 103 On.

to the wake of T101 (aligned with T77 at 312 deg). The contribution from the wake of T102 (aligned with T77 at 290 deg) is depicted by the rectangles. When the shift in the wake and its center is accounted for (Section 5.2), the maximum effects of the upwind turbine wake would be at an effective wind direction slightly below the angle of the alignment between the two turbines under consideration. It should be pointed out that the frequency of occurrence of wind directions below 293 deg and beyond 305 deg is quite low, as shown in Figure 12. In addition, the wind speed is generally low for wind directions below 293 deg; the total energy generated in this wind regime is insignificant. Under the predominant wind conditions, i.e., wind directions between 297 and 303 deg, the wind is essentially blowing inbetween T101 and T102, creating the least obstruction when the second row of turbines is turned on. The power loss further increases with both the first and second rows of turbines turned on.

Energy Loss or Deficit

To provide a reasonable estimate of the power deficit within the turbine array, we averaged the power outputs over all the wind directions, which effectively takes into account the probability distribution of the wind direction at the test site during the field experiment. The corresponding wind speed and direction distributions for that period are shown in Figure 61; the mean wind speed and directions are 10.7 m/s and 300 deg. Figures 62 through 65 illustrate the turbine power averaged over all directions for T102, T103, T101, and T77, respectively. Based on these results, we may estimate the total in-wake energy production, E_w, during that period by summing up the product of the frequency occurrence of the wind speed bins and the power output, or

$$E_w = \Sigma_S \, P_w(S) \, p(S) \tag{4}$$

where $P_w(S)$ is the in-wake power output averaged over all wind directions and $p(S)$ is the probability distribution of the wind speed. Similarly, the corresponding energy production in the absence of upwind wakes, E_o, is

$$E_o = \Sigma_S \, P_o(S) \, p(S) \tag{5}$$

where $P_o(S)$ is the unobstructed power output. Conversion of the energy to kilowatt-hours may be made by dividing the sum by 8 to account for the 7.5-min

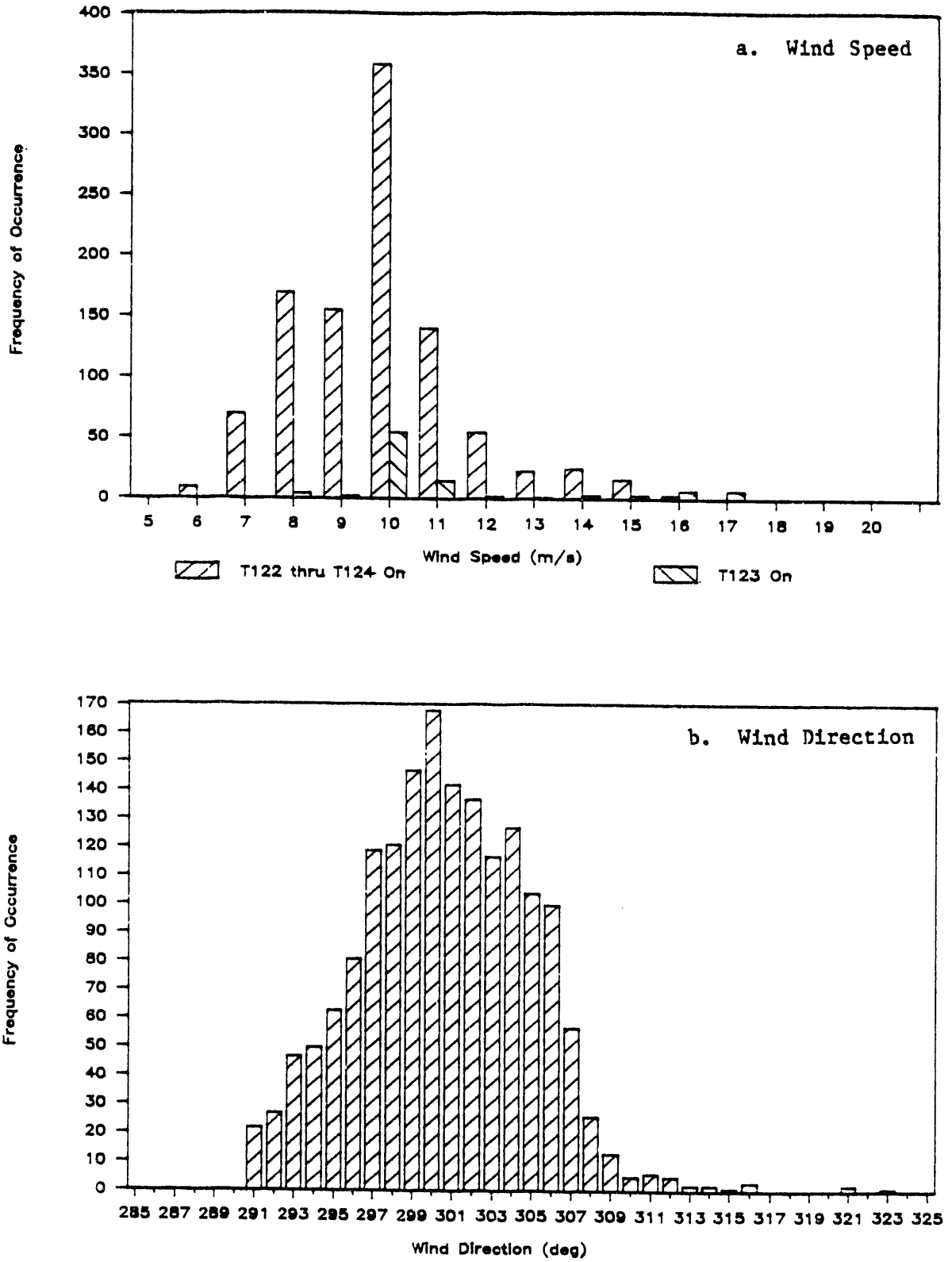

Figure 61. Distributions of the Wind Speed and Direction Derived from the Wind Data Measured During the Field Experiments.

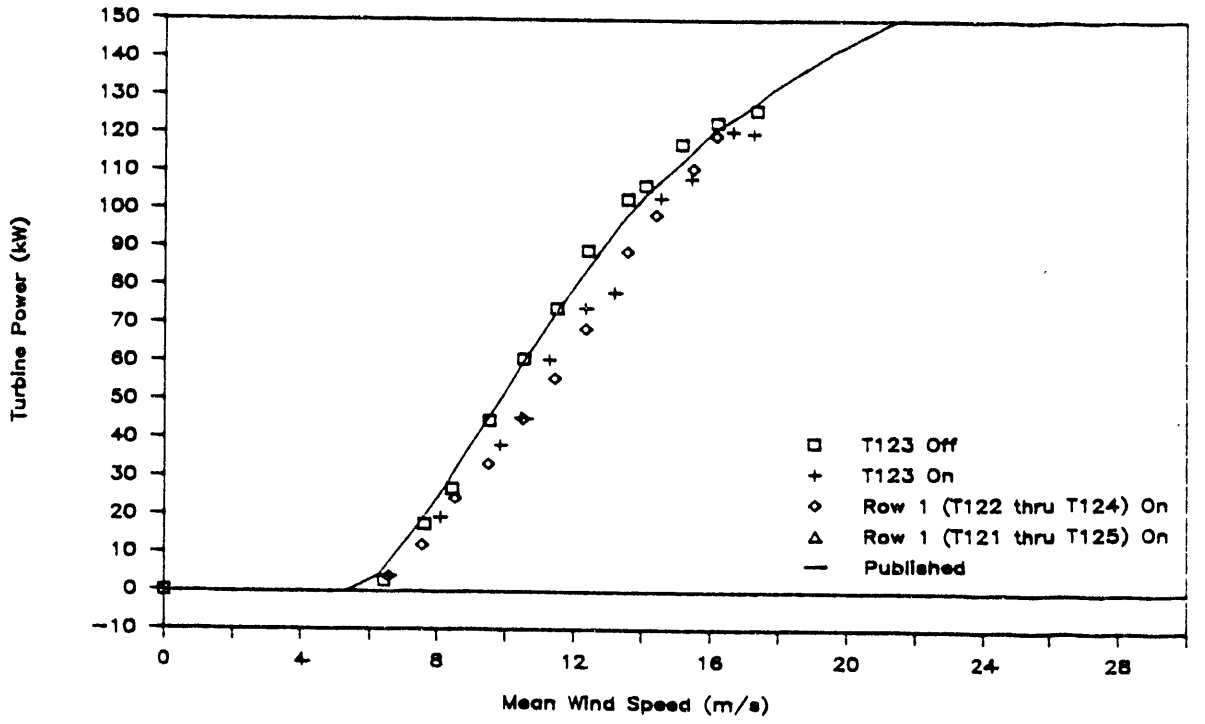

Figure 62. Turbine Power Averaged over All Wind Directions for T102.

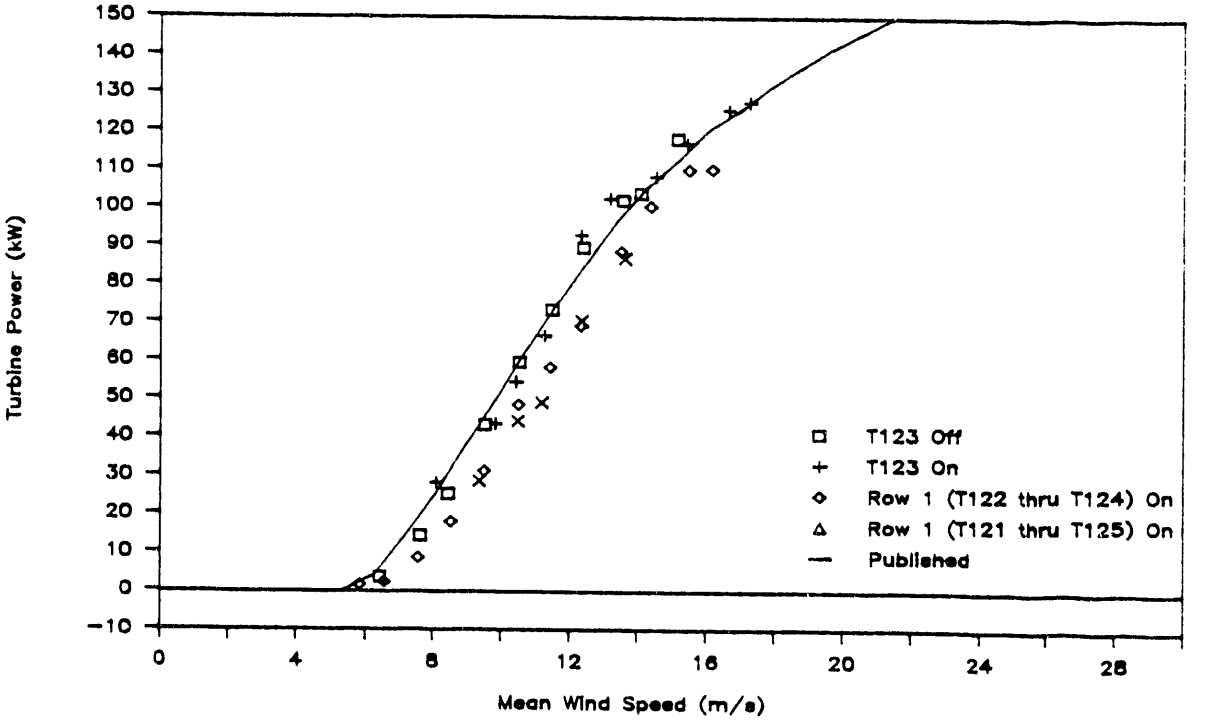

Figure 63. Turbine Power Averaged over All Wind Directions for T103.

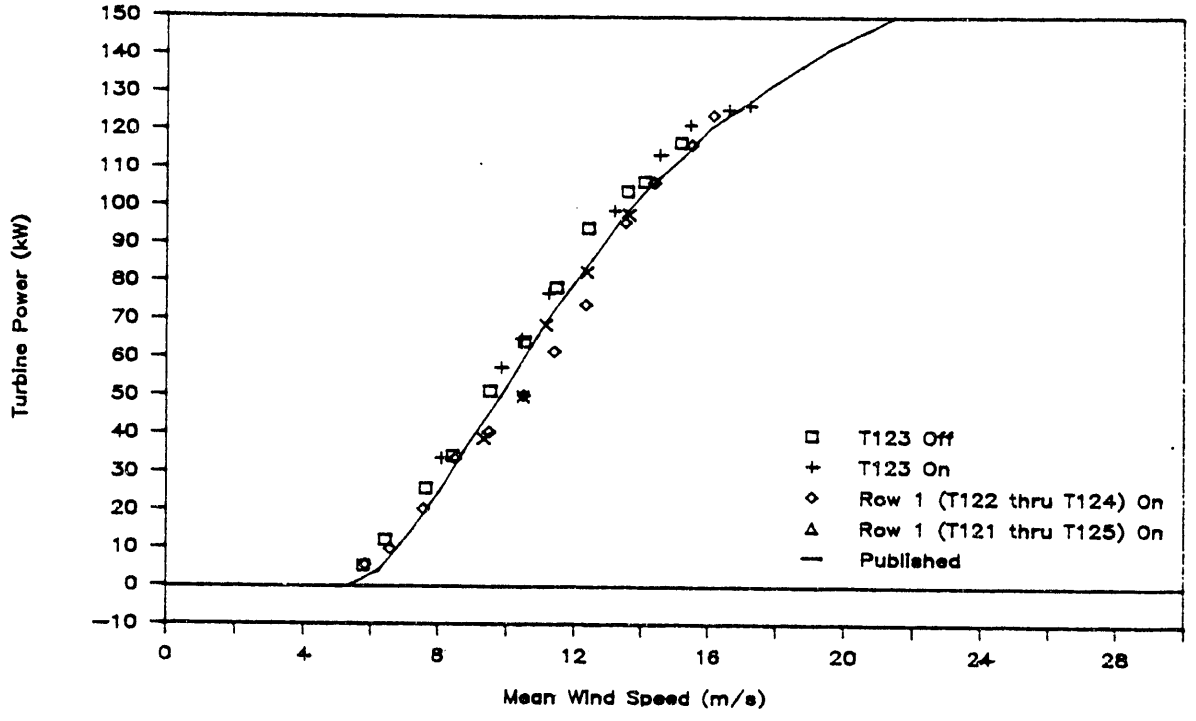

Figure 64. Turbine Power Averaged over All Wind Directions for T101.

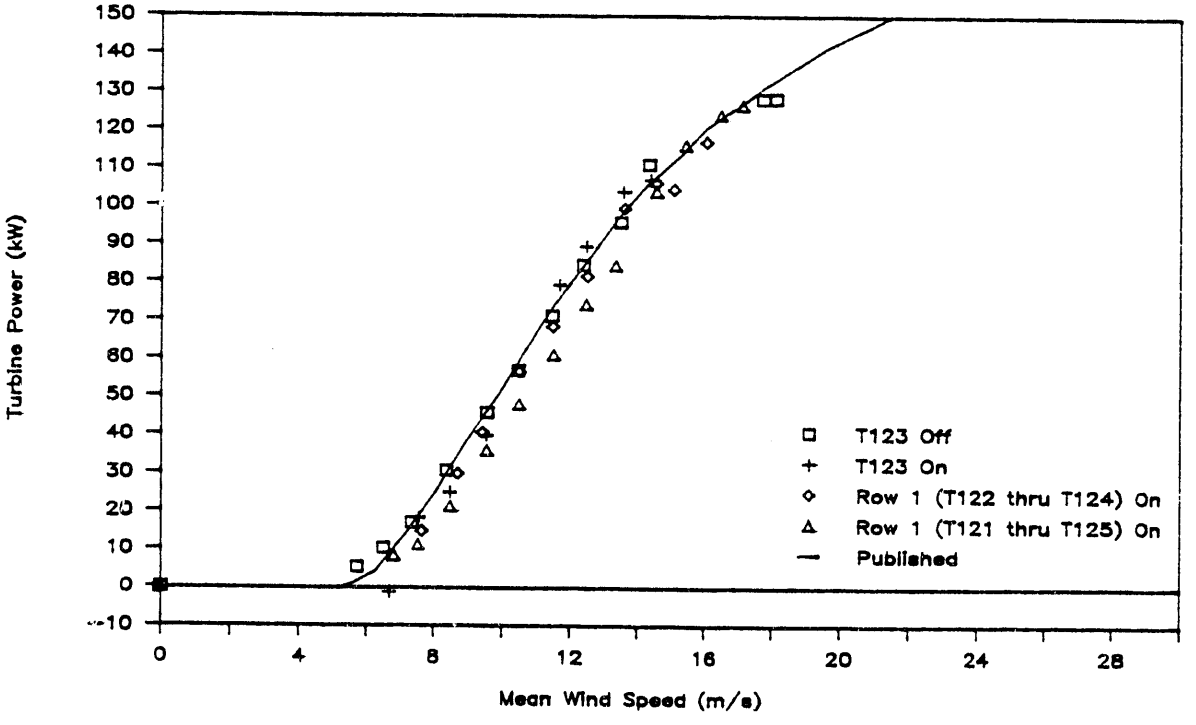

Figure 65. Turbine Power Averaged over All Wind Directions for T77.

averages. The difference between the unobstructed energy output and the in-wake energy output is the energy loss, E_l:

$$E_l = E_o - E_w \quad , \tag{6}$$

and the normalized difference is the energy deficit, E_d:

$$E_d = E_l / E_o \quad . \tag{7}$$

The energy deficit measured from the four turbines under various turbine on/off configurations together with the corresponding sampling size is listed in Table 3

From the energy loss measured at T101 through T102, several trends are evident. First, the results from T102 show that the energy deficit is about 14% when T123 was on and increases to 20% when T122 through T124 were on. Because the predominant wind direction between 297 and 303 deg essentially aligned the wake of T123 with T102, especially when the 5-deg mean shift of the wake is taken into consideration, the energy deficit represents the maximum value. With the addition of the wakes of the two outside turbines, T121 and T125, the energy deficit drops about 2%, which is within the error of the measurement. In other words, the presence of the wakes of these two turbines

Table 3. Energy Deficit Estimated from the Field Data

	T101	T102	T103	T77
T123 On [12.4 hrs]*	-0.004	0.14	0.03	----
Row 1 (T122 through T124) On [126 hrs]	0.17	0.20	0.20	0.03
Row 1 (T121 through T125) On [2.5 hrs]	0.11	0.18	0.21	----
T102 On [3.4 hrs]	----	----	----	-0.003
Row 2 (T101 through T103) On [24.2 hrs]	----	----	----	0.05
Rows 1 and 2 (T101 through T103 and T122 through T124) On [202 hrs]	----	----	----	0.15

*Numbers in brackets are total hours of samples.

has little influence on the power generated at T102. The energy deficits of T101 and T103 are insignificant when T123 was on, as the predominant wind direction is off the alignment between T123 and T101 or between T123 and T102. The energy deficits of these two turbines increase to 17 and 20%, respectively, when T122 and T124 were on. Again, there is little change in the energy losses when the outside two turbines T121 and T125 were turned on, with the exception of a 6% drop for T101. The significance of the results with T121 through T125 on, however, should be de-emphasized due to the relatively small sample size (i.e., 2.6 hr).

The last column in Table 3 lists the energy deficits at T77. The energy deficit is about 3% with T122 through T124 (row 1) on. There is only a slight increase of about 2% when T122 through T124 were off and T101 through T103 (row 2) were on. As discussed earlier, the predominant wind with a direction around 300 deg blew through the gap between T101 and T102 and avoided direct impact of either wake on T77, resulting in a 0% deficit when T102 was on. Consequently, the wake effects from the second row of turbines are minimized, leading to a relatively small energy deficit. The energy loss jumps from 5% to 15% when both upwind rows of turbine were turned on, indicating a nonlinear enhancement of the wake effects. Under these configurations, the void between the two wakes generated from T101 and T102 is filled in by those generated from T122 through T124. It is anticipated that a large energy deficit would result if all three turbines are lined up with the predominant wind direction.

Comparison of the energy losses between T102 and T77 operating in a similar array configuration indicates that the wake-producing turbine directly upwind of the energy-producing turbine has the most impact when the predominant wind direction aligns with the orientation of the two turbines. The presence of upwind wakes immediately adjacent to the primary upwind turbine has secondary effects on the energy production of the downwind turbine. The wakes from the turbines farther away crosswind from the primary turbine have practically no influence on the energy production of the downwind turbine of interest. From results presented in Figures 62 through 64, we estimated the power deficit averged over all wind directions as a function of the mean wind speed. The general trend of decreasing power deficit with increasing wind speed is observed from Figure 66, in which the power deficits of the three turbines T101 through T103 are plotted with the second row of turbines (T122 through T124) turned on. By and large, the trend of decreasing power deficit with

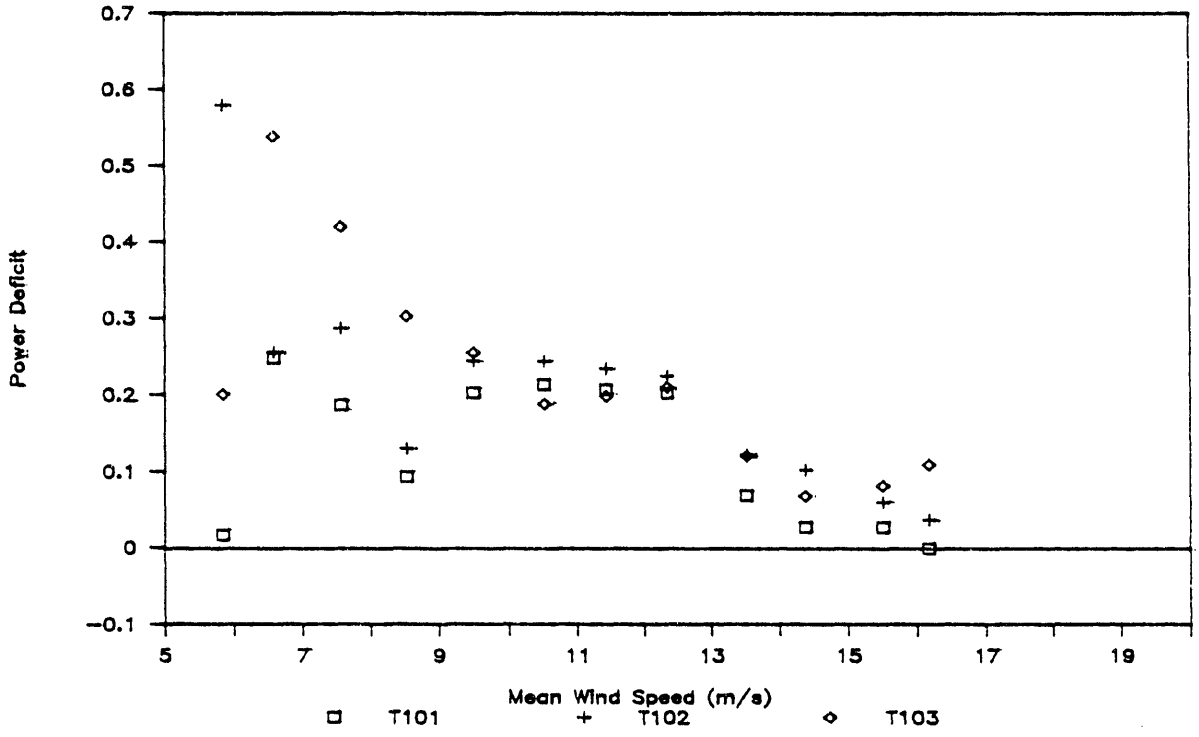

Figure 66. Turbine Power Deficits Averaged over All Wind Directions for T103, T102, and T101 with Various Turbine On/Off Configurations.

increasing wind speed is evident for wind speeds above 9 m/s. At the low-wind-speed end, the trend is not obvious because of the relatively large amount of data scatter that appears when the turbine power is low and the turbine may be operating in and out of motoring and generating modes. In addition, we anticipate that the wind field would be more susceptible to the influence of local terrain features, which could be a main source of the large data scatter. We believe that the envelope of the data for wind speeds below 9 m/s would be a reasonable representation of the power deficit, judging from the results of the velocity deficit and power loss discussed above. For practical purposes, however, the power deficit at low wind speeds should have insignificant contribution to the total energy loss, because the total energy is derived from medium- to high-wind-speed regimes.

The energy loss of 15 to 20% measured during the field experiment represents the high-end value and is not a realistic representation of the annual energy loss at the Tehachapi site. There are two major factors that would significantly reduce the annual energy loss. The first pertains to the practical limit of turbine availability for energy production. On the average, we would expect the availability of the turbines for energy production to be about 90 to 95%. This would allow downtime for repair and regular maintenance of the turbines. In other words, any upwind turbine would be on 90 to 95% of the time, with somewhat lower probability when all upwind turbines are on simultaneously. As a result, the overall power deficit would be lower than that obtainable with the entire upwind rows of turbines on simultaneously. Consider a 95% availability, a reduction of 7% in the energy loss is expected when the probability of the on/off configurations of the upwind row is taken into account (20% reduction for 90% availability).

The second factor relates to the wind-speed dependency of the power deficit and the annual wind speed distribution. From Table 1, the hourly averaged wind speeds measured at the Tehachapi site in July and August were among the lowest for 1984-85. High wind speeds were measured during the months of April through June and October in those two years. The annual average is about 1.22 times higher than the July or August average according to Table 1. The higher the averaged wind speed, the lower the energy loss results, because the power deficit decreases with increasing wind speed (Figure 65).

The actual energy loss may then be estimated according to Equations (4) through (7) by using the power deficit (Figure 66), the actual wind speed

distribution for a particular site, and the unobstructed power curve of the turbine under consideration. Correction may be made by taking into account the availability of the turbines for energy production.

For illustration, we will estimate the annual energy loss for 1986. The actual and predicted wind speed distributions are given in Table 4. From Equations (4) through (7), the annual energy loss is estimated to be 11%. Here, the power deficit used in the above derivation corresponds to the envelope of the data presented in Figure 66. When a 95% availability is assumed, the 11% loss further reduces to 10%, which is half the 20% deficit measured during the field experiment.

By the same token, assuming the energy deficit may be linearly superposed, the annual deficit for a turbine two rows downwind would add less than 3% to the 10% value. The 3% deficit, which corresponds to that measured at T77 with the upwind row of turbines at 16D (Table 3), reduces to about 1.5% when the 1986 wind speed distribution is used at 95% availability.

In an operating windfarm, the terrain is often more rugged than at the test site. Perfect alignment of more than two to three rows in both vertical and crosswind directions may be quiet difficult. Under this condition, the array effects reduce significantly, while micrositing effects become important.

Table 4. 1986 Observed and Projected Hourly Wind Speed Distribution (Station 2101)

Observed Mean Speed: 18.4 m/s
Projected Mean Speed: 20.9 m/s

Wind Speed (m/s)	Frequency of Occurrence		Wind Speed (m/s)	Frequency of Occurrence	
	Measured	Projected		Measured	Projected
0.45	237	74	18.3	75	77
0.89	128	140	18.8	84	71
1.34	162	155	19.2	68	68
1.79	216	172	19.7	53	61
2.24	268	207	20.1	45	57
2.68	332	224	20.6	54	53
3.13	344	254	21.0	37	48
3.58	370	265	21.5	34	44
4.02	396	284	21.9	29	40
4.47	391	293	22.4	22	36
4.92	387	295	22.8	20	34
5.36 (cut-in)	410	299	23.2	14	29
5.81	408	298	23.7	15	27
6.26	342	294	24.1	14	23
6.70	292	294	24.6	7	21
7.15	250	285	25.0	13	18
7.60	196	281	25.5	4	15
8.04	169	274	25.9	13	13
8.50	167	265	26.4	3	11
8.94	169	256	26.8 (cut-off)	5	9
9.39	151	246	27.3	3	7
9.83	168	235	27.7	4	5
10.3	138	223	28.2	3	4
10.7	150	211	28.6	0	4
11.2	141	199	29.0	1	3
11.6	152	188	29.5	0	3
12.0	138	176	30.0	1	3
12.5	151	167	30.4	0	3
13.0	157	157	30.8	0	2
13.4	140	149	31.3	0	2
13.9	128	141	31.7	0	2
14.3	116	133	32.2	0	1
14.8	115	127	32.6	0	1
15.2	109	118	33.0	0	1
15.6	105	113	33.5	0	1
16.1	106	107	34.0	0	1
16.5	91	99	34.4	0	1
17.0	95	96	34.9	0	0
17.4	77	87	35.3	0	0
17.9	77	82	35.8	0	0

6. SUMMARY AND RECOMMENDATIONS

In this section, we summarize the important findings derived from the field experiment. Several findings have shed light on the wake structure of a VAWT and the effects of upwind wakes on the performance of downwind turbines. Based on these findings, recommendations are made to advance our understanding of VAWT array effects and to optimize the design and operation of windfarms.

6.1 Summary

From the field data, we derived a wide range of information, including the ambient wind field and the velocity and power/energy deficits, under various turbine on/off configurations. Our strategy was to obtain measurements of the maximum array effects as the first priority and then to obtain progressively subtle variations. In the following, we summarize the important findings regarding array effects on turbine performance. These findings could lead to the development of practical criteria and guidelines for turbine designers and manufacturers, windfarm developers and operators, and utilities, with a final goal of establishing a cost-effective wind energy system as a viable means for generating safe and clean energy.

6.1.1 Ambient Wind Field

(1) Under normal meteorological conditions, the ambient wind field is thermally driven and displays a relatively consistent pattern, as shown in Figures 9 and 10. The wind speed record shows the presence of two main troughs at about 6:00 and 11:00 with speeds below the cut-in value of 5.4 m/s. After the second trough, the wind speed continues to rise and peaks in the late afternoon. In the presence of a weak high-pressure system off the coast, the wind blew all day long and the thermal effects became secondary. For wind speeds above 9 m/s, the wind direction is confined within a narrow window between 295 and 310 deg.

(2) The terrain in the vicinity has a gentle upslope of 7 deg on the average. Several local features, such as a change in the local slope, a small gorge near T122 and a turn on the upslope hill with a gradient perpendicular to the predominant wind direction near T125, create some perturbations to the otherwise relatively uniform ambient wind field. For example, the mean wind speed in the vicinity of the second row of turbines (T101 through

T103) is lower than that measured at the upwind reference tower by up to 10% depending on the wind speed. A reduction on this order should be taken into account when the power curve of a particular turbine is constructed.

(3) The vertical wind profiles at -2D and 3D reveal several characteristics typical of a developing boundary layer (overspeed zone), as the flow rises from the valley floor to the top of Cameron Ridge. No flow reversal, however, was experienced at any part of the upslope region upwind of the turbine/tower array, as is in the case of flow over a bluff (Walker and Wade, 1987). The vertical shear is significantly weaker at -2D than at 3D. It increases with increasing wind speed at -2D, but the trend reverses at 3D. Consequently, the difference in the shear between the two locations decreases with increasing wind speed, indicating that the recovery of the developing boundary layer requires a shorter fetch to complete when the wind speed, and thus the terrain-generated turbulence, increases.

6.1.2 Velocity Deficit

(1) The background velocity deficit with all the turbines turned off displays a similar pattern at various locations, although the absolute values differ (Figure 16). The background deficit was subsequently removed from the velocity deficit derived from various turbine on/off configurations. There is a significant change in the trend of the background deficit at wind speeds below 7 m/s, including a sharp increase in the wind direction with increasing wind speed. At these low wind speeds, the turbines often operated in a transition state between the modes of generating and motoring, especially when the wind field was highly fluctuating. Therefore, interpretation of the results should be made with discretion in this low-wind-speed regime.

(2) From the velocity deficit measured along the major axis of the turbine array (308 deg), we discovered several important findings:

- The maximum velocity deficit was detected in the wind direction bin between 298 and 303 deg, which is about 5 to 10 deg off the major axis of the turbine array. Such an offset in the wake center is due to asymmetry induced by the rotation of the blades, as discussed in Section 5.2.3.

- When the primary turbine (T123) is turned on alone, the maximum velocity deficit tends to decrease linearly with increasing wind speed and asymptotically to zero at the high-wind-speed end. This trend reverses at the low-wind-speed end at distances as close as 3D when the two turbines adjacent to T123 (T121 and T122) are also turned on. Such a trend reveral is an indirect effect due to additional unsteadiness (vortex shedding) and turbulence generated by the adjacent turbines, because significant overlapping of the wakes is not expected at such a short distance. This finding is consistent with the prediction of a shorter near-wake length by Lissaman et al. (1982) as one of the major array effects. As the wind speed or Reynolds number increases, the ambient turbulence becomes stronger while the blade-to-wind speed ratio reduces, which in turn reduces the effectiveness of the turbine-generated turbulence. As a result, no noticeable difference was observed in the maximum velocity deficit for wind speeds beyond 10 m/s.

- The vertical gradient of the velocity is higher below 13.7 m than above (Figures 16 and 32). This is a direct consequence of the presence of the vertical wind shear with high turbulence near ground level in the developing boundary layer. The high turbulence enhances entrainment and mixing near the ground and reduces the velocity deficit accordingly.

(3) From the cross-wake profiles of velocity deficit, we derived additional information some of which is typical of wakes generated by VAWTs:

- Other than the trend reversal of decreasing velocity deficit with increasing wind speed at low wind speeds, there are no other systematic differences detectable from the cross-wake deficit profiles in wakes generated by a single turbine and by a row of turbines separated by 3D. This indicates that any perturbations on the velocity deficit are less than 3 to 5%, which is the minimum level that can be detected from the deficit data due to the inherent relatively high scatter in the wind speed data.

- o The cross-wake deficit profiles with T123 on and T122 through T124 on all show a shift in the wake and its center with a maximum value of about 10 deg in the near wake (1.5D) at low wind speeds below 9 m/s. The shift reduces with increasing wind speed and with increasing downwind distance. A mean shift of about 5 deg is observed at 5D and 6.5D.

- o The wake width in a linear dimension increases with increasing downwind distance but at a rate below that of a constant-angle spread. At a given downwind distance, the wake width decreases with increasing wind speed. This indicates that the increase in entrainment and mixing that leads to wake spread does not keep up with the pace of the increase in advection that limits the wake spread. Outside the wake, there exists an accelerating zone exists, as demonstrated by the presence of a negative velocity deficit.

6.1.3 Power and Energy Deficit

(1) The power curves constructed from the power measurements during the field experiment compare well with the published data by FloWind (Figure 47), with the wind sensor located 2D upwind of the turbine. The agreement deteriorates with increasing separation between the wind sensor and the turbine (Figures 48 through 50). Good agreement may be restored once the local terrain effects on the wind speed are accounted for (Figure 51). At wind speeds beyond about 15 m/s, the power curves of two of the nine turbines (T123 and T124) level off, a symptom of a premature stall of the blades. Our experience in unsteady aerodynamics (Liu, 1986b; McCroskey, 1981) leads us to believe that the symptom is related to the dynamic stall phenomenon. The two turbines showing the stall symptom are located at the leading edge of Cameron Ridge where the turbulent boundary layer is relatively thin (Figure 15). In a steady flow, vigorous dynamic stall is unlikely to take place. Thickening in the boundary layer may promote dynamic stall for the downwind turbines, which greatly delays the stall to higher wind speeds.

(2) From the power curves of T102 and T77 derived from measurements under various turbine on/off configurations, the array effects on the performance of downwind turbines are clearly observed while the velocity deficit is not apparent.

- The turbine power measurements are direct means of gauging the effects of wakes generated by upwind turbines. The power loss and deficit derived from turbine power outputs under various turbine on/off configurations provide reasonably accurate information to assess the array effects, while the corresponding velocity deficit fails to do so. One of the main reasons favorable to the power output is that it is proportional to the third power of the wind speed. In addition, the array effects can only be estimated by areal integrating the velocity deficit profiles derived from extremely limited point measurements.

- The power loss or deficit depends on both the wind speed and direction, as anticipated. For an array with 8D downwind by 3D crosswind separations, the primary wake-producing turbine has the dominant effects on the performance of the downwind turbine. The turbines immediately adjacent to the primary turbine have only secondary effects, whereas the turbines farther away have insignificant effects. The power deficit reaches a maximum when the predominant wind is in the direction that aligns the wake of the upwind primary turbine with the downwind turbine under consideration. For a realistic representation of the power loss or deficit, the values averaged over all wind directions were used. The power loss maximizes at medium wind speeds around 12 m/s, whereas the power deficit tends to descrease with increasing wind speed (Figure 65).

- The above finding indicates that the cut-in speed for a VAWT within an array should increase according to the number of rows of upwind turbines. Otherwise, the turbine would be operating frequently in the motoring mode as a result of the induced power deficit in the presence of the upwind turbine wakes. This not only reduces the turbine efficiency in power production but also imposes an extra burden on the control system, thus shortening the lifetime of components such as brake shoes due to an unnecessary increase in the number of on/off cycles.

- The energy production of a turbine during the field experiment was derived by summing the product of the wind-speed frequency of occurrence and the power output in the corresponding wind-speed bin. The energy deficit is then the difference between the unobstructed energy and the in-wake energy normalized by the former. During the field experiment from mid July to early August, the energy deficits of T102 in the second row were measured to be about 14% and 20% when the primary turbine (T123) and the upwind row of turbines (T122 and T123) were on, respectively. The power deficits of T77 in the third row under similar conditions show noticeably lower values, 0% and 5%, due to misalignment of the predominant wind direction with the orientation of the wake-producing turbine (T102 or T101) and T77. When the first row of turbines (T122 through T124) and both the first and second rows of turbines (T122 through T124 and T101 through T103) were on, the power deficits of T77 were 3% and 15%. Evidently, the void between the two wakes of T101 and T102 was filled in by the wakes of the first row of turbines, indicating a nonlinear enhancement of the wake effects.

- The 15 to 20% energy deficit is not a realistic representation of the annual averages. For the Tehachapi site, the months of July and August are in the ebb of the primary wind season, with a monthly average wind speed noticeably lower than that in April or May. Because the power deficit decreases with increasing wind speed, the energy deficit measured during the field experiment therefore represents the high-end values. In addition, a 95% availability of the turbines for energy production would result in about a 7% reduction in the energy deficit. Based on the 1986 wind-speed distribution at the Tehachapi site, the energy deficit estimated for T102 is 11%, which reduces to 10% when a 95% availability is assumed. By the same token, we estimate a 1.5 to 2% increase in the annual energy deficit for a turbine two rows downwind, provided a linear superposition of the energy deficit is assumed.

6.2 Recommendations

Based on the findings of the field experiment, we recommend the following for improving the design and operation of VAWT windfarms as well as for furthering our understanding of array effects on the performance of VAWTs:

(1) The field results show that the wind speed sensor should be located very close to the turbine in order to attain a good correlation between the power output and the wind speed. Although we have demonstrated that a separation of 2D does yield reasonable results in a selected test site with relatively regular terrain features, this distance may be too large in other areas where the terrain features are more rugged, which is not unusual for a typical windfarm environment. Currently, the on/off configuration of a VAWT cluster (three at the FloWind windfarm) is controlled by a nearby wind sensor, which monitors the cut-in and cut-off wind speeds. There is evidence that some of the sensors do not perform as expected due to a micrositing phenomenon. It was subsequently discovered that the power output was far superior to the velocity deficit in sensing the turbine array effects on the performance of a downwind turbine. Therefore, we recommend that the power output be used in conjunction with the wind speed as the controlling parameters. Such a dual-parameter system would avoid motoring of the turbines at low wind speeds. This would not only improve the windfarm performance efficiency but also increase the lifetime of mechanical components. Furthermore, the availability of the power output at all times would help diagnose premature mechnical failures.

(2) This field experiment was one of the most extensive investigations of the performance of VAWTs in an operating windfarm. Only limited analysis of the data set has been conducted so far, and the results reported herein are by no means exhaustive. We have only examined the "maximium effects" in terms of the array effects on the performance of downwind turbines. For example, we have not touched upon the effects of background turbulence, although its role in reducing the velocity deficit has been indirectly demonstrated in examining the wind shear effects (Section 5.2.2). To investigate its effects in more detail, we could bin the velocity and power deficits into several ranges of background turbulence level. In addition,

results of the wind speed measured with the polystyrene propellers should be analyzed to investigate the high-frequency wind components induced by the rotors. Such information would provide insight to the resulting asymmetry of the wake of a VAWT.

(3) It is concluded in Section 5.2.3 that data scatter is relatively large in the velocity deficit derived by binning the data according to the wind speed and direction. It is recommended that an alternate analysis strategy may be adopted by comparing the results from back-to-back series of runs with different turbine on/off configurations. Such a comparison would minimize the variations in the environmental conditions, which tend to mask the effects of interest in the binned results. This strategy may be applied in deriving both the velocity and power deficits in an attempt to improve the accuracy in assessing the array effects on the performance of downwind VAWTs.

(4) As discussed in Section 5.3.2, the method for estimating the annual energy deficit [Equations (4) through (7)] based on the derived power deficit (Figure 65), the power output and the wind speed distribution may be applied to other sites and different turbine types. The power deficit for a range of practical array configurations should be derived and verified. Generalization of the method may be made to include the joint probability distribution of the wind speed and direction [Equation (3)], if needed. Such a method is a convenient tool for optimizing the design of a windfarm by selecting proper turbine types for a given site with known or estimated wind resources and terrain characteristics. In an established windfarm, the method may be used to derive information for management and planning purposes. For the utilities, information from individual windfarms may be summarized for wind energy management.

5760R

APPENDIX

QUALITY ASSURANCE

A set of experimental procedures was developed and implemented that governed the various key activities associated with the turbine wake project. These procedures included, but were not limited to, the following items:

(1) Calibration of sensors (Section 4.1.3).

(2) Classification of test conditions (Section 4.1.2 and Figure 6).

(3) Verification of computer software (Sections 3.1 and 6).

(4) Validation of meteorological data.

(5) Assurance of data quality.

The Participant and the PNL personnel had considerable experience in conducting full-scale wake studies under DOE sponsorship (e.g., Liu et al., 1983; Renne and Buck, 1985). In particular, the field experiment was similar to the wake measurement project using a DAF 500-kW VAWT (Renne and Buck, 1985) at the SCE test facility near San Gorgonio Pass, California. We followed closely the quality assurance (Q/A) program adopted in that project with due modifications.

The quality assurance activities were adopted to ensure data representativeness, completeness, precision and accuracy. A goal of the Cooperative Agreement Program initiated by DOE's Solar Energy Research Institute is to obtain high-quality data at operating windfarms suitable for the intended use by the wind energy community.

A detailed test plan was designed (Liu, 1986a) based on historical and recent data obtained at the Tehachapi FloWind windfarm. The final test site and test periods were selected based on an optimum assessment of the topography, the wind resources, the wind system and array configuration, and instrument capabilities. The tower array and sensor placement were designed to ensure maximum data stratification and spatial coverage and adequate redundancy.

Data recorded on different systems were processed with care to ensure the incorporation of calibration coefficients and corrections for sensor bias and limitations. Extensive measurements for the ambient wind field were conducted to compare wind speed measurements using Gill anemometers and Maximum cup anemometers. Corrections for the terrain effects on the local wind field (i.e., micrositing effects) were derived based on the measurements of the

ambient wind field. At the reference tower 2D upwind of the primary turbine (T123), we installed a Gill and cup anemometer together with a wind direction sensor at z = 13.7 m so that both wind speed and direction were measured independently by two separate instruments. A total of nine F-17 VAWTs were instrumented for power measurements. This again was done to ensure sufficient areal coverage and data redundancy. Intercomparison of wind speed and direction measurements using different sensors was made to ensure consistency of the field data. The essential specifications of the instruments used in the field experiments are summarized in Section 3.3. Refer to the manufacturers operational manual for detailed information.

Meteorological data in terms of pressure and temperature were measured at a nearby FloWind research trailer with an existing computer recording system. Manual readings of both temperature and barometric pressure were frequently made. For temperature information, we also included the record made at the Tehachapi City Fire Department.

The wind system was routinely maintained by the FloWind O&M crews according to the preventive maintenance schedules and procedures. Maintenance of the tower array and wind sensors was conducted by FloWind onsite research personnel, with additional support from the O&M crews. PNL personnel also visited the site several times during the course of the field experiment to check the integrity of the stack-up towers and the alignment of the Gill anemometers and the wind direction sensor.

5760R

REFERENCES

Baker, R. W., and Walker, S. N. (1982) "Wake Studies at the Goodnoe Hills MOD-2 Site," Technical Report prepared for the Bonneville Power Administration, October.

Hiester, T. R., Mercer, J. E., and Tremoulet, O. L. (1983) "The FloWind Vertical Axis Wind Turbine," Presented at the Energy Sources Technology Conference & Exhibition, Houston, Texas, 1 January to 3 February.

Ho, C.-M. (1983) "An Alternative Look at the Unsteady Separation Phenomenon," Symposium on Recent Advances in Aerodynamics and Aeroacoustics, Standford University, August, 11 pp.

Lissaman, P. B. S. (1979) "Energy Effectiveness of Arbitrary Arrays of Wind Turbines," J. of Energy, Vol. 3, pp. 323-328.

Lissaman, P. B. S., Gyatt, G. W., and Zalaly, A. D. (1982) "Numeric Modeling Sensitivity Analysis of the Performance of Wind Turbine Arrays," Technical Report PNL-4183, Pacific Northwest Laboratory, June.

Lissaman, P. B. S., Zambrano, T. G., and Gyatt, G. W. (1983) "Wake Structure Measurements at the Mod-2 Cluster Test Facility at Goodnoe Hills," Technical Report PNL-4572, Pacific Northwest Laboratory, March.

Liu H.-T. (1986a) "Final Test Plan for Field Investigation of a Wake Structure Downwind of a VAWT in a Windfarm Array," Flow Research Technical Communication No. 201, March.

Liu H.-T. (1986b) "Effects of Atmospheric Turbulence and Gust on the Performance of a Wortmann FX 63-137 Wing," Proc. Int. Conf. on Aerodynamics at Low Reynolds Numbers, the Royal Aeronautical Society, London, UK, October 15-18, 25 pp.

Liu, H.-T., Hiester, T. R., Waite, J. W., Tacheron, P. H., and Srnsky, R. A. (1983) "Flow Visualization Study of a Mod-2 Turbine Wake," Technical Report PNL-4535, Pacific Northwest Laboratory, June (also presented at the 1983 ASES Meeting, June 1-3).

Liu, H.-T., Geller, E. W., and Cooper, M. (1985) "An Environmental Aerodynamic Test System for Low-Reynolds-Number Applications," Proc. of the Conference on Low Reynolds Number Airfoil Aerodynamics, University of Notre Dame, Notre Dame, Indiana, 16-18 June.

MacCready (1966) "Mean Wind Speed Measurements in Turbulence," J. Appl. Meteorology, Vol. 5, pp. 219-225.

McCroskey (1981) "The Phenomenon of Dynamic Stall," NASA Technical Memo. No. 81264, Ames Research Center, Moffett Field, California, March.

Rauscher, M. (1953) Introduction to Aeronautical Dynamics, John Wiley & Son, p. 245.

Renne, D. S., and Buck, J. W. (1985) "Measurements and Analysis of the Wake of a DAF 500-kW Vertical Axis Wind Turbine," Southern California Edison Report No. 85-RD-9.

Vermeulen, P. E. J. (1980) "An Experimental Analysis of Wind Turbine Wakes," Proc. Third Int. Symp. on Wind Energy Systems, BHRA Fluid Engineering, Cranfield, Bedford, England, pp. 431-450.

Vermeulen, P. E. J., Builtjes, P. J. H., Dekker, J., and Bueren, G. L. V. (1979) "An Experimental Study of the Wake Behind a Full Scale Vertical Axis Wind Turbine," TNO Report 79-06118, Organization for Industrial Research, Apeldoorn, The Netherlands.

Walker, S. N., and Wade, J. E. (1987) "Local Flow Measurements for Micrositing," Technical Report PWE-87-823, Pacific Wind Energy, Inc., August.

5760R

END

DATE FILMED

12/4/92